Theory of Chirality Induced Spin Selectivity in Two Terminal Transport

Huisman, K.H.

DOI
10.4233/uuid:c3f5e791-2eb5-426a-8067-a1e3b488bd0a

Publication date
2023

Document Version
Final published version

Citation (APA)
Huisman, K. H. (2023). *Theory of Chirality Induced Spin Selectivity in Two Terminal Transport*. [Dissertation (TU Delft), Delft University of Technology]. https://doi.org/10.4233/uuid:c3f5e791-2eb5-426a-8067-a1e3b488bd0a

THEORY OF CHIRALITY INDUCED SPIN SELECTIVITY IN TWO TERMINAL TRANSPORT

THEORY OF CHIRALITY INDUCED SPIN SELECTIVITY IN TWO TERMINAL TRANSPORT

Proefschrift

ter verkrijging van de graad van doctor
aan de Technische Universiteit Delft,
op gezag van de Rector Magnificus prof. dr. ir. T.H.J.J. van der Hagen,
voorzitter van het College voor Promoties,
in het openbaar te verdedigen op donderdag 2 november 2023 om 10:00 uur

door

Karssien Hero HUISMAN

Master of Science in Physics and Astronomy, Universiteit van Amsterdam, Nederland
geboren te Amsterdam, Nederland

Dit proefschrift is goedgekeurd door de promotoren.

Samenstelling promotiecommissie:

Rector magnificus,	voorzitter
prof. dr. J.M. Thijssen	Technische Universiteit Delft, promotor
prof. dr. ir. H.S.J. van der Zant	Technische Universiteit Delft, copromotor
Onafhankelijke leden:	
prof. dr. ir. B.J. van Wees	Rijksuniversiteit Groningen
prof. dr. J.M. van Ruitenbeek	Universiteit Leiden
prof. dr. F.C. Grozema	Technische Universiteit Delft
prof. dr. J. Fransson	Universiteit Uppsala, Zweden
prof. dr. Y.M. Blanter	Technische Universiteit Delft, *reservelid*

Keywords: Magneto-transport, Onsager reciprocity, Büttiker reciprocity, Voltage probes, Coulomb interactions, Mean-field theory, (non-)collinear Hubbard one approximation, Vibrational modes, Spin-orbit coupling, Stray fields, Chirality Induced Spin Selectivity

Printed by: [PRINTER]

Front & Back: [Description of the figure on the Front and on the Back of the Disseration]

Casimir PhD Series, Delft-Leiden 2023-32

ISBN 978-90-8593-579-7

An electronic version of this dissertation is available at
http://repository.tudelft.nl/.
All research-code relevant for this dissertation are available at 4TU.Centre for Research Data via:
https://doi.org/10.4121/a92cc537-201c-4fd0-a3b7-6329f33667c1.v1.

Voor Edzo & Madeleine, aan wie ik alles te danken heb.

CONTENTS

SUMMARY

In this thesis we perform a theoretical study on the Chirality Induced Spin Selectivity effect in the context of two-terminal measurements for realistic parameters. In two-terminal measurements on chiral molecules one of the leads is magnetized and the current is measured for opposite magnetizations. In experiment it is found that the currents for opposite magnetizations are different for finite bias voltage. We call this finite difference a magnetocurrent. The magnetocurrent is odd in bias voltage and the size of the effect of the order of a few percent. Our aim is to explain this effect through modeling junctions with interactions and the spin-orbit where we always use choose realistic parameters.

In **chapter 1** we give an introduction to the different experiments that have been performed on the Chirality Induced Spin Selectivity effect. We focus on the two-terminal measurements and discuss Onsager reciprocity and Büttiker reciprocity. We conclude that Onsager reciprocity must always be explicitly verified in experiment and theory. Lastly we conclude that interactions have to be present to explain the Chirality Induces Spin selectivity.

In **chapter 2** we model a two-terminal junction containing helicene and gold with realistic parameters. Interactions are introduced through Büttiker voltage probes and we are interested in the size of the effect (magnetoresistance) in the currents. We conclude that the magnetoresistance vanishes if interactions are absent, in line with the Büttiker reciprocity theorem. When interactions are present a finite magnetoresistance appears and for realistic parameters it is of the order 0.1% and vanishes if the spin-orbit coupling (in the gold and the molecule) is set to zero. We explicitly verify the Onsager-reciprocity theorem such that the magnetocurrent around zero bias voltage is non-linear. The magnetocurrent is found to be dominantly even in bias voltage, contrary to the odd signature found in experiment.

In **chapter 3** we model a molecule as a tight binding chain with nearest neighbour hopping and next-nearest neighbour spin-orbit coupling. Interactions are modelled through on-site Coulomb interactions in the Hartree-Fock and Hubbard One approximation. The leads are take in the wide-band limit. The magnetocurrent is found to satisfy Onsager reciprocity and to be dominantly odd in bias voltage for strong Coulomb interactions in both approximations. The size of the effect is of the order 0.1% for a realistic choice of parameters.

In **chapter 4** we model a molecule as a tight binding chain with nearest neighbour hopping and nearest neighbour spin-orbit coupling. Interactions are modelled through on-site Coulomb interactions in the Hartree-Fock and Hubbard One approximation. The bias dependence of the magnetocurrent for semi-infinite leads and wide-band limit leads is studied. We find that the magnetocurrent is exactly even for leads in the wide band limit and exactly odd for semi-infinite leads in both approximations. These numerical findings are supported by the theoretical analyses and originate from the bipartite-lattice symmetry and time-reversal properties of the Green's function. We also demonstrate the validity of Onsager reciprocity and we find an effect that is of the order 0.1% for realistic parameters.

In **chapter 5** we study the effect of vibrational modes in the off-resonance regime for chiral molecules. The magnetocurrent is found to satisfy the Onsager-reciprocity theorem and its is dominantly even in bias voltage. The magnetocurrent becomes non-zero when the bias voltage matches the energy of the vibrational mode and the size of the effect is of the order 0.1% for realistic parameters.

SAMENVATTING

In deze thesis voeren we een theoretische studie uit over het chiraliteit geïnduceerde spin selectieve effect in de context van systemen met twee elektrodes voor realistiche parameters. In metingen voor systemen met twee elektrodes betreffende chirale moleculen wordt één van de elektrodes gemagnetiseerd en de stroom wordt gemeten voor tegenovergestelde magnetisaties. In het experiment wordt gemeten dat de stroom voor tegenovergestelde magnetisatie richtingen van elkaar verschilt voor een eindig bias voltage. Wij noemen dit eindige verschil een magnetostroom. De magnetostroom is oneven in het bias voltage en de grootte van het effect is van de orde van een paar procent. Ons doel is om dit effect te verklaren door interacties en de spin-baan koppeling in de theoretische beschrijving van het systeem op te nemen waarbij er altijd gebruik wordt gemaakt van realistische parameters.

In **hoofdstuk 1** geven we een introductie over de verschillende soorten experimenten die gedaan zijn in de context van chiraliteit geïnduceerde spin selectiviteit. Uiteindelijk zullen we ons concentreren op twee elektrode metingen en zullen we Onsager reciprociteit en Büttiker reciprociteit bespreken. We concluderen dat Onsager reciprociteit altijd expliciet geverifieerd moet worden in het experiment én in de theorie. Tot slot concluderen we dat interacties aanwezig moeten zijn in de theoretische beschrijving om het chiraliteit geïnduceerde spin selectieve effect te verklaren.

In **hoofdstuk 2** modelleren we een junctie die bestaat uit een heliceen molcuul met gouden elektrodes voor realistische parameters. Interacties worden geïntroduceerd door Büttiker voltage probes en we zijn geïnteresseerd in de grootte van het effect (magnetoweerstand). We concluderen dat de magnetoweerstand nul wordt als interacties afwezig zijn, in overeenstemming met Büttiker reciprociteit. Wanneer interacties worden meegenomen verschijnt er voor realistische parameters een eindige magnetoweerstand die van de orde 0.1% is en verdwijnt als de spin-baan koppeling (in het goud en in het heliceen molecuul) op nul wordt gezet. Onsager reciprociteit wordt expliciet geverifieerd zodanig dat de magnetostroom rond het bias voltage nul non-lineair is. De magnetostroom in onze studie is dominant even in het bias voltage, in tegenstelling tot het signatuur dat gevonden wordt in het experiment.

In **hoofdstuk 3** modelleren we een molecuul in als een eindige “tight-binding” ketting met naaste buren hopping en naaste-naaste buren hopping afkomstig van de spin-baan koppeling. Interacties worden gemodelleerd als Coulomb interacties tussen elektronen die zich op hetzelfde site bevinden met tegenovergestelde spin in de Hartree-Fock en Hubbard-One benadering. De elektrodes worden gemodelleerd in de wijde banden limiet. De magnetostroom voldoet aan Onsager reciprociteit en de magnetostroom is dominant oneven in het bias voltage voor sterke Coulomb interacties in beide benaderingen. De orde van grootte van het effect is van de orde 0.1% voor realistische parameters.

In **hoofdstuk 4** modelleren we een molecuul in als een eindige “tight-binding” ketting met naaste buren hopping en naaste buren hopping afkomstig van de spin-baan koppeling. Interacties worden gemodelleerd als Coulomb interacties tussen elektronen die zich op hetzelfde site bevinden met tegenovergestelde spin in de Hartree-Fock en Hubbard-One benadering. De bias voltage afhankelijkheid van de magnetostroom wordt onderzocht voor semi-oneindige elektrodes en elektrodes in de wijde banden limiet. Een theoretische analyse gebaseerd, op de tweedelige rooster en tijdsomkeer symmetrie van de Green's functies, toont aan dat de voltage afhankelijkheid van de magnetostroom exact even is in de wijde banden limiet en exact oneven is voor de semi-oneindige elektrodes in beide benaderingen. Onze numerieke resultaten ondersteunen deze theoretische analyse. We tonen wederom aan dat aan Onsager reciprociteit wordt voldaan en dat de orde van grootte voor realistische parameters 0.1% is.

In **hoofstuk 5** bestuderen we het effect van vibrationele "modes" in het uit-resonante regime voor chirale moleculen. De magnetostroom voldoet aan Onsager reciprociteit en is dominant even in het bias voltage. De magnetostroom wordt niet-nul wanneer het bias voltage gelijk is aan de eigenfrequentie van de vibrationele "mode" en de grootte van het effect is van de order 0.1% voor realistische parameters.

1

INTRODUCTION

The Chirality Induced Spin Selectivity (CISS) effect is measured across different types of experiments for chiral molecules. We focus on two-terminal transport experiments with chiral molecules where a non-zero magnetocurrent is measured. Magnetocurrent is defined as the difference between the charge currents at finite bias in a two terminal device for opposite magnetizations of one of the leads. Our aim is to develop a theory to explain the appearance and bias voltage dependence of this magnetocurrent. In order to do so we discuss the Onsager reciprocity theorem in detail. We conclude that in order to understand the CISS effect, electrons must interact amongst themselves or with vibrational modes. In the following chapters the signature and size of the magnetocurrent for the different types of interactions are discussed.

1.1. CHIRALITY INDUCED SPIN SELECTIVITY

Chirality induced spin selectivity (CISS) is a broad term that is used to describe phenomena observed across different types of experiments concerning chiral molecules. These experiments entail photo-emission, enantiospecific adsorption, two terminal transport, Hall-type and chemical reactions (for an extensive overview see ref [1]).

Chirality is the property a stationary object can have and it means that there are two different configurations which are related to each other by by a mirror operation. These two configurations cannot be made to coincide by applying rotations on them. The term chirality is derived from the ancient Greek word for hand: $\chi\epsilon\iota\rho$ (kheir) and, not surprisingly, an example of a chiral object is a hand. Molecules can also be chiral and example is shown in figure 1.1, the molecules are each others mirror image and cannot be superimposed by applying rotations.[1] Other examples of organic chiral molecules are helicene, DNA,proteins,sugars etc. and also some anorganic molecules such as copper oxide and perovskites can be made chiral. Helicene and DNA molecules are shaped like a helix

---

[1] Barron[2] made a further distinction of chirality for moving (rather than stationary) objects. A moving object is said to be “truly chiral” if its time-reversed image cannot be superimposed with its mirror image.

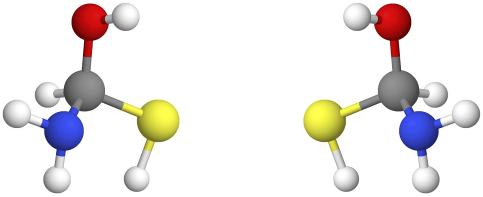

Figure 1.1: The molecule on the right is the mirror image of the molecule on the left. These molecules cannot be made to coincide by applying rotations and translations, therefore they are chiral.

and their chirality is indicated by the direction in which the helix turns, which is either clockwise or anti-clockwise when looking along the helical axis.

1.2. PHOTO-EMISSION EXPERIMENTS

Before the first observation of CISS, Mayer and Kessler[3] found that a vapor of chiral, camphorlike molecules containing an ytterbium atom ($Yb(hfc)_3$), show an asymmetry between the transmission probability of electrons initially polarized parallel and anti-parallel to the electron beam axis. This asymmetry changed sign between the enantiomers of the molecule. Later experiments with bromocamphor,[4] dibromocamphor and $X(hfc)_3$ (with X = Yb,Pr,Eu,Er)[5] also showed this asymmetry. It was found that the asymmetry grows with the atomic number of atoms added to the camphor (Br,Yb,Pr,Eu,Er) and that the asymmetry became large when there were resonances in the cross-section corresponding to temporary ion formation.[4,5]

The first observation of CISS was made in the photo-emission experiment of Ray et al.[6] in 1999. In this experiment electrons where photo-excited from a gold substrate, then passed through a layer of chiral molecules attached to this substrate and the transmission for spin up and spin down electrons was measured. The polarization of the incoming light can induce an asymmetry for spin up and spin down electrons in the outgoing electron beam, even for a bare gold substrate (the asymmetry is zero for linearly polarized light). Surprisingly, it was found that a layer of chiral molecules attached to the gold substrate changed this asymmetry significantly for spin up and spin down electrons than the bare gold substrate. Other studies confirmed that this effect also occurred for other chiral molecules such as double stranded DNA molecules[7,8] on gold, helicene[9] on copper & gold, oligopeptides[10] on Au and copper oxide - gold films.[11]

1.3. TWO-TERMINAL TRANSPORT

In two terminal transport experiments on chiral molecules[12–24] one lead is magnetized and the currents for positive and negative magnetization are measured as a function of bias voltage (see fig. 1.2). The CISS effect manifests itself as the appearance of a magnetocurrent. Magnetocurrent is the observation that the currents for non-zero bias voltage differ for opposite magnetizations of the lead. The magnetocurrent is dominantly odd in bias voltage and values of the order 6% – 90% have been measured. In this thesis we will focus on the theory of two terminal transport of CISS experiments.

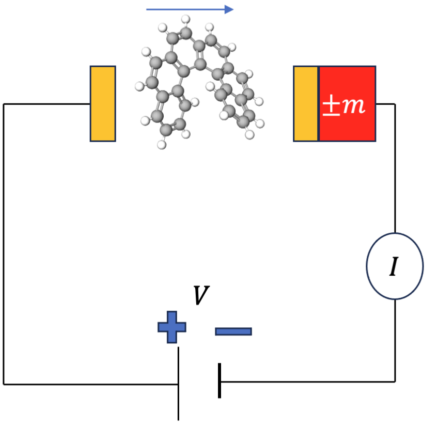

Figure 1.2: Schematic of a two terminal experiment. A bias voltage V is applied and the current I that runs through the chiral helicene molecule is measured for the positive ($+m$) and negative ($-m$) magnetization.

Yang, van Wees and van der Wal[25] pointed out the importance of Onsager-Casimir reciprocity in experiments. Onsager-Casimir reciprocity[26–28] prohibits magnetocurrent from being observed in two-terminal junctions voltage, in the regime where the current scales linearly with the bias voltage. Astonishingly, several experiments[13–15,18,21,23,29] seem to show violation of Onsager-Casimir reciprocity for reasons that are not yet known. An example of current-voltage curves that violate Onsager-Casimir reciprocity is shown in fig. 1.3a & 1.3b. In ref fig. 1.3a the currents for positive and negative magnetization are plotted. At zero bias voltage the slopes of the currents for positive and negative magnetization differ, thereby implying that the corresponding magnetocurrent in fig. 1.3b is linear in bias voltage and Onsager-Casimir reciprocity is violated. However in some of these experiments the currents for positive and negative magnetization show a plateau of zero current around zero bias voltage (like the one in fig. 1.3c) such that the demonstration of Onsager-Casimir reciprocity is not really convincing. In order for Onsager reciprocity to be tested experimentally for devices with chiral molecules, the currents near zero bias voltage need to be dominantly linear in bias voltage and be significantly nonzero. To the best of our knowledge ref. [30] is one of the first experiments that has explicitly verified Onsager reciprocity for a junction with chiral molecules.

Naturally the question arises what can break Onsager-Casimir reciprocity in two terminal experiments? To answer that question, let us first give a short recap on Onsager reciprocity (see ref. [31] for more details). Onsager started his derivation by considering the entropy near its maximum i.e. near thermodynamic equilibrium. Equilibrium for a two terminal system means that temperatures and chemical potentials for the left and right lead are equal (i.e. $T_\mathrm{L} = T_\mathrm{R}$ and $\mu_\mathrm{L} = \mu_\mathrm{R}$).[32] The system is driven out of equilibrium by a bias voltage V and the current I, in the linear response regime, scales as: $I \propto G_1 V$, with G_1 the linear conductance coefficient. Another important consideration is how quantities such as magnetic field, velocity, force, etc. change under reversal of time i.e. if the quantities considered are time-even or time-odd. The linear conductance coefficient for a two terminal system depends on time-even quantities, denoted as x_n

and time-odd quantities, denoted as $\tilde{x}_q$ such that $G_1 = G_1(x_1,...,x_N,\tilde{x}_1,...,\tilde{x}_Q)$. Under reversal of time $t \to -t$, time-even quantities remain the same ($x_n \to x_n$) while time-odd quantities change sign ($\tilde{x}_q \to -\tilde{x}_q$). From Onsager's derivation[26,27] it follows that the linear conductance coefficient for a two terminal system is invariant under reversal of the arrows of time:

$$G_1(x_1,...,x_N,\tilde{x}_1,...,\tilde{x}_Q) = G_1(x_1,...,x_N,-\tilde{x}_1,...,-\tilde{x}_Q). \tag{1.1}$$

The magnetic field m in the lead is a time-odd quantity, thus this implies that linear conductance coefficients are equal for opposite magnetizations $G_1(m) = G_1(-m)$. This in turn implies that the magnetocurrent can only scale non-linearly with bias voltage.[25,33–35] Lastly it should be noted that the reciprocity theorem is generic: it does not rely on a specific description of the scattering process. Therefore we expect that any theory should reproduce Onsager's reciprocity theorem or provide strong reasons for its violation: vibrational modes or Coulomb interactions cannot invalidate the theorem. The only criterion is that the system is near equilibrium. Nevertheless the meaning of Onsager's reciprocity theorem in the context of two terminal transport experiments on molecules has been topic of debate.[36,37]

1.4. BROKEN RECIPROCITY ?

Experimental work of[38–40] showed that self-assembled monolayers of chiral molecules can magnetize when put on a nonmagnetic gold surface at room temperature. We call this spontaneous magnetization m_χ. This magnetization changes with the chirality of the molecules[40] and it decreases over time.[39] In this section we will discuss the implications of these experimental findings for two terminal transport, theories based on spin-accumulation in one of the leads[41,42] and possible experimental errors in light of the Onsager reciprocity theorem.

We consider two extreme scenarios. In the first scenario the spontaneous magnetization m_χ changes sign with the magnetization of the leads and the linear conductance satisfies: $G_1(m, m_\chi) = G_1(-m, -m_\chi)$, in agreement with the Onsager reciprocity theorem. In the second scenario the self-assembled monolayer of molecules act a spin valve. This means that, for some unknown reason, the spontaneous magnetization m_χ does not change at all upon reversal of the magnetization m in the leads, the linear conductance coefficients for positive and negative magnetization of the lead are $G_1(m, m_\chi)$ and $G_1(-m, m_\chi)$ respectively. According to the Onsager reciprocity theorem these coefficients can be unequal to each other, since time-reversal would flip the sign of *b*oth magnetizations m, m_χ and therefore non-reversal of m_χ implies violation of the Onsager reciprocity. Firstly the question is whether a spontaneous magnetization m_χ is expected from theory and secondly the question is how the spontaneous magnetization changes with the magnetization in the leads.

Hedegård[43] pointed out that the relative motion of electrons, magnetic dipole-dipole coupling can serve as a source for a spontaneous magnetization. He concluded that neither of these is a viable source of spontaneous magnetization. A 'back of the envelope' calculation[44] tells us that the dipolar interaction energy between two magnetic dipoles $\boldsymbol{m}_1$ and $\boldsymbol{m}_2$ (of the order of a few Bohr magneton) separated by a few Å is of the order 10^{-4} eV, which is well below the energy scale set by room-temperature ($T = 300$ K)

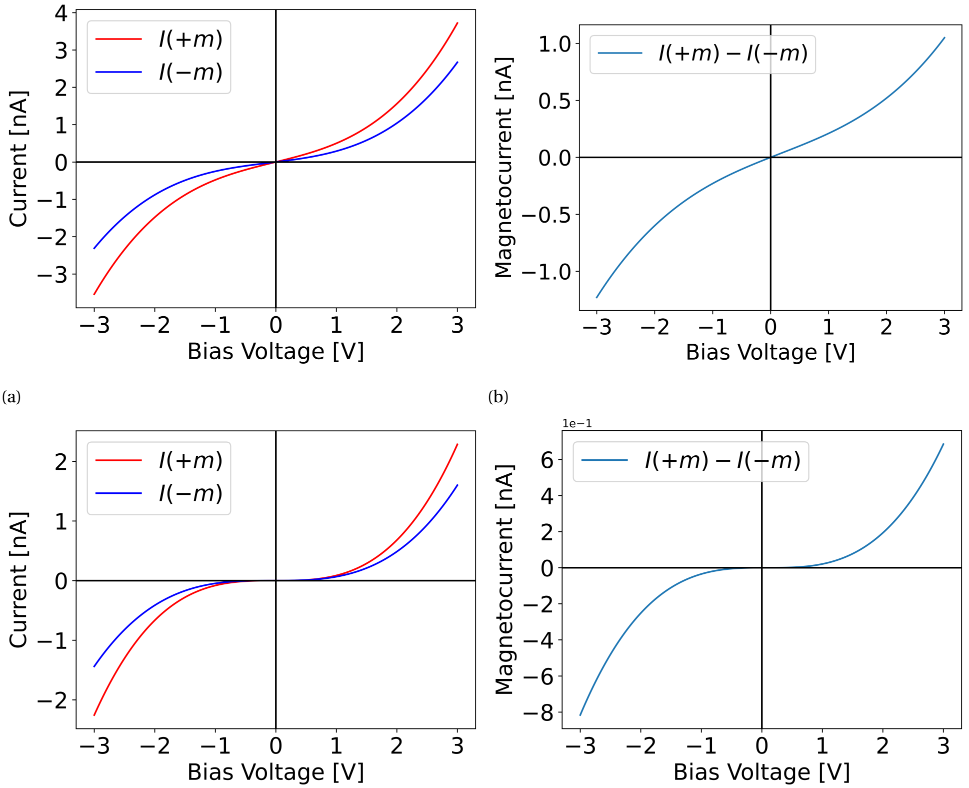

(a) (b) (c) (d)

Figure 1.3: **(a)** The figure shows the current as a function of bias voltage for positive and negative magnetization of the lead. Around zero bias voltage the slopes for positive and negative magnetization differ. **(b)** The difference between the positive and negative magnetization of figure 1.3a. It shows that the magnetocurrent is linear around zero bias voltage and dominantly odd in V. **(c)** The current for positive and negative magnetization as a function of bias voltage for a chiral molecule. Around zero bias voltage the currents show a plateau behaviour. **(d)** Difference between the current for up and down magnetization in fig. 1.3c The difference is dominantly odd in bias voltage V. Note that none of these figures are made with actual experimental data, but rather serve as an illustration for the violation of Onsager reciprocity.

: $k_B T \approx 2.5 \cdot 10^{-2}$ eV. Therefore thermal fluctuations will destroy any spontaneous magnetization at such temperatures. Hedegård[43] also pointed out that exchange interactions (of electrons with the surroundings of the molecule) are important. This is understood through Stoner's criterion,[45] which implies that an interacting system can lower its ground state energy by building up a finite magnetization.

In other studies[46,47] exchange effects were taken into account. When molecules are adsorbed onto a nonmagnetic lead, a positive (m_{up}) and a negative (m_{down}) magnetic ground state were found, by varying the packing density of the molecules.[46] When a vibrational spin-dependent coupling[47] was taken into account, a magnetization was obtained for a molecule coupled to a nonmagnetic substrate.

There are some problems with large ensembles of molecules spontaneously magnetizing. First of all we are dealing with organic molecules and gold, two materials that are paramagnetic at room temperature and unlike for example Fe or Co do not have an unpaired electron in their outer shell. Then suddenly, when put together, they seem to become ferromagnetic. Secondly, we have the randomising effect of temperature which will destroy any magnetization above the critical temperature (the temperature below which the system is magnetic and above which it is non-magnetic). Nevertheless magnetization of self-assembled monolayers of molecules has been observed at 300 K far above a typical critical temperature.[40] It is topic of debate whether the effect of exchange interactions can explain this spontaneous magnetization.

Now let us address the question how the spontaneous magnetization m_χ changes with the magnetization in the leads. Let us assume that self-assembled monolayers of chiral molecules form an Ising model (although a Heisenberg model is probably more realistic). This monolayer is adsorbed onto a substrate and it is considered near equilibrium. In the Landau theory[2] of phase transitions the free energy of the Ising model, in the presence of an external magnetic field h, is approximated as $F = -hm + rm^2 + sm^4$, valid when the system is close to the critical temperature. Let us assume that the temperature in experiment is below the critical temperature. The field h causes the minimum of the free energy that is opposite in sign to h to become metastable and the minimum which is aligned with the same sign as h to become stable in free energy, making the latter minimum more likely. We call the magnetization corresponding to the stable minimum of the free energy at external magnetization h, $m_\chi(h)$ (see fig. 1.4) and it can be seen that it changes sign with the external magnetization $m_\chi(h) = -m_\chi(-h)$.

Upon reversal of the external field h, a system initially in the global minimum state $m_\chi(h)$, may stick in the state which has now become metastable $m_{\text{meta}}(-h)$ (see fig. 1.4)), implying violation of reciprocity. After some time, the system is however expected to relax to the stable minimum and Onsager reciprocity is then restored: $G_1(h, m_\chi) = G_1(-h, -m_\chi)$. Some authors have argued that a finite spin current[42] or spin-transfer torque[41] induce a spin-accumulation close the the molecule-lead interface. This means that the chemical potential for up and down spin is unequal $\mu_s = \mu_\uparrow - \mu_\downarrow \neq 0$. It has been topic of debate whether this spin-accumulation can break Onsager reciprocity. Due to spin being a time-odd quantity it flips under reversal of time and thus the spin-accumulation: $\mu_s \to -\mu_s$ is a time odd-quantity. Onsager reciprocity implies that: $G_1(m, \mu_s) = G_1(-m, -\mu_s)$. We therefore expect that any sane theory finds the equilibrium spin-accumulation

---

[2] Landau theory neglects fluctuations and is not correct for $d < 4$.

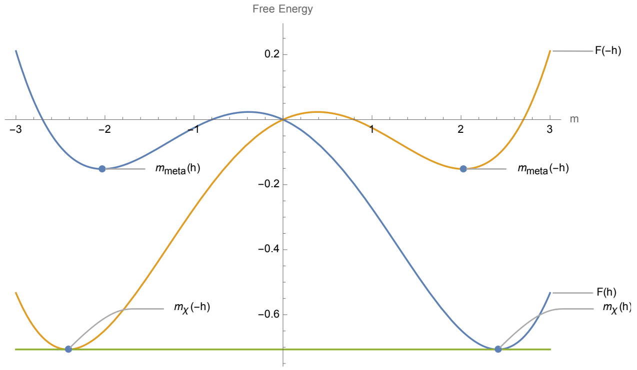

Figure 1.4: Free Energy of Landau theory as a function of the systems magnetization for a system where an external magnetization h is applied. The figure shows that the minima of the free energy $m_\chi(h)$ and $m_\chi(-h)$ are opposite in sign and that the free energy obtain the same value in its minimum for positive and negative external magnetization. The metastable magnetizations for positive $m_{\text{meta}}(h)$ and negative magnetization $m_{\text{meta}}(-h)$ are indicated in the Free energy.

to change sign when the magnetization is flipped.

One could argue that a spin accumulation in one of the leads closely resembles a spontaneous magnetization in that lead. From the perspective of the molecule the leads acquire a spin-accumulation and from the extended molecule perspective (i.e. the molecule and a part of the leads) a part of the lead magnetizes i.e. there is an imbalance between spin-up and spin-down electrons. This accumulation/magnetization is expected to always change sign between the opposite magnetizations, due to Onsager reciprocity. In conclusion, the effect of spin-accumulation can only transiently cause Onsager reciprocity to be broken. Moreover, the leads outside of the extended molecule are in equilibrium; hence also from the perspective of the leads this accumulation of spin will change sign between the opposite magnetizations of the lead.

When considering time-even quantities, the force exerted by the leads on the molecule is of great importance. Force is a time-even quantity and Onsager reciprocity requires it to remain unchanged when the magnetization of the lead is reversed. If the substrate on which the molecules are are attached has is only weakly magnetized, the magnetic lead will either be attracted or repelled by the substrate, resulting in a different force that is exerted on the molecule for the opposite magnetizations of the lead. Of course it is assumed that in experiment such effects are taken into account by looking at the force-distance curves.

1.5. RECIPROCITY ABIDING MAGNETOCURRENT

In this thesis we will not focus on mechanisms that could break Onsager's reciprocity theorem. Rather, we analyse models with well-defined physical mechanisms and we will always explicitly verify that Onsager reciprocity holds.

Now let us move on to the task of developing theoretical models that allow for a non-zero magnetocurrent in the first place. As a start, we recall that in photo-emission experiments it was shown that a layer of chiral molecules induces an asymmetry in the transmission for spin up and spin down electrons. It is because of this reason that early theory has focused on the spin dependence of the transmission which can be induced by spin-orbit coupling and some form of chirality. Another condition for the transmission to be asymmetric for spin up and spin down electron is that, for a two terminal system, the leads must support more than one spin-degenerate channel.[48,49] It is known that the spin-orbit coupling of the molecule's constituents can induce an asymmetry of the order 10^{-5}% for helicene[50] (where the s, $p_{\mathrm{x,y}}$ orbitals were projected out), six to seven orders of magnitude smaller than is observed in experiment. When taking the spin-orbit coupling of a gold substrate into account, the effect is of the order of a few percent for a chiral chain of carbon atoms[51] or for a helicene molecule.[34,52]

Although a spin dependent transmission may be interesting, it does however not guarantee a finite magnetocurrent. In fully coherent two terminal transport, the absence of a magnetocurrent extends to the nonlinear regime as well, this is called Büttiker reciprocity.[53] In order to see a magnetocurrent in the nonlinear regime, coherence must be broken; this is done through interactions of the electrons with vibrational modes[54] or among themselves , through the Coulomb interactions.[55]

We conclude that there are three important points when developing a two terminal transport theory for CISS. The first point is Onsager-Casimir reciprocity that states the linear conductance coefficients are equal for the opposite magnetizations of one of the leads $G_1(m) = G_1(-m)$. Deviations from Onsager are not expected and therefore theory should reproduce it or provide strong reasons for its violation.[56] The second one is the bias dependence of the magnetocurrent which in two terminal transport experiments is found to be dominantly odd in the bias voltage. Theory has found that interactions modeled by a decoherence node[33] yield a magnetocurrent dominantly even in bias voltage. A model including spin-dependent electron phonon coupling[57] finds an odd magnetocurrent, however it seems that the currents for opposite magnetizations seem to have a different slope at zero bias voltage, indicating that Onsager reciprocity does not hold. The last point is the size of the effect, the polarization of the charge current, defined as the magnetocurrent divided by the sum of the opposite currents: $P_C = \frac{I(m)-I(-m)}{I(m)+I(-m)}$. In experiment, values varying from 6%-90% are observed, while theory finds for large values of the spin-orbit coupling an effect which is of the order 0.1% for Büttiker voltage probes[34] or Coulomb interactions.[35,58] Fransson[55] found an effect of the order of the order of a few percent, when taking Coulomb interactions and spin-orbit coupling for a chiral molecule into account, although the Fermi-level in his work lies well outside the molecular spectrum.

1.6. THIS THESIS

This thesis is structured as follows. In chapter 2 we model a molecular junction for realistic parameters and introduce interactions through Büttiker voltage probes. In chapter 3 and 4 we model bipartite asymmetric and bipartite symmetric structures respectively with spin-orbit coupling and on-site Coulomb interactions. In chapter 5 we investigate the effect of vibrational modes on the magnetocurrent in the off-resonance regime.

REFERENCES

(1) Aiello, C. D.; Abendroth, J. M.; Abbas, M.; Afanasev, A.; Agarwal, S.; Banerjee, A. S.; Beratan, D. N.; Belling, J. N.; Berche, B.; Botana, A., et al. A Chirality-Based Quantum Leap. *ACS Nano* **2022**, *16*, PMID: 35318848, 4989–5035.

(2) Barron, L. Fundamental Symmetry Aspects of Chirality. **1987**.

(3) Mayer, S.; Kessler, J. Experimental Verification of Electron Optic Dichroism. *Phys. Rev. Lett.* **1995**, *74*, 4803–4806.

(4) Mayer, S.; Nolting, C.; Kessler, J. Electron scattering from chiral molecules. *Journal of Physics B: Atomic, Molecular and Optical Physics* **1996**, *29*, 3497.

(5) Nolting, C.; Mayer, S.; Kessler, J. Electron dichroism - new data and an experimental cross-check. *Journal of Physics B: Atomic, Molecular and Optical Physics* **1997**, *30*, 5491.

(6) Ray, K.; Ananthavel, S. P.; Waldeck, D. H.; Naaman, R. Asymmetric Scattering of Polarized Electrons by Organized Organic Films of Chiral Molecules. *Science* **1999**, *283*, 814–816.

(7) Ray, S. G.; Daube, S. S.; Leitus, G.; Vager, Z.; Naaman, R. Chirality-Induced Spin-Selective Properties of Self-Assembled Monolayers of DNA on Gold. *Phys. Rev. Lett.* **2006**, *96*, 036101.

(8) Göhler, B.; Hamelbeck, V.; Markus, T. Z.; Kettner, M.; Hanne, G. F.; Vager, Z.; Naaman, R.; Zacharias, H. Spin Selectivity in Electron Transmission Through Self-Assembled Monolayers of Double-Stranded DNA. *Science* **2011**, *331*, 894–897.

(9) Kettner, M.; Maslyuk, V. V.; Nürenberg, D.; Seibel, J.; Gutierrez, R.; Cuniberti, G.; Ernst, K.-H.; Zacharias, H. Chirality-Dependent Electron Spin Filtering by Molecular Monolayers of Helicenes. *The Journal of Physical Chemistry Letters* **2018**, *9*, PMID: 29618210, 2025–2030.

(10) Kettner, M.; Göhler, B.; Zacharias, H.; Mishra, D.; Kiran, V.; Naaman, R.; Waldeck, D. H.; Sęk, S.; Pawłowski, J.; Juhaniewicz, J. Spin Filtering in Electron Transport Through Chiral Oligopeptides. *The Journal of Physical Chemistry C* **2015**, *119*, 14542–14547.

(11) Ghosh, K. B.; Zhang, W.; Tassinari, F.; Mastai, Y.; Lidor-Shalev, O.; Naaman, R.; Möllers, P.; Nürenberg, D.; Zacharias, H.; Wei, J., et al. Controlling Chemical Selectivity in Electrocatalysis with Chiral CuO-Coated Electrodes. *The Journal of Physical Chemistry C* **2019**, *123*, 3024–3031.

(12) Liu, T.; Wang, X.; Wang, H.; Shi, G.; Gao, F.; Feng, H.; Deng, H.; Hu, L.; Lochner, E.; Schlottmann, P., et al. Linear and Nonlinear Two-Terminal Spin-Valve Effect from Chirality-Induced Spin Selectivity. *ACS Nano* **2020**, *14*, PMID: 33136367, 15983–15991.

(13) Lu, H.; Xiao, C.; Song, R.; Li, T.; Maughan, A. E.; Levin, A.; Brunecky, R.; Berry, J. J.; Mitzi, D. B.; Blum, V., et al. Highly Distorted Chiral Two-Dimensional Tin Iodide Perovskites for Spin Polarized Charge Transport. *Journal of the American Chemical Society* **2020**, *142*, PMID: 32602710, 13030–13040.

(14) Huizi-Rayo, U.; Gutierrez, J.; Seco, J. M.; Mujica, V.; Diez-Perez, I.; Ugalde, J. M.; Tercjak, A.; Cepeda, J.; San Sebastian, E. An Ideal Spin Filter: Long-Range, High-Spin Selectivity in Chiral Helicoidal 3-Dimensional Metal Organic Frameworks. *Nano Letters* **2020**, *20*, PMID: 33170013, 8476–8482.

(15) Koplovitz, G.; Primc, D.; Ben Dor, O.; Yochelis, S.; Rotem, D.; Porath, D.; Paltiel, Y. Magnetic Nanoplatelet-Based Spin Memory Device Operating at Ambient Temperatures. *Advanced Materials* **2017**, *29*, 1606748.

(16) Nguyen, T. N. H.; Rasabathina, L.; Hellwig, O.; Sharma, A.; Salvan, G.; Yochelis, S.; Paltiel, Y.; Baczewski, L. T.; Tegenkamp, C. Cooperative Effect of Electron Spin Polarization in Chiral Molecules Studied with Non-Spin-Polarized Scanning Tunneling Microscopy. *ACS Applied Materials & Interfaces* **2022**, *14*, PMID: 35960822, 38013–38020.

(17) Rahman, M. W.; Firouzeh, S.; Pramanik, S. Carrier localization and magnetoresistance in DNA-functionalized carbon nanotubes. *Nanotechnology* **2021**, *32*, 455001.

(18) Kulkarni, C.; Mondal, A.; Das, T.; Grinbom, G.; Tassinari, F.; Mabesoone, M.; Meijer, E.; Naaman, R. Highly Efficient and Tunable Filtering of Electrons' Spin by Supramolecular Chirality of Nanofiber-Based Materials. *Advanced Materials* **2020**, *32*, DOI: `10.1002/adma.201904965`.

(19) Kiran, V.; Mathew, S.; Cohen, S.; Hernandez Delgado, I.; Lacour, J.; Naaman, R. Helicenes-A New Class of Organic Spin Filter. *Advanced materials (Deerfield Beach, Fla.)* **2016**, *28*, DOI: `10.1002/adma.201504725`.

(20) Xie, Z.; Markus, T. Z.; Cohen, S. R.; Vager, Z.; Gutierrez, R.; Naaman, R. Correction to Spin Specific Electron Conduction through DNA Oligomers. *Nano Letters* **2012**, *12*, PMID: 22132798, 523–523.

(21) Al Bustami, H.; Koplovitz, G.; Primc, D.; Yochelis, S.; Capua, E.; Porath, D.; Naaman, R.; Paltiel, Y. Single Nanoparticle Magnetic Spin Memristor. *Small* **2018**, *14*, 1801249.

(22) Bullard, G.; Tassinari, F.; Ko, C.-H.; Mondal, A. K.; Wang, R.; Mishra, S.; Naaman, R.; Therien, M. J. Low-Resistance Molecular Wires Propagate Spin-Polarized Currents. *Journal of the American Chemical Society* **2019**, *141*, PMID: 31411873, 14707–14711.

(23) Tassinari, F.; Jayarathna, D.; Kantor-Uriel, N.; Davis, K.; Varade, V.; Achim, C.; Naaman, R. Chirality Dependent Charge Transfer Rate in Oligopeptides. *Advanced Materials* **2018**, *30*, 1706423.

(24) Bloom, B. P.; Kiran, V.; Varade, V.; Naaman, R.; Waldeck, D. H. Spin Selective Charge Transport Through Cysteine Capped Cdse Quantum Dots. *Nano Letters* **2016**, *16*, PMID: 27336320, 4583–4589.

(25) Yang, X.; van der Wal, C. H.; van Wees, B. J. Spin-Dependent Electron Transmission Model for Chiral Molecules in Mesoscopic Devices. *Phys. Rev. B* **2019**, *99*, 024418.

(26) Onsager, L. Reciprocal Relations in Irreversible Processes. I. *Phys. Rev.* **1931**, *37*, 405–426.

(27) Onsager, L. Reciprocal Relations in Irreversible Processes. II. *Phys. Rev.* **1931**, *38*, 2265–2279.

(28) Casimir, H. B. G. On Onsager's Principle of Microscopic Reversibility. *Rev. Mod. Phys.* **1945**, *17*, 343–350.

(29) Mondal, A. K.; Preuss, M. D.; Ślęczkowski, M. L.; Das, T. K.; Vantomme, G.; Meijer, E. W.; Naaman, R. Spin Filtering in Supramolecular Polymers Assembled from Achiral Monomers Mediated by Chiral Solvents. *Journal of the American Chemical Society* **2021**, *143*, PMID: 33926182, 7189–7195.

(30) Hossain, M. A.; Illescas-Lopez, S.; Nair, R.; Cuerva, J. M.; Álvarez de Cienfuegos, L.; Pramanik, S. Transverse magnetoconductance in two-terminal chiral spin-selective devices. *Nanoscale Horiz.* **2023**, *8*, 320–330.

(31) Vita, A. D., *Non-Equilibrium Thermodynamics*; First Edition; Springer: 2022, pp 12, 25–26, 29–32.

(32) Jacquet, P. A. ThermoElectric Transport Properties of a Chain of Quantum Dots with Self-Consistent Reservoirs. *Journal of Statistical Physics* **2009**, *134*, 709–748.

(33) Yang, X.; van der Wal, C. H.; van Wees, B. J. Detecting Chirality in Two-Terminal Electronic Nanodevices. *Nano Letters* **2020**, *20*, PMID: 32672980, 6148–6154.

(34) Huisman, K. H.; Thijssen, J. M. CISS Effect: A Magnetoresistance Through Inelastic Scattering. *The Journal of Physical Chemistry. C, Nanomaterials and Interfaces* **2021**, *125*, 23364–23369.

(35) Huisman, K. H.; Heinisch, J.-B. M.-Y.; Thijssen, J. M. Chirality-Induced Spin Selectivity (CISS) Effect: Magnetocurrent–Voltage Characteristics with Coulomb Interactions I. *The Journal of Physical Chemistry C* **2023**, *127*, 6900–6905.

(36) Naaman, R.; Waldeck, D. H. Comment on "Spin-dependent electron transmission model for chiral molecules in mesoscopic devices". *Phys. Rev. B* **2020**, *101*, 026403.

(37) Yang, X.; van der Wal, C. H.; van Wees, B. J. Reply to "Comment on 'Spin-dependent electron transmission model for chiral molecules in mesoscopic devices"'. *Phys. Rev. B* **2020**, *101*, 026404.

(38) Kumar, A.; Capua, E.; Kesharwani, M. K.; Martin, J. M. L.; Sitbon, E.; Waldeck, D. H.; Naaman, R. Chirality-induced spin polarization places symmetry constraints on biomolecular interactions. *Proceedings of the National Academy of Sciences* **2017**, *114*, 2474–2478.

(39) Meirzada, I.; Sukenik, N.; Haim, G.; Yochelis, S.; Baczewski, L. T.; Paltiel, Y.; Bar-Gill, N. Long-Time-Scale Magnetization Ordering Induced by an Adsorbed Chiral Monolayer on Ferromagnets. *ACS Nano* **2021**, *15*, PMID: 33591720, 5574–5579.

(40) Ben Dor, O.; Yochelis, S.; Radko, A.; Vankayala, K.; Capua, E.; Capua, A.; Yang, S.-H.; Baczewski, L.; Parkin, S. Magnetization Switching in Ferromagnets by Adsorbed Chiral Molecules Without Current or External Magnetic Field. *Nature Communications* **2017**, *8*, 14567.

(41) Alwan, S.; Dubi, Y. Spinterface Origin for the Chirality-Induced Spin-Selectivity Effect. *Journal of the American Chemical Society* **2021**, *143*, PMID: 34460242, 14235–14241.

(42) Dalum, S.; Hedegård, P. Theory of Chiral Induced Spin Selectivity. *Nano Letters* **2019**, *19*, PMID: 31265313, 5253–5259.

(43) Hedegård, P. Chiral-Induced Spin Selectivity in Capacitively Coupled Molecules. *The Journal of Physical Chemistry A* **2022**, *126*, PMID: 35575635, 3157–3166.

(44) Ashcroft, N. W.; Mermin, N. D., *Solid State Physics*; Saunders College Publishing: 1976, pp 673–674.

(45) Stoner, E. C. Collective electron ferromagnetism. *Proceedings of the Royal Society of London. Series A. Mathematical and Physical Sciences* **1938**, *165*, 372–414.

(46) Dianat, A.; Gutierrez, R.; Alpern, H.; Mujica, V.; Ziv, A.; Yochelis, S.; Millo, O.; Paltiel, Y.; Cuniberti, G. Role of Exchange Interactions in the Magnetic Response and Intermolecular Recognition of Chiral Molecules. *Nano Letters* **2020**, *20*, PMID: 32786950, 7077–7086.

(47) Fransson, J. Charge Redistribution and Spin Polarization Driven by Correlation Induced Electron Exchange in Chiral Molecules. *Nano Letters* **2021**, *21*, 3026–3032.

(48) Kiselev, A. A.; Kim, K. W. Prohibition of equilibrium spin currents in multiterminal ballistic devices. *Phys. Rev. B* **2005**, *71*, 153315.

(49) Bardarson, J. H. A proof of the Kramers degeneracy of transmission eigenvalues from antisymmetry of the scattering matrix. *Journal of Physics A: Mathematical and Theoretical* **2008**, *41*, 405203.

(50) Geyer, M.; Gutierrez, R.; Mujica, V.; Cuniberti, G. Chirality-Induced Spin Selectivity in a Coarse-Grained Tight-Binding Model for Helicene. *The Journal of Physical Chemistry C* **2019**, *123*, 27230–27241.

(51) Zöllner, M. S.; Varela, S.; Medina, E.; Mujica, V.; Herrmann, C. Insight Into the Origin of Chiral-Induced Spin Selectivity From a Symmetry Analysis of Electronic Transmission. *Journal of Chemical Theory and Computation* **2020**, *16*, PMID: 32271568, 2914–2929.

(52) Rebergen, M. A Study of Induced Spin Selectivity in Chiral Molecules, MSc thesis, Delft University of Technology, 2018.

(53) Büttiker, M. Symmetry of Electrical Conduction. *IBM Journal of Research and Development* **1988**, *32*, 317–334.

(54) Fransson, J. Vibrational Origin of Exchange Splitting and Chirality Induced Spin Selectivity. *Physical Review B* **2020**, DOI: `10.1103/PhysRevB.102.235416`.

(55) Fransson, J. Chirality-Induced Spin Selectivity: The Role of Electron Correlations. *The Journal of Physical Chemistry Letters* **2019**, *10*, PMID: 31657931, 7126–7132.

(56) Evers, F.; Aharony, A.; Bar-Gill, N.; Entin-Wohlman, O.; Hedegård, P.; Hod, O.; Jelinek, P.; Kamieniarz, G.; Lemeshko, M.; Michaeli, K., et al. Theory of Chirality Induced Spin Selectivity: Progress and Challenges. *Advanced Materials* **2022**, *34*, 2106629.

(57) Das, T. K.; Tassinari, F.; Naaman, R.; Fransson, J. Temperature-Dependent Chiral-Induced Spin Selectivity Effect: Experiments and Theory. *The Journal of Physical Chemistry C* **2022**, *126*, 3257–3264.

(58) Huisman, K. H.; Heinisch, J. B. M. Y.; Thijssen, J. M. CISS effect: Magnetocurrent–voltage characteristics with Coulomb interactions. II. *The Journal of Chemical Physics* **2023**, *158*, 174108, DOI: `10.1063/5.0148748`.

2

BÜTTIKER VOLTAGE PROBES

One of the manifestations of chirality-induced spin selectivity (CISS) is the magnetoresistance in two-terminal transport measurements on molecular junctions. This chapter investigates the effect of spin-orbit coupling in the leads on the polarization of the transmission. A helicene molecule between two gold contacts is studied using a tight binding model. In order to study the occurrence of magnetoresistance, which is prohibited in coherent transport, as a consequence Büttiker reciprocity, we add Büttiker probes to the system in order to incorporate inelastic scattering effects. We show that for a strict two-terminal system without inelastic scattering the magnetoresistance is strictly zero in the linear and nonlinear regimes. We show that for a two-terminal system with inelastic scattering, a nonzero magnetoresistance does appear in the nonlinear regime, reaching values of the order of 0.1%. Our calculations show that for a two-terminal system respecting time-reversal symmetry and charge conservation, a nonzero magnetoresistance can only be obtained through inelastic scattering. However spin-orbit coupling in the leads in combination with inelastic scattering modelled with the Büttiker voltage probe method cannot explain the magnitude of the magnetoresistance measured in experiments.

Part of this chapter has been published in the *Journal of Physical Chemistry C* **2021**, *125*, 42, 23364–23369 [1].

2.1. INTRODUCTION

In two-terminal transport experiments,[2–10] polarizations of the current i.e. magnetoresistances (MRs, see eq. (2.2) for the definition) ranging from 6% to 90% have been measured for self assembled monolayers (SAMs) of chiral molecules. This MR is a manifestation of the connection between chirality of the molecular structure and spin selectivity, commonly denoted as the CISS effect. Theoretical efforts have been geared towards explaining the existence of CISS in transport including quantitative estimates for the MR.

Most theoretical work done on CISS focuses on calculating the spin-polarization of the transmission (SPT, see eq. (2.1)). The spin-orbit coupling of the molecule's constituents is too weak to explain the CISS effect. In ref [11] the molecule helicene was studied and a maximum spin-polarization of the transmission of the order 10^{-5}% was found. When decoherence is taken into account, by adding on-site imaginary terms to the Hamiltonian, a maximum spin-polarization of the transmission of 0.3% was found. As in this approach the particle number is not conserved, the system is no longer strictly two-terminal and it therefore does not explain the MR unless in the experiment electrons are leaking from the device into another reservoir than the source or drain. In two-terminal transport experiments, heavy metals such as gold, platinum and silver are often used. These metals are known to have strong spin-orbit coupling. Previous theoretical work has studied the effect of large spin-orbit coupling in gold leads on the spin-polarization of the transmission[12,13] in density functional theory and tight binding models.[14,15] Spin-polarizations of the transmission reaching values of 1%[12] and 5%[13] were found. Another interesting proposal for obtaining sizeable spin polarization was put forward by Dalum and Hedegård.[16] They noticed that close to degeneracies in the spectrum, the eigenstates of the Hamiltonian rotate away significantly from the unperturbed states, leading to substantial spin polarization. Until recently, most theoretical work that tried to explain the CISS effect, focused on calculating the spin-polarization of the transmission but it has now been realized that spin-polarization of the transmission does not necessarily lead to the occurrence of a MR.

Two fundamental reciprocity theorems are very important when considering the nonzero MR measured in experiments and putting it in a theoretical perspective. The first is the Onsager-Casimir reciprocity[17,18] which implies that for a two-terminal interacting system the MR can only be nonzero in the nonlinear regime. The second is the Büttiker reciprocity theorem.[19] This theorem, that is based on time-reversal symmetry and unitarity of the S-matrix, prohibits MR to occur for two-terminal non-interacting systems irrespective of the regime (linear/nonlinear, see sec. 2.2.2), even when the spin-polarization of the transmission is nonzero. In order to obtain a nonzero MR, interactions must be included. In refs [20] and [21] the effects of the Coulomb interactions and a coupling to vibrational modes were studied respectively and a nonzero MR was found.

Nonzero MR can be obtained by breaking charge conservation but in the experiment the leakage currents are often too small to justify this as a cause of a MR. In this chapter we focus on another option: electrons that scatter inelastically while conserving their number during the process. We construct a tight binding model for a junction in which helicene is coupled to 2 gold electrodes which have strong spin-orbit coupling. Büttiker probes are added in order to model inelastic scattering while maintaining charge conservation. We denote the system with Büttiker probes as an interacting system and the system without Büttiker probes as a non-interacting system. Tight binding has the advantage over a quantum-chemical calculation that inelastic effects can easily be included through Büttiker probes. Also, it is easy to study the effect of changing couplings and interaction parameters.

We first validate our model by calculating the spin-polarization of the transmission and comparing this to density functional theory results.[12,13] The first goal is to verify the occurrence of a MR and to investigate its magnitude when Büttiker probes are active. The second goal is to address the characteristics features of the MR and compare it with the characteristics found in experiment.

In section 2.2.1 the spin-polarization of the transmission is defined. In section 2.2.2 the MR is defined and it is explained what restrictions are imposed on the MR by Büttiker and Onsager-Casimir reciprocity together with the implications for experimental observables. In sec. 2.2.3 a description of the non-interacting system is given. In sec. 2.2.4 the Büttiker probes and their parameters are described. The results for the non-interacting and interacting system are given in section 2.3.1 and 2.3.2 respectively. In section 2.4 we present conclusions.

2.2. COMPUTATIONAL DETAILS

2.2.1. THEORY: SPIN-POLARIZATION OF THE TRANSMISSION

The spin-polarization of the transmission from the right to the left lead is defined as:

$$P_z(E) = \frac{T_{\mathrm{RL}}^{\uparrow\uparrow} + T_{\mathrm{RL}}^{\downarrow\uparrow} - T_{\mathrm{RL}}^{\uparrow\downarrow} - T_{\mathrm{RL}}^{\downarrow\downarrow}}{T_{\mathrm{RL}}}. \tag{2.1}$$

Here $T_{\mathrm{RL}}^{\mathrm{ss}'}$ is the energy-dependent transmission probability for an electron in the right lead with spin $\mathrm{s} = \uparrow, \downarrow$ (quantised in the z -direction, which we take as the direction of the transmission) to be transmitted to the left lead with spin $\mathrm{s}' = \uparrow, \downarrow$ and $T_{\mathrm{RL}} = \sum_{\mathrm{s},\mathrm{s}' \in \{\uparrow,\downarrow\}} T_{\mathrm{RL}}^{\mathrm{ss}'}$, with T_{RL} the total transmission probability from right to left. In the non-equilibrium Green's function (NEGF) formalism, the transmission function is given by the Meir-Wingreen formula $T_{\mathrm{RL}}(E) = \mathrm{Tr}[\mathbf{G}(E)\mathbf{\Gamma}_{\mathrm{R}}\mathbf{G}(E)^{\dagger}\mathbf{\Gamma}_{\mathrm{L}}(E)]$, with $\Gamma_{\mathrm{L,R}}(E)$ the imaginary part of the self-energy of the left and right lead respectively and $\mathbf{G}(E)$ the retarded Green's function which is given by $\mathbf{G}(E) = (E\mathbf{1} - \mathbf{H} - \Lambda_{\mathrm{L}} - \Lambda_{\mathrm{R}} + \frac{i}{2}\Gamma_{\mathrm{L}} + \frac{i}{2}\Gamma_{\mathrm{R}})^{-1}$. Here $\mathbf{1}$ is the unit-matrix, $\mathbf{H}$ is the Hamiltonian of the scattering region in figure 2.1 and $\Lambda_{\mathrm{L,R}}$ the real part of the self energy of the left, right lead respectively. Below, we drop the explicit dependence of the transmission on energy E.

2.2.2. MAGNETORESISTANCE AND THE RECIPROCITY THEOREMS

We define the MR as the normalized difference of the currents for the up and down magnetization $m, -m$ of the lead:

$$MR = \frac{I(m) - I(-m)}{I(m) + I(-m)}. \tag{2.2}$$

For a two-terminal system which respects current conservation, the net current into the left lead is calculated with:

$$I(m,V) = \frac{e}{h}\int_{-\infty}^{\infty} T_{\mathrm{RL}}(m)\Big(f_{\mathrm{L}}(E) - f_{\mathrm{R}}(E)\Big)dE, \tag{2.3}$$

where $f_{\mathrm{L}}(E), f_{\mathrm{R}}(E)$ are the Fermi-Dirac distributions of the left and right lead respectively and m is the magnetization of the left lead. The chemical potentials for spin up and down electrons in the left/right lead are equal i.e. $\mu_i^{\uparrow} = \mu_i^{\downarrow}$ for i = L, R. Assuming symmetric capacitive coupling to the left and right lead, the chemical potentials of the left and right leads are $E_{\mathrm{F}} + \frac{V}{2}$ and $E_{\mathrm{F}} - \frac{V}{2}$ respectively with E_{F} the Fermi energy and V the bias voltage. The current can be expanded in the bias voltage:

$$I(m,V) = G_1(m)V + G_2(m)V^2 + G_3(m)V^3 + \dots \tag{2.4}$$

We define $\Delta I(m,V)$ as the difference between the currents for positive and negative magnetization. Using eq. (2.4) we can write $\Delta I(m,V)$ as:

$$\begin{aligned}\Delta I(m,V) &\equiv I(m,V) - I(-m,V)\\ &= \Big[G_1(m) - G_1(-m)\Big]V + \Big[G_2(m) - G_2(-m)\Big]V^2 + \Big[G_3(m) - G_3(-m)\Big]V^3 + \dots\end{aligned} \tag{2.5}$$

We define the odd and even part of $\Delta I(m,V)$ as:

$$A(m,V) = \frac{1}{2}\Big[\Delta I(m,V) - \Delta I(m,-V)\Big] = \Big[G_1(m) - G_1(-m)\Big]V + \Big[G_3(m) - G_3(-m)\Big]V^3 + \dots, \tag{2.6}$$

$$B(m,V) = \frac{1}{2}\Big[\Delta I(m,V) + \Delta I(m,-V)\Big] = \Big[G_2(m) - G_2(-m)\Big]V^2 + \Big[G_4(m) - G_4(-m)\Big]V^4 + \dots, \tag{2.7}$$

respectively.

In ref. [19] it was shown that for a two-terminal system time-reversal symmetry and unitarity of the S-matrix (which expresses charge conservation) imply that $T_{\mathrm{RL}}(m) = T_{\mathrm{RL}}(-m)$. This relation is known as the Büttiker reciprocity theorem for two-terminal systems. Combining this relation with eq. (2.3) it trivially follows that: $I(m,V) = I(-m,V)$. Combining this with eq. (2.5), we obtain:

$$\Delta I(m,V) = \Big[G_1(m) - G_1(-m)\Big]V + \Big[G_2(m) - G_2(-m)\Big]V^2 + \Big[G_3(m) - G_3(-m)\Big]V^3 + \dots = 0. \tag{2.8}$$

From this it follows that: $G_n(m) = G_n(-m)$ for $n = 1, 2, ..$ if Büttiker reciprocity holds. Time-reversal symmetry and unitarity of the S-matrix prohibit a finite $\Delta I(m,V)$ in the linear and nonlinear regime for a two-terminal system without interactions.

On the other hand Onsager-Casimir reciprocity holds for systems with interactions. Onsager-Casimir reciprocity implies that $I(m,V) = I(-m,V)$ in the linear regime: $G_1(m) =$

$G_1(-m)$,[17,18] i.e. the linear coefficient is an even function of the magnetization. This means that the differential conductance evaluated at $V=0$ is identical for opposite magnetizations:

$$G_1(m) \equiv \frac{dI(m,V=0)}{dV} = \frac{dI(-m,V=0)}{dV} = G_1(-m). \tag{2.9}$$

For the non linear-coefficients: $G_2(m), G_3(m), \ldots$ in principle we can have: $G_n(m) \neq G_n(-m)$[22–24] for $n \geq 2$. In ref. [24] it was shown that electron interactions allow for a second order contribution (odd in m) $\alpha m V^2$ to the current from which clearly $G_2(m) \neq G_2(-m)$. Another example of this is the electrical magnetochiraleffect[25] which gives (for small bias voltages) a second order contribution to the current[15] $G_2(m) = G^0(\chi) m$ (with $G^0(\chi)$ a coefficient which depends on the chirality χ) for which also $G_2(m) \neq G_2(-m)$. In ref. [26] a rigorous analysis based on full counting statistics derived relations between the coefficients $G_n(m), G_n(-m)$ under microscopic reversibility. As expected the Onsager-Casimir relation $G_1(m) = G_1(-m)$ was found. From this work it can also be concluded that microscopic reversibility does not imply that the nonlinear coefficients for opposite magnetizations are equal: $G_n(m) \neq G_n(-m)$ for $n \geq 2$.

We now expand the MR (eq (2.2)) in the bias voltage for an interacting system. Defining $\Delta G_n(m) \equiv G_n(m) - G_n(-m)$ and $\overline{G}_n(m) \equiv G_n(m) + G_n(-m)$. We can write the MR as:

$$MR = \frac{\Delta G_1(m) V + \Delta G_2(m) V^2 + \ldots}{\overline{G}_1(m) V + \overline{G}_2(m) V^2 + \ldots}. \tag{2.10}$$

Onsager-Casimir reciprocity implies $\Delta G_1(m) = 0$, so that eq. (2.10) simplifies to: $MR = \frac{\Delta G_2(m) V + \ldots}{\overline{G}_1(m) + \overline{G}_2(m) V + \ldots}$, showing that the MR vanishes at zero bias. Remarkably in ref. [2] a nonzero MR was found at zero bias which seems in contradiction with the Onsager-Casimir reciprocity.

The analysis in this section and refs [22–24, 26] imply that interactions play a crucial role in obtaining a MR.

2.2.3. TIGHT BINDING HAMILTONIAN

Our Slater-Koster Tight Binding model addresses four parts of a transport junction i) semi-infinite gold leads without spin-orbit coupling ii) a block of 3 × 3 × 3 gold atoms with spin-orbit coupling, iii) a sulfur anchoring group and iv) a helicene molecule. A schematic picture of the scattering region is shown in figure 2.1. The outer 3 × 3 layers of gold atoms on the left and right side each have a semi-infinite gold lead without spin-orbit coupling attached to it see figure 2.1.

For parts i) and ii) the Slater-Koster tight binding parametrization of ref. [27] will be used; for a detailed description see section 2.5.1 of the Appendix. The tight binding parameters reported in ref. [28] are used for the anchoring group. For a detailed description of part iii) see Appendix section 2.5.1. We use the full Slater-Koster tight binding model of helicene reported in ref. [11] and the Slater-Koster tight binding parameters are given in the Appendix 2.5.1. Only the 2p,2s orbitals of carbon atoms are considered. A [n]helicene molecule consist of a chain of n benzene rings. Helicene

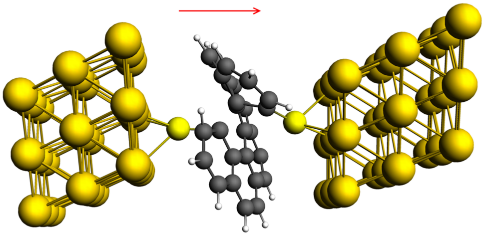

Figure 2.1: Reprinted with permission from [13]. Copyright 2018, M.P. Rebergen. Schematic picture of the scattering region. The gold spheres are gold atoms, the bright yellow spheres are sulfur atoms and the grey spheres in the middle are carbon atoms. To this scattering region semi-infinite gold lead are attached.

has two enantiomeric states: P and M related by mirror symmetry. The numerical calculations were performed using the Kwant code [29]. For details regarding the implementation in Kwant see section 2.5.1 of the Appendix. Our Python code is available on `https://github.com/khhuisman/CISS_effect`.

2.2.4. BÜTTIKER PROBES

In order to model interactions, we use Büttiker probes; virtual leads that are attached to each site of the molecule. Büttiker probes can act as a "dephasing probe" or a "voltage probe" to model elastic and inelastic processes respectively.[30,31] In ref. [32] it was shown that for an Aharonov-Bohm junction a dephasing probe does not lead to a finite MR in the linear, nor in the nonlinear regime, but a voltage probe does lead to a nonzero MR in the nonlinear regime, confirming the findings of ref [23]. Therefore in our model we use voltage probes. The Büttiker probe acts as a voltage probe if the total *charge* current into the probe is zero. The chemical potential of the probe is determined in a self-consistent manner such that the total charge current into the probe is zero. However, there is a finite net *energy* current going into each virtual lead which represents energy being dissipated into an external environment (the Büttiker probe), while respecting charge conservation (in contrast to refs [11, 15] where the addition of on-site imaginary terms leads to loss of particles). The Hamiltonian of a virtual lead is modeled as a semi-infinite linear chain (see Appendix section 2.5.1).

We define a probe to be a collection of virtual leads. For the [6]helicene molecule we have 26 carbon atoms to which we can attach a virtual lead. One probe containing several leads, with one and the same chemical potential, can be attached to several sites. Alternatively a virtual lead, characterised by a single chemical potential, can be connected to more than one carbon atoms.

The hopping parameter within the lead is t_0 and t_{leak} is the coupling between the lead and the carbon atom. In order to cover a wide range of energies, we choose t_0 to be large compared to the Slater-Koster tight binding hopping parameters of carbon (see Appendix section 2.5.1), hence we take $t_0 = 50$ eV. We distinguish three regimes: $t_{\text{leak}} > t_0$, $t_{\text{leak}} = t_0$ and $t_{\text{leak}} < t_0$.

We varied the attachment position of the probe(s), the amount of leads in a single probe, the coupling between the probe and the molecule: t_{leak} and the amount of independent probes consisting of one lead. In Appendix section 2.5.4 we prove that a voltage probe always satisfies the Onsager-Casimir reciprocity: $G_1(m) = G_1(-m)$.

2.3. RESULTS

2.3.1. TWO-TERMINAL JUNCTION, NON-INTERACTING

In fig. 2.2a the spin-polarization of the transmission (see eq. (2.1)) for [6]P,M- helicene is shown for an unmagnetized lead and we find a maximum absolute value of the spin-polarization of the transmission of 2%, which is comparable with the density functional theory studies[12,13] (see Appendix section 2.5.1 for the result of the ref [13]). In fig. 2.2a we also see that the spin-polarization of the transmission is exactly opposite in sign for [6]P,M- helicene as expected (see Appendix section 2.5.2). In figure 2.2b the spin-polarization of the transmission for [12]P-helicene and [6]P-helicene for an unmagnetized lead are plotted. The spin-polarization of the transmission is seen to increase with the length of the molecule as was found in ref [12]. Dalum and Hedegård[16] find an increased spin-polarization of the transmission at degeneracies of the molecular spectrum. The frontier levels do not show degeneracies beyond the usual Kramer's degeneracy. Moreover the spin-orbit coupling of the gold supersedes the effect highlighted by these authors.

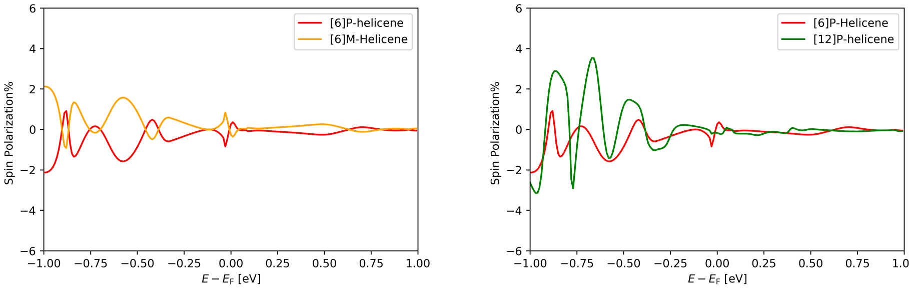

(a)

(b)

Figure 2.2: **(a)** Spin-polarization for the gold-sulfur - [6] P and M helicene unmagnetized junction as a function of energy in red, orange respectively. E_F is the Fermi energy of gold in electronvolt (eV). **(b)** Spin-polarization for [6, 12]P-helicene in the unmagnetized junction as a function of energy. E_F is the Fermi energy of gold in electronvolt (eV). The figure shows an increase in spin-polarization when the length of the molecule is increased.

We now turn to a system with a magnetized lead. In figure 2.3a the transmissions $T_{RL}(m), T_{RL}(-m)$ are plotted in blue, red respectively as a function of energy. We see that for every energy these transmissions are equal: $T_{RL}(m) = T_{RL}(-m)$, confirming that Büttiker reciprocity holds for our two-terminal system. The currents $I(m), I(-m)$ are plotted in figure 2.3b in blue and in red respectively as a function of bias voltage V and are calculated using eq. (2.3) for a Fermi energy of gold $E_F = -5.3$ eV at $T = 0$ K. They are obviously identical, confirming that the MR for this non-interacting system is zero in the linear and nonlinear regime, even though there is a nonzero spin-polarization of the transmission in the bias window $[E_F - \frac{V}{2}, E_F + \frac{V}{2}]$ for the magnetized system (not plotted).

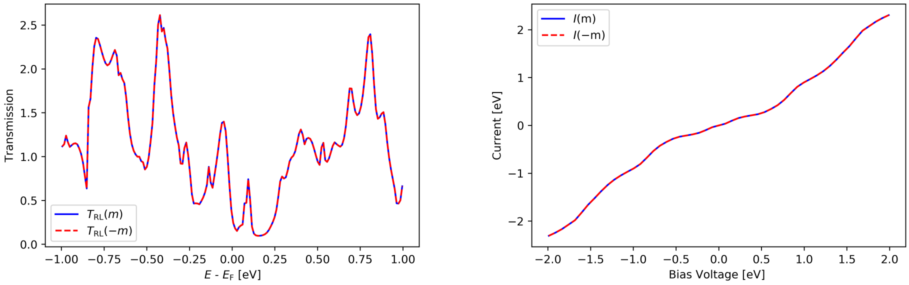

(a) (b)

Figure 2.3: **(a)** Transmission from right to left for $E_F = -5.3$ eV, and the magnetizations $m = \pm 2.1$ of the left lead. The difference between $T_{RL}(m)$ and $T_{RL}(-m)$ is zero. **(b)** The charge current $I(m)$ in eV into the left lead for the magnetizations $\pm m$ increases and shows no difference between $I(m), I(-m)$.

2.3.2. TWO-TERMINAL JUNCTION, INELASTIC SCATTERING

Varying the attachment position, the order of magnitude of the MR varies between of 10^{-2}% and 10^{-1}%. In fig. 2.4a the MR is plotted for [6]M,P- helicene. We see that its sign changes between the enantiomers of the molecule, as was found in experiments.[3,5,9,10] In fig. 2.4a there is a MR around zero bias (except at $V = 0$ there MR = 0 as expected see sec. 2.2.2), which is allowed by Onsager-Casimir because the MR only arises in the nonzero difference between higher order contributions (ΔG_n for $n \geq 2$) to $\Delta I(m, V)$ see eq. (2.10).

In figure 2.4b we show the odd and even parts of $\Delta I(m, V)$ in red and in blue, see eqs. (2.6) and (2.7). The fact that the voltage probe satisfies Onsager-Casimir reciprocity (see Appendix 2.5.4) ensures that there are no contributions to $\Delta I(m, V)$ which are linear in V. This means that the odd part in figure 2.4b must be nonlinear in nature. The even part of the $\Delta I(m, V)$ in figure 2.4b can only scale with $V^2, V^4, \ldots$ which by definition is nonlinear. In figure 2.4b we see the even contribution to $\Delta I(m, V)$ dominates. Experimental results on CISS imply that $\Delta I(m, V)$ has an odd part which is larger than the even contribution.[2,5–10]

One might expect that adding more independent probes leads to more inelastic scattering and therefore a larger MR, however this turns out not to be the case. We calculated the MR for up to and including 4 independent probes and found that the MR did not increase with the number of independent probes. The order of magnitude of the largest MR stayed below 0.1%. We also varied the amount of leads in one independent probe. For this case the amount of probes did not change the order of magnitude of the MR.

We found that the MR primarily depends on the spin-orbit coupling of the gold whereas the effect of the spin-orbit coupling from the carbon atoms on the MR is negligible, and it vanishes when the spin-orbit coupling is switched off altogether. So far, the potential across the molecule has been kept constant. If we apply a linear drop to the on-site potential along the helix axis of the molecule, the maximum MR remains of the same order of 0.1%.

Fransson[20] has studied a model capturing the coupling between the electrons and the vibrational modes. He obtained a significant MR only when including a coupling to the spin-orbit hopping term in the Hamiltonian. This term has a rather specific form and our generic Büttiker probes may fail to represent this. Fransson finds that the MR scales with the coupling between electrons and vibrational modes. In contrast, the Büttiker probe method used here, gives a MR which quickly saturates to a (rather low) MR value when increasing the coupling parameter t_{leak}. Further research into the specific form of the self-energy and the construction of an appropriate Büttiker probe seems useful. The question remains why substantial MR is found in experiments. Maybe this is a consequence of interactions like the ones we study in this chapter, but it can also be that in the experiments on SAMs, part of the current is leaking into reservoirs other than the two terminals of the voltage source.

It could be that SAMs of chiral molecules allow for molecule-molecule or molecule-substrate interactions. These interactions might manifest themselves as a magnetization of the substrate as was measured in ref [33]. How this magnetization effects the currents in two-terminal junctions is unclear. Whether CISS is a single molecule property or rather a property of SAMs remains an open question. More experiments on single-molecule (rather than SAMs), two-terminal junctions are highly desirable.

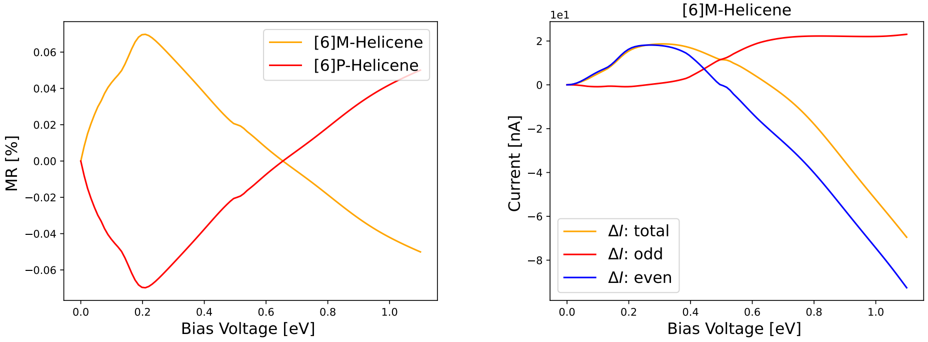

(a)

(b)

Figure 2.4: **(a)** The MR in percentage for the gold- sulfur-[6] P and M helicene junction with 1 probe consisting of 1 lead attached, as a function of bias voltage in red and orange respectively. The MR changes sign between the enantiomers of the molecule. **(b)** The even and odd part in V of $\Delta I(m,V)$ in blue and red respectively as a function of bias voltage.

2.4. Conclusion

We have constructed a tight binding model that includes spin-orbit coupling in the gold leads and found a spin-polarization of the transmission comparable to that found in density functional theory studies on a similar system.[12,13] Furthermore the spin-polarization of the transmission changes sign between the enantiomers of the molecule and increases with the length of the molecule. In line with the Büttiker reciprocity theorem, we find that the MR vanishes in the linear and nonlinear regime in the non-interacting system even though the spin polarized transmission is finite.

Adding Büttiker probes yields a magnetoresistance beyond the linear regime. The spin-orbit coupling in the leads in combination with inelastic scattering modeled through local Büttiker probes gives a nonzero MR of the order 0.1%, which is 1-2 orders of magnitude smaller than the MR found in the experiments.[2–10] The MR only arises in the nonzero difference between higher order contributions ($\Delta G_n \neq 0$ for $n \geq 2$), satisfying Onsager-Casimir reciprocity. Furthermore we find that the MR changes sign between the enantiomers of the molecule as was found in refs [3, 5, 9, 10] and contrary to experiment $\Delta I(m, V)$ has an even contribution in bias voltage which is larger than the odd contribution.

2.5. APPENDIX

2.5.1. TIGHT BINDING MODEL

GOLD LEADS

For the block of 3 × 3 × 3 gold atoms with spin-orbit coupling and the semi-infinite gold leads the SKTB parametrization of ref [27] is used. It considers the 5d, 6s, 6p orbitals of gold; the atomic spin-orbit coupling has a dominant contribution from the 5d-orbitals. The onsite Hamiltonian (without spin) is:

$$\mathbf{H}_{\mathrm{onsite,gold}} = \mathrm{diag}(\epsilon_\mathrm{s}, \epsilon_\mathrm{p}, \epsilon_\mathrm{p}, \epsilon_\mathrm{p}, \epsilon_\mathrm{xy}, \epsilon_{\mathrm{x}^2-\mathrm{y}^2}, \epsilon_\mathrm{xz}, \epsilon_\mathrm{yz}, \epsilon_{\mathrm{z}^2}). \tag{2.11}$$

Here is ϵ_i is the energy of orbital i, the values are listed in table 2.1. The Slater-Koster parameters for nearest-neighbour (NN) and next-NN (NNN) hopping are displayed in table 2.2.

In the cubic harmonic basis: d_xy,$\mathrm{d}_{\mathrm{x}^2-\mathrm{y}^2}$,$\mathrm{d}_\mathrm{xz}$,$\mathrm{d}_\mathrm{yz}$,$\mathrm{d}_{\mathrm{z}^2}$ basis, the spin-orbit coupling Hamiltonian becomes with $\mathbf{s}_\mathrm{i} = \frac{1}{2}\sigma_\mathrm{i}$ ($\hbar = 1$) and i = x, y, z:

$$\mathbf{H}_{\mathrm{SOC}} = \xi_{5\mathrm{d}}\mathbf{L}\cdot\mathbf{S} = \xi_{5\mathrm{d}} \begin{pmatrix} 0 & 2i\mathbf{s}_\mathrm{z} & -i\mathbf{s}_\mathrm{x} & i\mathbf{s}_\mathrm{y} & 0 \\ -2i\mathbf{s}_\mathrm{z} & 0 & i\mathbf{s}_\mathrm{y} & i\mathbf{s}_\mathrm{x} & 0 \\ i\mathbf{s}_\mathrm{x} & -i\mathbf{s}_\mathrm{y} & 0 & -i\mathbf{s}_\mathrm{z} & i\sqrt{3}\mathbf{s}_\mathrm{y} \\ -i\mathbf{s}_\mathrm{y} & -i\mathbf{s}_\mathrm{x} & i\mathbf{s}_\mathrm{z} & 0 & -i\sqrt{3}\mathbf{s}_\mathrm{x} \\ 0 & 0 & -i\sqrt{3}\mathbf{s}_\mathrm{y} & i\sqrt{3}\mathbf{s}_\mathrm{x} & 0 \end{pmatrix}. \tag{2.12}$$

Here $\xi_{5\mathrm{d}}$ is the spin-orbit coupling parameter. which takes on the value 0.3 – 0.4 eV.[27,34] We take $\xi_{5\mathrm{d}} = 0.3$ eV. The 6s orbitals do not have an atomic SOC and the 6p orbitals do not have a significant atomic SOC respectively.

In experiment the gold substrate usually is placed on a nickel, a metal with negligible SOC, therefore the semi-infinite gold lead has the atomic SOC turned “off” i.e. $\xi_{5d} = 0$ only the 3 × 3 × 3 block of gold atoms have the atomic SOC turned “on” i.e. $\xi_{5\mathrm{d}} = 0.3$ eV. In order to calculate the MR we need to magnetize the left lead. We take a magnetization of the left lead m, pointing in the z-direction. This leads to the Hamiltonian:

$$\mathbf{H}^{\mathrm{mag}}_{\mathrm{lead,L}} = \sum_{\mathrm{i}\in\mathrm{L},\mu} c^\dagger_{\mathrm{i},\mu} c_{\mathrm{i},\mu} m\sigma_\mathrm{z}, \tag{2.13}$$

Onsite energy	Rydberg
ϵ_s	0.56220
ϵ_p	1.27897
ϵ_{d1}	0.26097
ϵ_{d2}	0.25309

Table 2.1: The onsite energies of the 6s, 6p and 5d orbitals of gold taken from table 6.62 of ref [27] in Rydberg. Here d1 refers to the d_{xy}, d_{xz}, d_{yz} orbitals and d2 to the $d_{x^2\text{-}y^2}$, d_{z^2} orbitals and p to the p_x, p_y, p_z orbitals.

Slater-Koster parameters	Nearest Neigbour (NN)	Next-NN
$V_{ss\sigma}$	-0.0668	0.00277
$V_{pp\sigma}$	0.17866	0.03707
$V_{pp\pi}$	-0.01645	-0.01025
$V_{dd\sigma}$	-0.04971	-0.00305
$V_{dd\pi}$	0.02624	0.0024
$V_{dd\delta}$	-0.00457	-0.00057
$V_{sp\sigma}$	0.09721	0.00261
$V_{sd\sigma}$	-0.04722	-0.00784
$V_{pd\pi}$	0.01896	-0.00762
$V_{pd\sigma}$	-0.06399	0.0047

Table 2.2: The nearest neighbour and next-nearest neighbour Slater-Koster parameters of gold in the orthogonal basis taken from table 6.62 of ref [27] in Rydberg.

which is added to the onsite Hamiltonian of the left semi-infinite gold lead eq. (2.11). Here m is the magnetization in eV, $c^{\dagger}_{i,\mu}$ & $c_{i,\mu}$ are the fermionic creation and annihilation operators respectively, i labels the sites of the left lead, μ labels the 6p, 6s, 5d orbitals (9 orbitals total), σ_z is the Pauli z-matrix.

HELICENE MODEL

We use the full SKTB model of helicene reported in ref [11], sec. 1.1 and the parameters given in table 2.3. Only the 2p and 2s orbitals of carbon atoms are considered in this model. A [n]helicene molecule consist of a chain of n benzene rings. Helicene has two enantiomeric states: P and M. For P-helicene the helix turns clockwise and for M-helicene the helix turns counter-clockwise along the helix axis.

ANCHORING GROUP

Carbon and gold do not form a bond very easily and therefore an anchoring group is used to attach the molecule to the leads. The anchoring group consists of a sulfur atom which forms bonds well with a carbon atom of helicene and with gold atoms on the surface. A DFT study was performed to see which orbitals of sulfur and gold and sulfur and carbon contributed most to the electron hopping. Detailed quantum chemical calculations, carried out with the code ADF from SCM[35] show that the 3p orbitals of the sulfur atom and the 6s & 5d orbitals of gold atom, the 2p orbitals of carbon atom respectively are key in the hopping process[28] forming a a hollow configuration. The DFT study showed an

Slater-Koster parameters	eV
$V_{\mathrm{ss}\sigma}$	-7.92
$V_{\mathrm{sp}\sigma}$	8.08
$V_{\mathrm{pp}\sigma}$	7.09
$V_{\mathrm{pp}\pi}$	-3.44
Onsite energies	eV
ϵ_{s}	-18
$\epsilon_{\mathrm{pp}\sigma}$	-18
$\epsilon_{\mathrm{pp}\pi}$	-10.5
Spin - Orbit Coupling	eV
ξ_{p}	6×10^{-3}
Geometric Parameters	Å
a_0	1.4
b_0	3.6

Table 2.3: The Slater-Koster parameters of carbon, onsite energies, SOC parameter and geometric parameters taken from table 1 of [11] in eV and in Ångström. We also take $||\boldsymbol{E}=0||$ for the electric field $\boldsymbol{E}$.

onsite energy of sulfur of $E_{\mathrm{S}} = -6.21$ eV and the hopping matrix elements are listed in table 2.4 and 2.5 in eV.

VIRTUAL LEADS

The Hamiltonian of a virtual lead (Büttiker probe) is given by:

$$\mathbf{H}_{\text{virt. lead}} = \sum_{\mathrm{i}=0,\mu}^{\mathrm{i}=\infty} u_0 \, d^{\dagger}_{\mathrm{i},\mu} d_{\mathrm{i},\mu} \hat{\mathbb{1}}_{\mathrm{s}} + t_0 \, d^{\dagger}_{\mathrm{i},\mu} d_{\mathrm{i}+1,\mu} \hat{\mathbb{1}}_{\mathrm{s}} + \mathrm{h.c.}, \tag{2.14}$$

$$\mathbf{H}_{\text{coup.}} = t_{\text{leak}} \sum_{\mu} d^{\dagger}_{0,\mu} a_{\mathrm{x},\mu} + a^{\dagger}_{\mathrm{x},\mu} d_{0,\mu}. \tag{2.15}$$

Here u_0 is the onsite energy, t_0 the hopping parameter, $d^{\dagger}_{\mathrm{i},\mu}, d_{\mathrm{i},\mu}$ are the fermionic creation and annihilation operators, i labels the sites of the virtual lead, μ labels the orbitals (4 orbitals total) and $\hat{\mathbb{1}}_{\mathrm{s}}$ is the 2×2 identity matrix. The coupling between the first site of the virtual lead and the carbon atom is described by eq. (2.15), here $a_{\mathrm{x},\mu}$ is the annihilation operator of an electron on site x in orbital μ of helicene and t_{leak} is the coupling strength . In principle every carbon atom of helicene has a semi-infinite lead described by eqs. (2.14), (2.15) to it. The current going into each virtual lead is calculated with formulas described in section 2.5.5. We use the Newton - Raphson method to determine $\mu_{\mathrm{B}}(m)$ such that $I_{\mathrm{B}}(m) = 0$ the convergence criterion is that $|I_{\mathrm{B}}(m)| \leq 10^{-13}$.

Au_1 - S	$3p_x$	$3p_z$	$3p_z$
6s	1.31	-2.20	3.471
$5d_{xy}$	0.557	0.376	-1.14
$5d_{x^2-y^2}$	-0.92	-0.431	-0.809
$5d_{xz}$	-0.508	-0.987	0.701
$5d_{yz}$	-1.04	0.852	-1.32
$5d_{z^2}$	0.622	-1.158	-0.681

Au_2 - S	$3p_x$	$3p_z$	$3p_z$
6s	1.33	2.22	3.50
$5d_{xy}$	-0.555	0.367	1.16
$5d_{x^2-y^2}$	-0.933	0.458	-0.796
$5d_{xz}$	-0.513	1.02	0.73
$5d_{yz}$	1.07	0.836	1.35
$5d_{z^2}$	0.654	1.20	-0.674

Au_3 - S	$3p_x$	$3p_z$	$3p_z$
6s	-2.323	0.004	3.191
$5d_{xy}$	-0.004	1.083	0.01
$5d_{x^2-y^2}$	-0.191	-0.007	1.279
$5d_{xz}$	1.302	0.004	-1.166
$5d_{yz}$	0.008	-0.825	-0.003
$5d_{z^2}$	-0.921	-0.003	-0.712

Table 2.4: Hopping matrix elements between the 6s,5d orbitals of gold and 3p orbitals of sulfur in eV for gold atoms 1,2,3.

C - S	$3p_x$	$3p_z$	$3p_z$
2s	-3.3	-0.323	7.863
$2p_x$	-2.1	0.21	-2.851
$2p_x$	0.208	-3.822	-0.266
$2p_z$	-3.031	-0.288	3.294

Table 2.5: Hopping matrix elements between the 2p,2s orbitals of carbon and 3p orbitals of sulfur in eV.

IMPLEMENTATION IN KWANT

For the TB calculation a crucial detail for the implementation in Kwant is explained here. The Kwant package comes with a file called **leads.py**. In that file the function *modes* is defined:

```
def modes(h_cell, h_hop, tol = 1e6, stabilization = None,
          *, particle_hole = None,time_reversal = None,
          chiral=None, projectors = None).
```

We changed the variable *stabilization* from the default *None* to (False,False). Alternatively we can change it to (True,False), (False, True) or (True,True), we found that it did not matter for our calculation. By changing *stabilization* in this way the internal algorithms Kwant uses are changed such that it accurately calculates the transmission. When one does not change *stabilization* this will result in a transmission that will diverge to unrealistic values for some energies.

SPIN POLARIZATION DFT STUDY

Figure 2.5 shows the transmission for spin up and spin down electrons: $G^{\uparrow}$ and $G^{\downarrow}$ of ref. [13]. Here a DFT study for a 2T noninteracting system such as the one studied in this paper was done making use of the wide-band limit. Figure 2.5 show a SPT (defined here as $\frac{G_{\uparrow}-G_{\downarrow}}{G_{\uparrow}+G_{\downarrow}}$) of the order 1%, similar to the SPT found in this paper.

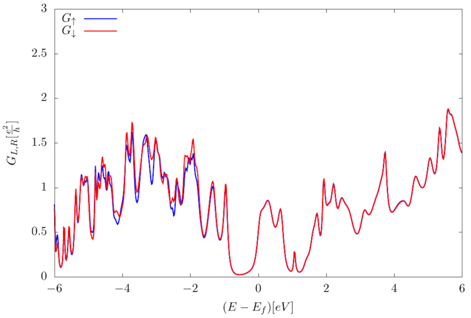

Figure 2.5: Reprinted with permission from [13]. Copyright 2018, M.P. Rebergen. The transmission for spin up and spin down electrons: $G^{\uparrow}$ and $G^{\downarrow}$ respectively as a function of energy E of the DFT study of ref [13]. E_f is the Fermi energy of gold.

2.5.2. SIGN CHANGE OF SPIN-POLARIZATION OF TRANSMISSION

Helicene with helical axis pointing in the z-direction has two enantiomeric states that can be interconverted by applying the mirror operation: $\mathscr{M}_{\mathrm{y}} : \mathrm{y} \rightarrow -\mathrm{y}$. In ref [36] the effects of rotation operations by π $\mathscr{C}_2$ around a longitudinal,transverse and planar axis (l, t, p respectively) and mirror operations $\mathscr{M}$ in a longitudinal,transverse plane on the transmission for a 2T junction were studied. For our tight binding model (see fig. 2.6) we identify l, t, p = z, y, x, thus the mirror operation y → −y corresponds to the mirror operation $\mathscr{M}_{\mathrm{l}}$. In sec. 2.5.3 the effect of $\mathscr{M}_{\mathrm{y}}$ on the Hamiltonian is explained.

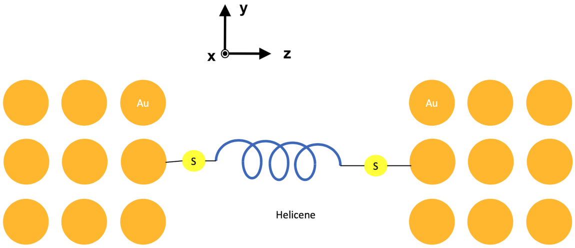

Figure 2.6: Schematic picture of the tight binding model. The helix axis of helicene lies along the z-axis.

For $\mathscr{M}_\mathrm{l}$ we have the relations from figure 3 of ref [36]:

$$T_\mathrm{RL}^{\sigma_\mathrm{s}\sigma'_\mathrm{s}} \rightarrow T_\mathrm{RL}^{\overline{\sigma_\mathrm{s}\sigma_\mathrm{s}}'} \text{ for spin in the s = z,x direction,} \tag{2.16}$$

$$T_\mathrm{RL}^{\sigma_\mathrm{s}\sigma'_\mathrm{s}} \rightarrow T_\mathrm{RL}^{\sigma_\mathrm{s}\sigma'_\mathrm{s}} \text{ for spin in the s = y direction.} \tag{2.17}$$

Where σ_s is the spin quantized along s axis and $\overline{\sigma_\mathrm{s}}$ indicates that the spin σ_s is flipped. For the spin-polarization P_z in the z-direction

$$P_\mathrm{z} = \frac{T_\mathrm{RL}^{\uparrow\uparrow} + T_\mathrm{RL}^{\downarrow\uparrow} - T_\mathrm{RL}^{\uparrow\downarrow} - T_\mathrm{RL}^{\downarrow\downarrow}}{T_\mathrm{RL}^{\uparrow\uparrow} + T_\mathrm{RL}^{\downarrow\uparrow} + T_\mathrm{RL}^{\uparrow\downarrow} + T_\mathrm{RL}^{\downarrow\downarrow}}, \tag{2.18}$$

the mirror operation implies that

$$P'_\mathrm{z} = \mathscr{M}_\mathrm{y}(P_\mathrm{z}) = \frac{T_\mathrm{RL}^{\downarrow\downarrow} + T_\mathrm{RL}^{\uparrow\downarrow} - T_\mathrm{RL}^{\downarrow\uparrow} - T_\mathrm{RL}^{\uparrow\uparrow}}{T_\mathrm{RL}^{\uparrow\uparrow} + T_\mathrm{RL}^{\downarrow\uparrow} + T_\mathrm{RL}^{\uparrow\downarrow} + T_\mathrm{RL}^{\downarrow\downarrow}} = -P_\mathrm{z}. \tag{2.19}$$

Thus we have shown that the spin-polarization P_z changes sign under $\mathscr{M}_\mathrm{y}$. This is equivalent to the statement that the spin-polarization changes sign between the enantiomers of the molecule. Note that for spin quantized along the x, y axis we have: $P_\mathrm{x} \rightarrow -P_\mathrm{x}$ and $P_\mathrm{y} \rightarrow P_\mathrm{y}$ (P_y is invariant) under $\mathscr{M}_\mathrm{l}$.

2.5.3. MIRROR OPERATION

The goal is to show how the mirror operation: $\mathscr{M}_\mathrm{y} : \mathrm{y} \rightarrow -\mathrm{y}$ affects the different parts of the Hamiltonian: i) The onsite spin-orbit coupling Hamiltonian (the onsite energies clearly do not change under $\mathscr{M}_\mathrm{y}$) and ii) the hopping elements (of gold-gold, carbon-gold, sulfur-gold and carbon-carbon).

Spin-Orbit Coupling: Under $\mathscr{M}_\mathrm{y}$, spin and orbital angular momentum transforms as:

$$\mathbf{S} = (\mathbf{S}_\mathrm{x}, \mathbf{S}_\mathrm{y}, \mathbf{S}_\mathrm{z}) \overset{\mathscr{M}_\mathrm{y}}{\rightarrow} (-\mathbf{S}_\mathrm{x}, \mathbf{S}_\mathrm{y}, -\mathbf{S}_\mathrm{z}), \tag{2.20}$$

$$\mathbf{L} = (\mathbf{L}_\mathrm{x}, \mathbf{L}_\mathrm{y}, \mathbf{L}_\mathrm{z}) \overset{\mathscr{M}_\mathrm{y}}{\rightarrow} (-\mathbf{L}_\mathrm{x}, \mathbf{L}_\mathrm{y}, -\mathbf{L}_\mathrm{z}). \tag{2.21}$$

This implies that the spin-orbit coupling Hamiltonian $\mathbf{H}_\mathrm{SOC} = \xi \mathbf{L} \cdot \mathbf{S}$ is invariant under $\mathscr{M}_\mathrm{y}$.

Hopping Matrices The SKTB matrix element: $H^{\mu,\nu}_{\mathrm{l,m,n}}$ is the hopping parameter between orbital μ and ν and l,m,n are the direction cosines. Under $\mathscr{M}_{\mathrm{y}}$ the SKTB hopping matrices transform as:

$$H^{\mu,\nu}_{\mathrm{l,m,n}} \to H^{\mu,\nu}_{\mathrm{l,-m,n}}. \tag{2.22}$$

This implies changes for hopping matrices of carbon-carbon, gold-gold, gold-sulfur and sulfur-carbon! The detailed transformation of the orbitals transform under $\mathscr{M}_{\mathrm{y}}$ can be deduced from the hopping matrices in the SKTB framework. Alternatively for the helicene molecule we can change the direction in which the helix rotates by letting $\Phi_i \to -\Phi_i$ in equation (1) of ref [11], since P,M helicene are distinct from each other in the clockwise/counterclockwise rotation of the helix. This change will alter the hopping element caculated in eqs. (4), (5) and (6) of ref [11].

2.5.4. BÜTTIKER PROBES AND ONSAGER-CASIMIR

Given that we can expand the current into the left lead in the bias voltage V as $I(m,V) = G_1(m)V + G_2(m)V^2 + G_3(m)V^3 + ...$, we have that:

$$G_1(m) = \frac{dI(m,V)}{dV}|_{V=0}. \tag{2.23}$$

The goal of this section is to show that $G_1(m) = G_1(-m)$ for a Büttiker voltage probe. For a system at finite temperature and $\mu_{\mathrm{L,R}} = E_{\mathrm{F}} \pm \frac{V}{2}$ the Fermi Dirac function and its derivative w.r.t bias voltage are:

$$f(E,\mu(V)) = \Big(\exp\big[\beta(E-\mu(V)\big]+1\Big)^{-1}, \tag{2.24}$$

$$\frac{\partial f(E,\mu(V))}{\partial V} = \beta\Big(\exp\big[\beta(E-\mu(V)\big]+1\Big)^{-1}\frac{\partial \mu(V)}{\partial V} = g(E,\mu)\frac{\partial \mu}{\partial V}. \tag{2.25}$$

For eq. (2.38) with i = L and j = R, B we have (where we drop $\frac{e}{h}$):

$$I_{\mathrm{L}}(m,V) = \int \Big[T_{\mathrm{BL}}(m) + T_{\mathrm{RL}}(m)\Big] f(E,\mu_{\mathrm{L}}) - T_{\mathrm{LB}}(m) f(E,\mu_{\mathrm{B}}) - T_{\mathrm{LR}}(m) f(E,\mu_{\mathrm{R}}) dE. \tag{2.26}$$

Thus the derivative $\partial_V I_{\mathrm{L}}(m,V)$, which we hereby define as $G_1(V,m)$, for a bias voltage - independent system is:

$$\begin{aligned}\partial_V I_{\mathrm{L}}((m,V)) \equiv G_1(V,m) = \int \frac{1}{2}\Big[T_{\mathrm{BL}}(m,E) + T_{\mathrm{RL}}(m,E)\Big] \times g(E,\mu_{\mathrm{L}}) + \frac{1}{2} T_{\mathrm{LR}}(m,E) \times g(E,\mu_{\mathrm{R}}) \\ - T_{\mathrm{LB}}(m) g(E,\mu_{\mathrm{B}}) \frac{\partial \mu_{\mathrm{B}}(V,m)}{\partial V} dE.\end{aligned} \tag{2.27}$$

And at $V = 0$ we have the expression:

$$\begin{aligned} G_1(V=0,m) = &\int \frac{1}{2}\Big[T_{\mathrm{BL}}(m,E)+T_{\mathrm{RL}}(m,E)+T_{\mathrm{LR}}(m,E)\Big]\times g(E,\mu=E_{\mathrm{F}}) \\ &- T_{\mathrm{LB}}(m)g(E,\mu_{\mathrm{B}}(0))\frac{\partial\mu_{\mathrm{B}}(V=0)}{\partial V}dE. \end{aligned} \tag{2.28}$$

To find $\frac{\partial\mu_{\mathrm{B}}(V,m)}{\partial V}$ we must turn to the current into the Büttiker probe: $I_{\mathrm{B}}(m)$. This current is given by eq. (2.38) with i = B and j = R, L (where we drop $\frac{e}{h}$):

$$I_{\mathrm{B}} = \int\Big[T_{\mathrm{LB}}(m)+T_{\mathrm{RB}}(m)\Big]f(E,\mu_{\mathrm{B}}) - T_{\mathrm{BL}}(m)f(E,\mu_{\mathrm{L}}) - T_{\mathrm{BR}}(m)f(E,\mu_{\mathrm{R}})dE. \tag{2.29}$$

For a voltage probe we have the condition that: $I_{\mathrm{B}}=0$. We take the derivative w.r.t. $I_{\mathrm{B}}(m)$ and the left hand side and right hand side of this expression:

$$\begin{aligned} \frac{d}{dV}I_{\mathrm{B}}(m) = &\int\Big[T_{\mathrm{LB}}(m,\mu_{\mathrm{B}}(V))+T_{\mathrm{RB}}(m,\mu_{\mathrm{B}}(V))\Big]g(E,\mu_{\mathrm{B}})\frac{\partial\mu_{\mathrm{B}}(V)}{\partial V} \\ &+ T_{\mathrm{BR}}(m)g(E,\mu_{\mathrm{R}})\frac{1}{2} - T_{\mathrm{BL}}(m)g(E,\mu_{\mathrm{L}})\frac{1}{2}dE = 0, \\ &\Rightarrow \\ \partial_V\mu_{\mathrm{B}}(V) = &\,\frac{1}{2}\frac{\int T_{\mathrm{BL}}(m)g(E,\mu_{\mathrm{L}}) - T_{\mathrm{BR}}(m)g(E,\mu_{\mathrm{R}})dE}{\int g(E,\mu_{\mathrm{B}})\big[T_{\mathrm{LB}}(m,\mu_{\mathrm{B}})+T_{\mathrm{RB}}(m,\mu_{\mathrm{B}})\big]dE}. \end{aligned} \tag{2.30}$$

We can take $\partial_V\mu_{\mathrm{B}}(V)$ outside of the integral since it does not depend on energy and in the last lign we put the integral signs back in. For $V=0$ we have $\mu_{\mathrm{L}}=\mu_{\mathrm{R}}=E_{\mathrm{F}}$ and because there can be no currents running at $V=0$ we have that $\mu_{\mathrm{B}}(V=0)=E_{\mathrm{F}}$. To prove this we can plug $\mu_{\mathrm{L}}=\mu_{\mathrm{R}}=\mu_{\mathrm{B}}(V=0)=E_{\mathrm{F}}$ into eq. (2.29):

$$I_{\mathrm{B}} = \int f(E,E_{\mathrm{F}})\Big[T_{\mathrm{LB}}(m)+T_{\mathrm{RB}}(m)-T_{\mathrm{RB}}(m)-T_{\mathrm{BL}}(m)\Big]dE = 0, \tag{2.31}$$

because $T_{\mathrm{LB}}(m)+T_{\mathrm{RB}}(m)-T_{\mathrm{RB}}(m)-T_{\mathrm{BL}}(m)=0$ (this follow from unitarity of the scattering matrix). This proofs $\mu_{\mathrm{B}}(V=0)=E_{\mathrm{F}}$ satisfies the probe condition $I_{\mathrm{B}}=0$. Plugging $\mu_{\mathrm{B}}(V=0)=E_{\mathrm{F}}$ into eq. (2.30) and relabeling the energy $E\rightarrow E_1$ we find:

$$\Rightarrow \partial_V\mu_{\mathrm{B}}(m,V=0) = \frac{1}{2}\frac{\int g(E_1,E_{\mathrm{F}})\Big[T_{\mathrm{BL}}(m)-T_{\mathrm{BR}}(m)\Big]dE_1}{\int g(E_1,E_{\mathrm{F}})\Big[T_{\mathrm{LB}}(m)+T_{\mathrm{RB}}(m)\Big]dE_1}. \tag{2.32}$$

Plugging eq. (2.32) back into eq. (2.28) gives (omitting E_{F}):

$$
\begin{aligned}
G_1(V=0,m) = \int \frac{1}{2}\Big[T_{\mathrm{BL}}(m)+T_{\mathrm{RL}}(m)+T_{\mathrm{LR}}(m)\Big]\times g(E) \\
- T_{\mathrm{LB}}(m)g(E)\frac{\int g(E_1)\Big[T_{\mathrm{BL}}(m,E_1)-T_{\mathrm{BR}}(m,E_1)\Big]dE_1}{\int g(E_1)\Big[T_{\mathrm{LB}}(m,E_1)+T_{\mathrm{RB}}(m,E_1)\Big]dE_1}.
\end{aligned}
\tag{2.33}
$$

Now we relabel the energy E in eq. (2.33) with E_2 and calculate:

$$
\begin{aligned}
\Delta G \equiv\, & G_1(V=0,m)-G_1(V=0,-m), \\
=\, & \frac{1}{2}\int \Big[T_{\mathrm{BL}}(m,E_2)+T_{\mathrm{RL}}(m,E_2)+T_{\mathrm{LR}}(m,E_2)+\ \ldots.(m\rightarrow -m)\Big]\times g(E_2)dE_2 \\
& -\int T_{\mathrm{LB}}(m,E_2)g(E_2)\frac{\partial\mu_{\mathrm{B}}(m,V=0)}{\partial V}dE_2+\int T_{\mathrm{LB}}(-m,E_2)g(E_2)\frac{\partial\mu_{\mathrm{B}}(-m,V=0)}{\partial V}dE_2.
\end{aligned}
\tag{2.34}
$$

We now use time-reversal symmetry ($T_{\mathrm{ij}}(m) = T_{\mathrm{ji}}(-m)$) and $T_{\mathrm{LB}}(m)+T_{RB}(m) = T_{\mathrm{BR}}(m)+T_{\mathrm{BL}}(m)$ (this follow from unitarity of the scattering matrix) to find:

$$
\begin{aligned}
\Delta G = \frac{1}{2a}\int g(E_1)g(E_2)\Big[2\times T_{\mathrm{LB}}(m,E_2)T_{\mathrm{BL}}(m,E_1) \\
+T_{\mathrm{LB}}(m,E_1)\Big(T_{\mathrm{BR}}(m,E_2)-T_{\mathrm{BL}}(m,E_2)-T_{\mathrm{LB}}(m,E_2)-T_{\mathrm{RB}}(m,E_2)\Big)\Big]dE_1dE_2.
\end{aligned}
\tag{2.35}
$$

Where $a=\int g(E,E_{\mathrm{F}})\Big[T_{\mathrm{LB}}(m)+T_{\mathrm{RB}}(m)\Big]dE$. If there are interactions then $a\neq 0$. Now we interchanges the labels E_2, E_1 in the first part of eq. (2.35) and find:

$$
\int g(E_1)g(E_2)\Big[2\times T_{\mathrm{BL}}(m,E_2)T_{\mathrm{LB}}(m,E_1)\Big]dE_1dE_2 = \int g(E_1)g(E_2)\Big[2\times T_{\mathrm{BL}}(m,E_1)T_{\mathrm{LB}}(m,E_2)\Big]dE_1dE_2.
\tag{2.36}
$$

Plugging eq. (2.36) back into eq. (2.35):

$$
\Delta G = \frac{1}{2a}\int g(E_1)g(E_2)\times T_{\mathrm{LB}}(m,E_1)\Big[T_{\mathrm{BR}}(m,E_2)+T_{\mathrm{BL}}(m,E_2)-T_{\mathrm{LB}}(m,E_2)-T_{\mathrm{RB}}(m,E_2)\Big]dE_1dE_2 = 0.
\tag{2.37}
$$

We can conclude that Onsager-Casimir reciprocity is satisfied for any temperature in the case of a Büttiker voltage probe, and $a\neq 0$. Again time-reversal symmetry and unitarity of the S-matrix imply that: $G_1(m)=G_1(-m)$.

2.5.5. CHARGE CURRENT FORMULA

For a system with multiple leads which respects unitarity of the S-matrix and which has magnetization m the current going into lead i is given by:

$$I_{\mathrm{i}}(m) = \frac{e}{h}\int_{-\infty}^{\infty}\sum_{\mathrm{j}\neq\mathrm{i}} T_{\mathrm{ji}}(m)\, f_{\mathrm{i}} - T_{\mathrm{ij}}(m)\, f_{\mathrm{j}}\; dE. \tag{2.38}$$

Here $T_{\mathrm{ji}}(m)$ is the transmission from lead j to lead i for a magnetization m of the system and f_{i} is the Fermi-Dirac function of lead i. There is an implicit sum over spins in $T_{\mathrm{ji}}(m) = \sum_{\mathrm{s,s'}\in\{\uparrow,\downarrow\}} T_{\mathrm{ji}}^{\mathrm{ss'}}(m)$. For a 2 terminal system which respects *current conservation*: $I_{\mathrm{L}} + I_{\mathrm{R}} = 0$, eq. (2.38) reduces to:

$$I(m) = \frac{e}{h}\int_{-\infty}^{\infty} T_{\mathrm{RL}}(m, E)\Big(f_{\mathrm{L}}(E) - f_{\mathrm{R}}(E)\Big)\, dE. \tag{2.39}$$

REFERENCES

(1) Huisman, K. H.; Thijssen, J. M. CISS Effect: A Magnetoresistance Through Inelastic Scattering. *The Journal of Physical Chemistry. C, Nanomaterials and Interfaces* **2021**, *125*, 23364–23369.

(2) Kulkarni, C.; Mondal, A.; Das, T.; Grinbom, G.; Tassinari, F.; Mabesoone, M.; Meijer, E.; Naaman, R. Highly Efficient and Tunable Filtering of Electrons' Spin by Supramolecular Chirality of Nanofiber-Based Materials. *Advanced Materials* **2020**, *32*, DOI: `10.1002/adma.201904965`.

(3) Aragonès, A. C.; Medina, E.; Ferrer-Huerta, M.; Gimeno, N.; Teixidó, M.; Palma, J. L.; Tao, N.; Ugalde, J. M.; Giralt, E.; Díez-Pérez, I., et al. Measuring the Spin-Polarization Power of a Single Chiral Molecule. *Small* **2017**, *13*, 1602519.

(4) Kiran, V.; Cohen, S.; Naaman, R. Structure Dependent Spin Selectivity in Electron Transport Through Oligopeptides. *The Journal of Chemical Physics* **2017**, *146*, DOI: `10.1063/1.4966237`.

(5) Kiran, V.; Mathew, S.; Cohen, S.; Hernandez Delgado, I.; Lacour, J.; Naaman, R. Helicenes-A New Class of Organic Spin Filter. *Advanced materials (Deerfield Beach, Fla.)* **2016**, *28*, DOI: `10.1002/adma.201504725`.

(6) Xie, Z.; Markus, T. Z.; Cohen, S. R.; Vager, Z.; Gutierrez, R.; Naaman, R. Correction to Spin Specific Electron Conduction through DNA Oligomers. *Nano Letters* **2012**, *12*, PMID: 22132798, 523–523.

(7) Al Bustami, H.; Koplovitz, G.; Primc, D.; Yochelis, S.; Capua, E.; Porath, D.; Naaman, R.; Paltiel, Y. Single Nanoparticle Magnetic Spin Memristor. *Small* **2018**, *14*, 1801249.

(8) Bullard, G.; Tassinari, F.; Ko, C.-H.; Mondal, A. K.; Wang, R.; Mishra, S.; Naaman, R.; Therien, M. J. Low-Resistance Molecular Wires Propagate Spin-Polarized Currents. *Journal of the American Chemical Society* **2019**, *141*, PMID: 31411873, 14707–14711.

(9) Tassinari, F.; Jayarathna, D.; Kantor-Uriel, N.; Davis, K.; Varade, V.; Achim, C.; Naaman, R. Chirality Dependent Charge Transfer Rate in Oligopeptides. *Advanced Materials* **2018**, *30*, 1706423.

(10) Bloom, B. P.; Kiran, V.; Varade, V.; Naaman, R.; Waldeck, D. H. Spin Selective Charge Transport Through Cysteine Capped Cdse Quantum Dots. *Nano Letters* **2016**, *16*, PMID: 27336320, 4583–4589.

(11) Geyer, M.; Gutierrez, R.; Mujica, V.; Cuniberti, G. Chirality-Induced Spin Selectivity in a Coarse-Grained Tight-Binding Model for Helicene. *The Journal of Physical Chemistry C* **2019**, *123*, 27230–27241.

(12) Zöllner, M. S.; Varela, S.; Medina, E.; Mujica, V.; Herrmann, C. Insight Into the Origin of Chiral-Induced Spin Selectivity From a Symmetry Analysis of Electronic Transmission. *Journal of Chemical Theory and Computation* **2020**, *16*, PMID: 32271568, 2914–2929.

(13) Rebergen, M. A Study of Induced Spin Selectivity in Chiral Molecules, MSc thesis, Delft University of Technology, 2018.

(14) Gersten, J.; Kaasbjerg, K.; Nitzan, A. Induced Spin Filtering in Electron Transmission Through Chiral Molecular Layers Adsorbed on Metals With Strong Spin-Orbit Coupling. *The Journal of chemical physics* **2013**, *139 11*, 114111.

(15) Liu, Y.; Xiao, J.; Koo, J.; Yan, B. Chirality-Driven Topological Electronic Structure of DNA-Like Materials. *Nature Materials* **2021**, DOI: `10.1038/s41563-021-00924-5`.

(16) Dalum, S.; Hedegård, P. Theory of Chiral Induced Spin Selectivity. *Nano Letters* **2019**, *19*, PMID: 31265313, 5253–5259.

(17) Onsager, L. Reciprocal Relations in Irreversible Processes. I. *Phys. Rev.* **1931**, *37*, 405–426.

(18) Onsager, L. Reciprocal Relations in Irreversible Processes. II. *Phys. Rev.* **1931**, *38*, 2265–2279.

(19) Büttiker, M. Symmetry of Electrical Conduction. *IBM Journal of Research and Development* **1988**, *32*, 317–334.

(20) Fransson, J. Vibrational Origin of Exchange Splitting and Chirality Induced Spin Selectivity. *Physical Review B* **2020**, DOI: `10.1103/PhysRevB.102.235416`.

(21) Fransson, J. Chirality-Induced Spin Selectivity: The Role of Electron Correlations. *The Journal of Physical Chemistry Letters* **2019**, *10*, PMID: 31657931, 7126–7132.

(22) Sánchez, D.; Büttiker, M. Magnetic-Field Asymmetry of Nonlinear Mesoscopic Transport. *Physical Review Letters* **2004**, *93*, DOI: `10.1103/physrevlett.93.106802`.

(23) Büttiker, M.; Sánchez, D. Interaction-Induced Magnetic Field Asymmetry of Nonlinear Mesoscopic Electrical Transport. *International Journal of Quantum Chemistry* **2005**, *105*, 906–913.

(24) Spivak, B.; Zyuzin, A. Signature of the Electron-Electron Interaction in the Magnetic-Field Dependence of Nonlinear I-V Characteristics in Mesoscopic Systems. *Physical Review Letters* **2004**, *93*, DOI: `10.1103/physrevlett.93.226801`.

(25) Rikken, G.; Fölling, J.; Wyder, P. Electrical Magnetochiral Anisotropy. *Physical review letters* **2002**, *87*, 236602.

(26) Saito, K.; Utsumi, Y. Symmetry in Full Counting Statistics, Fluctuation Theorem, and Relations Among Nonlinear Transport Coefficients in the Presence of a Magnetic Field. *Phys. Rev. B* **2008**, *78*, 115429.

(27) Papaconstantopoulos, D. A., *Handbook of the Band Structure of Elemental Solids*; Second Edition; Springer New York Heidelberg Dordrecht London: 2015, pp 295–299.

(28) Choi, K. Theoretical Report On the Hopping Between Gold and Sulfur in CISS Experiments, MSc thesis, Delft University of Technology, 2020.

(29) Groth, C. W.; Wimmer, M.; Akhmerov, A. R.; Waintal, X. Kwant: A Software Package for Quantum Transport. *New Journal of Physics* **2014**, *16*, 063065.

(30) Büttiker, M. Role of quantum coherence in series resistors. *Phys. Rev. B* **1986**, *33*, 3020–3026.

(31) Kilgour, M.; Segal, D. Inelastic effects in molecular transport junctions: The probe technique at high bias. *The Journal of Chemical Physics* **2016**, *144*, 124107, DOI: `10.1063/1.4944470`.

(32) Bedkihal, S.; Bandyopadhyay, M.; Segal, D. The Probe Technique far From Equilibrium: Magnetic Field Symmetries of Nonlinear Transport. *The European Physcial Journal B* **2013**, DOI: `10.1140/epjb/e2013-40971-7`.

(33) Ben Dor, O.; Yochelis, S.; Radko, A.; Vankayala, K.; Capua, E.; Capua, A.; Yang, S.-H.; Baczewski, L.; Parkin, S. Magnetization Switching in Ferromagnets by Adsorbed Chiral Molecules Without Current or External Magnetic Field. *Nature Communications* **2017**, *8*, 14567.

(34) Barreteau, C.; Spanjaard, D.; Desjonquères, M.-C. An Efficient Magnetic Tight-Binding Method for Transition Metals and Alloys. *Comptes Rendus Physique* **2016**, *17*, This is an open access article under the CC BY-NC-ND license, 406–429.

(35) Te Velde, G.; Bickelhaupt, F. M.; Baerends, E. J.; Fonseca Guerra, C.; van Gisbergen, S. J. A.; Snijders, J. G.; Ziegler, T. Chemistry With ADF2019. *J. Comput. Chem.* **2001**, *22*, 931–967.

(36) Chico, L.; Latgé, A.; Brey, L. Symmetries of Quantum Transport With Rashba Spin–Orbit: Graphene Spintronics. *Phys. Chem. Chem. Phys.* **2015**, *17*, 16469–16475.

3

NON-BIPARTICE STRUCTURES WITH COULOMB INTERACTIONS

One of the manifestations of chirality-induced spin selectivity (CISS) is the appearance of a magnetocurrent. Magnetocurrent is the observation that the charge currents at finite bias in a two terminal device for opposite magnetizations of one of the leads differ. Magnetocurrents can only occur in the presence of interactions, either of the electrons with vibrational modes or among themselves, through the Coulomb interaction. In experiments on chiral molecules assembled in monolayers the magnetocurrent seems to be dominantly cubic (odd) in bias voltage while theory finds a dominantly even bias voltage dependence. Thus far, theoretical work has predicted a magnetocurrent which is even bias. Here we analyze the bias voltage dependence of the magnetocurrent numerically and analytically involving the spin-orbit and Coulomb interaction (through the Hartree-Fock and Hubbard One approximations). For both approximations it is found that for strong Coulomb interactions the magnetocurrent is dominantly odd in bias voltage, confirming the symmetry observed in experiment.

Part of this chapter has been published in the *Journal of Physical Chemistry C* **2023**, *127*, 14, 6900–6905 [1].

3.1. INTRODUCTION

Chirality-induced spin selectivity (CISS) is a term that classifies a collection of experimental observations on chiral molecules. These observations were made in photo-emission,[2–5] Hall-type,[6,7] and transport experiments[8–16] (for an extensive overview see ref [17]). Photo-emission experiments show that a layer of chiral molecules has a different transmission probability for spin up and down electrons i.e. the transmission probability is spin dependent. Hall-type experiments show that self-assembled monolayers of chiral molecules magnetize when placed on a substrate. This magnetization changes with the chirality of the molecules[6] and it decreases over time.[7]

In two terminal transport experiments, CISS manifests itself as the appearance of magnetocurrent. Magnetocurrent is the observation that the currents for non-zero bias differ for opposite magnetizations of the lead.

Theory initially has mostly focused on the spin dependence of the transmission. The spin-orbit coupling of the molecule's constituents in combination with the chirality of the molecule induce an asymmetry in the transmission probability for spin up and down electrons of the order $10^{-5}\%$ when no decoherence is considered.[18] It has been shown that the chirality of the molecule in combination with the spin-orbit coupling of the substrate can induce an asymmetry in the transmission probability for spin up and down electrons of a few percent,[19,20] consistent with theoretical work on[21,22] and findings in photo-emission experiments. A spin dependent transmission does however not imply a magnetocurrent..[20,23,24]

Magnetocurrent simply is not possible in a fully coherent, noninteracting particle picture according to Büttiker's reciprocity theorem for two terminal systems[25] so that modelling beyond this simplified picture is necessary.[23]

Thus in addition to the chirality of the molecule and spin-orbit coupling, interactions need to be present[26] to obtain a magnetocurrent, in other words, interactions are a necessary ingredient for translating a spin dependent transmission into a non-zero magnetocurrent. Several authors have made attempts to reveal magnetocurrent in a theoretical description in chiral structures by including electron-phonon interactions,[27] electron-electron interactions[28] or a generic decoherence probe.[20,24] Some authors[29,30]have proposed alternative explanations based on chirality-induced interface magnetisation. In describing two terminal transport measurements of the CISS effect there are three points that need to be addressed by theory.

The first point is the Onsager-Casimir reciprocity, which states that the *linear* conductance terms at equilibrium are equal for opposite magnetizations : $G_1(m) = G_1(-m)$.[23,31–33] Deviations from Onsager-Casimir reciprocity are not expected and theories should therefore reproduce this, or provide a strong reason for their violation.[34]

The second point is the odd/even behaviour of the magnetocurrent ΔI in bias voltage. From Onsager-Casimir reciprocity it follows that the magnetocurrent ΔI is non-linear in bias voltage.[20,24] Experiments[9–16] find that the magnetocurrent is dominantly odd in bias voltage indicating that a cubic dependence dominates ($\Delta I \propto V^3$). The theoretical work of Yang, van der Wal and van Wees[24] modelled interactions with the vibrational modes via an extra node which is placed between the molecule and one of the leads, forcing the electrons to move through this node and thereby fully decohere. They found that the magnetocurrent is dominantly even in bias voltage ($\Delta I \propto V^2$). An analysis from our group that modelled interactions with the vibrational modes via the Büttiker voltage probe method and realistic parameters for the electronic structure came to the same conclusion.[20] Theoretical work of refs [26] and [35] for mesoscopic metallic samples (quantum Hall bar, chaotic cavity) finds that ΔI is dominantly even in bias voltage. In ref [36] ΔI is odd but it seems to violate Onsager-Casimir reciprocity since ΔI is linear in bias voltage. The discrepancy between the odd $\Delta I - V$ characteristics of the experiment and the even ones of the theory remains a puzzling problem and it is this discrepancy which is the main topic of this chapter.

The third point entails the size of the effect. In experiments it can reach values of 1-80 % while from theoretical model calculations for realistic parameters,[20,37] values of less than 1% have been reported. Fransson[28] found that for Coulomb interactions in the Hubbard One approximation the size of the CISS effect can reach values of the order 10%, although the Fermi level lies well outside the molecular spectrum.

In this chapter we will consider Coulomb interactions using the Hartree Fock approximation (HFA) and the Hubbard One approximation (HIA) for more or less realistic parameters, focusing on the bias voltage dependence of the magnetocurrent. The chapter is structured as follows: in sec. 3.2 we describe the scattering region, in sec. 3.3 we present our numerical results, in sec. 3.4 we give an explanation of our results and we present our main conclusions in sec. 3.5.

3.2. MODEL DESCRIPTION

The Hamiltonian of a molecular transport junction is given by:

$$\mathbf{H} = \mathbf{H}_{\text{os}} + \mathbf{H}_{\text{T}} + \mathbf{H}_{\text{SOC}} + \mathbf{H}_{\text{U}} + \mathbf{H}_{\text{lead-molecule}} + \mathbf{H}_{\text{leads}}, \tag{3.1}$$

where $\mathbf{H}_{\text{os}}$ is the on-site Hamiltonian, $\mathbf{H}_{\text{T}}$ is the hopping Hamiltonian, $\mathbf{H}_{\text{SOC}}$ is the hopping Hamiltonian due to spin-orbit coupling, $\mathbf{H}_{\text{U}}$ describes the Coulomb interactions, $\mathbf{H}_{\text{lead-molecule}}$ describes the coupling of the molecule to the leads and $\mathbf{H}_{\text{leads}}$ describes the Hamiltonian of the leads. The on-site Hamiltonian is given by $\mathbf{H}_{\text{os}} = \sum_k \epsilon_k \hat{n}_k$, the on-site energy will be set to zero ($\epsilon_k = 0$) throughout this chapter. The hopping Hamiltonian is given by $\mathbf{H}_{\text{T}} = -\sum_k t\, \hat{c}^{\dagger}_{k+1} \hat{c}_k +$ h.c., where t is the hopping parameter and h.c. denotes the hermitian conjugate. In this chapter the sites are arranged in a helix with radius a and pitch c. N is the number of sites within one winding and M is the number of windings such that MN is the total number of sites in the molecule. For the hopping Hamiltonian due to spin-orbit coupling we use the model of Fransson[28] which couples next-nearest neighbours $\mathbf{H}_{\text{SOC}} = \sum_k \lambda \big(i \vec{v}_k \cdot \vec{\sigma} \big) \hat{c}^{\dagger}_{k+2} \hat{c}_k + h.c.$, where λ is the spin-orbit coupling parameter, the components of $\vec{\sigma}$ are the Pauli-matrices, $\vec{v}_k = \vec{d}_{k+1} \times \vec{d}_{k+2}$ and $\vec{d}_{k+n} = (\vec{r}_k - \vec{r}_{k+n})/|\vec{r}_k - \vec{r}_{k+n}|$, with $\vec{r}_k$ the coordinates of site k on a helix: $\vec{r}_k = [a\cos\big(\phi_k\big), a\sin\big(\phi_k\big), c\frac{\phi_k}{2\pi}\frac{N}{NM-1}]$ and $\phi_k = \frac{2\pi(k-1)}{N}$, $k \in MN$. We take $M = 1, N = 8$ and $a = 1, c = 1$. Note that due to the spin-dependent hopping term the lattice is non-bipartite. $\mathbf{H}_{\text{U}}$ contains the Coulomb interactions, we take those to be on-site:

$$\mathbf{H}_{\text{U}} = U \sum_k \hat{n}_{k\uparrow} \hat{n}_{k\downarrow}, \tag{3.2}$$

with U the Coulomb interaction strength.

We model the leads using the wide-band limit, meaning that the self-energies are purely imaginary and independent of energy. The diagonal matrix elements of lead α that are coupled to the molecule are given by $\gamma(\mathbb{1} + p_z^\alpha \sigma_z)$ and are zero otherwise. Here γ is the coupling strength and $p_z^\alpha \in [-1,1]$ the magnetic polarization of lead α. For the right lead we take $p_z^{\mathrm{R}} = 0$ and we couple the left lead to the two leftmost sites and the right lead to the two right most sites.

We aim at using realistic parameters corresponding to a molecule consisting of carbon atoms. We take the hopping parameter $t = 2.4$ eV.[38] Due to the image-charge effect[39] the effective on-site Coulomb interaction of carbon, which for an isolated molecule is $U_C = 10.06$ eV,[40] will be lowered to an extent which sensitively depends on the molecule-lead separation. To investigate the effect of U on the bias dependence of the magnetocurrent we vary U to a maximum value of 4.8 eV. The spin-orbit coupling parameter of helicene is $\lambda = 6$ meV[18] (therefore $\lambda/t \approx 10^{-3}$). To also investigate its effect on the bias dependence of the magnetocurrent we will vary λ between $10^{-3}t$ and $10^{-1}t$. Furthermore we take $T = 300\ K$, the coupling strength the lead is taken $\gamma = 0.5$ eV[41] and $p_z^{\mathrm{L}} = 0.5$.

The Coulomb interactions cause a shift in the on-site energies of the Hamiltonian of $U/2$ causing the molecular spectrum to be symmetric around $U/2$ for bipartite lattices. At zero bias voltage the chemical potentials of the left and right lead are given by the Fermi energy E_{F}. In that case for $E_{\mathrm{F}} = \frac{U}{2}$ the molecule is charge neutral and E_{F} lies precisely between the highest occupied molecular orbital (HOMO) and lowest unoccupied molecular orbital (LUMO) energy. However in molecular junctions the molecule is rarely charge neutral due to charge transfer, which corresponds to $E_{\mathrm{F}} \neq \frac{U}{2}$ (lying either closer to the HOMO or LUMO energy). Therefore we also vary the Fermi energy between the energy of the HOMO and LUMO level.

In sec. 3.4 we state the retarded and advanced two-point Green's functions in the Hartree-Fock and the Hubbard One approximation derived with the equation of motion technique (analogous to ch. 12 of of ref. [42]). These Green's functions are expressed in terms of the average electron densities for site k with spin s: $\langle n_{ks}\rangle$, which we determine self consistently from the Green's functions see equation (eq. (3.11)). Every iteration m has an input and an output electron density and as convergence criterion for the m-th iteration we use: $|\langle n_{ks}^{in,m}\rangle - \langle n_{ks}^{out,m}\rangle| < 10^{-5}$. The Hamiltonian without interactions ($U = 0$) is defined as: $\mathbf{H}_0 = \mathbf{H}_{\mathrm{os}} + \mathbf{H}_{\mathrm{T}} + \mathbf{H}_{\mathrm{SOC}}$ and is constructed with the Kwant code[43] and the Qsymm code.[44] We have implemented a non-equilibrium transport code which can be found in `https://github.com/khhuisman/CISS_CoulombInteraction`.

In this code we determine the electron density as follows. Suppose we want to calculate the electron density for the decreasing or increasing bias voltages $\{0, V_1, V_2, \ldots\}$, ($|V_{i+1}| > |V_i|$). First of all we start our self-consistent calculation at zero bias voltage where we expect that every site is approximately half filled , therefore we take this as an initial guess ($\langle n_{ks}^{in,m=0}(V=0)\rangle = \frac{1}{2}$). Then we self-consistently determine the electron densities for $V = 0$ and obtain the converged result $\langle n_{ks}^{converged}(V=0)\rangle$. We then use these values as an initial guess for the next bias voltage V_1: $\langle n_{ks}^{in,m=0}(V=V_1)\rangle = \langle n_{ks}^{converged}(V=0)\rangle$. We always use the output of a self-consistent calculation as initial guess for the next bias voltage: $\langle n_{ks}^{in,m=0}(V=V_{i+1})\rangle = \langle n_{ks}^{converged}(V=V_i)\rangle$ to adiabatically connect the two solutions. This procedure is done separately for positive and negative bias and both times we start in $V = 0$. Furthermore we employ linear mixing of the electron densities meaning that the input for iteration $m+1$ is a linear combination of the input and output of iteration m: $\langle n_{ks}^{in,m+1}(V)\rangle = (1-\alpha)\langle n_{ks}^{out,m}(V)\rangle + \alpha\langle n_{ks}^{in,m}(V)\rangle$ characterized by the parameter $\alpha \in [0,1)$. The used values of α vary between the different Coulomb interaction strengths and are indicated in the code.

3.3. RESULTS

We now turn to a two terminal system with Coulomb interactions. The transmission then depends on the bias voltage V through the Coulomb potential, and in the HFA and HIA, this is expressed in terms of the electron densities, that depend on the bias voltage applied to the molecule. This means that the transmission becomes voltage dependent: $T_{\mathrm{LR}}(m) \to T_{\mathrm{LR}}(m,V) = T_{\mathrm{LR}}(m, \langle n_{1\uparrow}(m,V)\rangle, \langle n_{1\downarrow}(m,V)\rangle, ..., \langle n_{ks}(m,V)\rangle)$. The current into the left lead is then given by:

$$I(m,V) = \frac{e}{h}\int_{-\infty}^{\infty} T_{\mathrm{LR}}(m,V)\Big(f_{\mathrm{L}} - f_{\mathrm{R}}\Big)dE, \tag{3.3}$$

where $f_\alpha = f(E,\mu_\alpha,\beta)$ is the Fermi-Dirac distribution of the lead α with chemical potential μ_α at $\beta = \frac{1}{k_{\mathrm{B}}T}$ with T the temperature of the lead. The transmission is given by $T_{\mathrm{LR}} = \mathrm{Tr}\Big[\boldsymbol{\Gamma}_{\mathrm{L}}\mathbf{G}^{+}\boldsymbol{\Gamma}_{\mathrm{R}}\mathbf{G}^{-}\Big]$ with $\mathbf{G}^{+}$ the retarded Green's function. Assuming symmetric capacitive coupling to the left and right lead, the chemical potentials of the left and right leads are $E_{\mathrm{F}} + \frac{V}{2}$ and $E_{\mathrm{F}} - \frac{V}{2}$ respectively, with E_{F} the Fermi energy and V the bias voltage. Using eq. (3.3) we can write the magnetocurrent as:

$$\begin{aligned} \Delta I(m,V) &\equiv I(m,V) - I(-m,V) \\ &= \frac{e}{h}\int_{-\infty}^{\infty}\Big[T_{\mathrm{LR}}(m,V) - T_{\mathrm{LR}}(-m,V)\Big](f_{\mathrm{L}} - f_{\mathrm{R}})dE. \end{aligned} \tag{3.4}$$

In figure 3.1, $\Delta I(m,V)$ is plotted as a function of bias voltage in the HFA and HIA respectively. In fig. 3.1a the magnetocurrent is plotted for $E_{\mathrm{F}} \neq \frac{U}{2}$ in the HFA and we see that for small U/t (upper panels) the magnetocurrent is dominantly even in bias voltage and for large U/t (lower panels) the magnetocurrent is dominantly odd in bias voltage for $E_{\mathrm{F}} \neq \frac{U}{2}$. In fig. 3.1b the magnetocurrent is plotted for $E_{\mathrm{F}} \neq \frac{U}{2}$ in the HIA and we see that it is a dominantly odd function of the bias voltage. In fig. 3.1c and 3.1d we see that $\Delta I(m,V)$ is dominantly odd in voltage for $E_{\mathrm{F}} = \frac{U}{2}$. From the numerical results it is clear that $\Delta I(m,V)$ is dominantly odd in bias voltage in both the HFA and HIA for most cases, the only exception being $E_{\mathrm{F}} \neq \frac{U}{2}$ for small $U/t < 1$ in the HFA for which the magnetocurrent is dominantly even. Here we simply stated our numerical results, in sec. 3.4 we present a theoretical analyses to explain them. Now follow some other results, our calculation shows that in both the HFA and HIA the polarization of the current $P_C(V) = \frac{I(m,V)-I(-m,V)}{I(m,V)+I(-m,V)}$ is less than 1% even if relatively large values of the spin-orbit coupling parameter are used. Also it is found that when the molecule changes its chirality, $\Delta I(m,V)$ exactly changes sign $\Delta I(m,V) \to -\Delta I(m,V)$. Furthermore if the spin-orbit coupling parameter is set to zero, the magnetocurrent vanishes. In Appendix 3.6.4 we

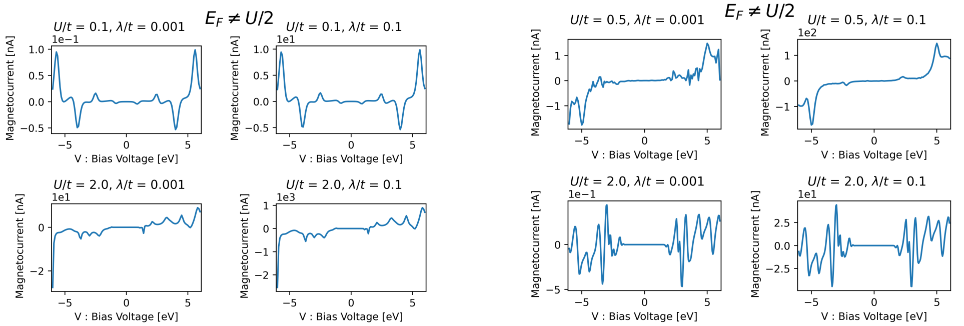

(a) HFA

(b) HIA

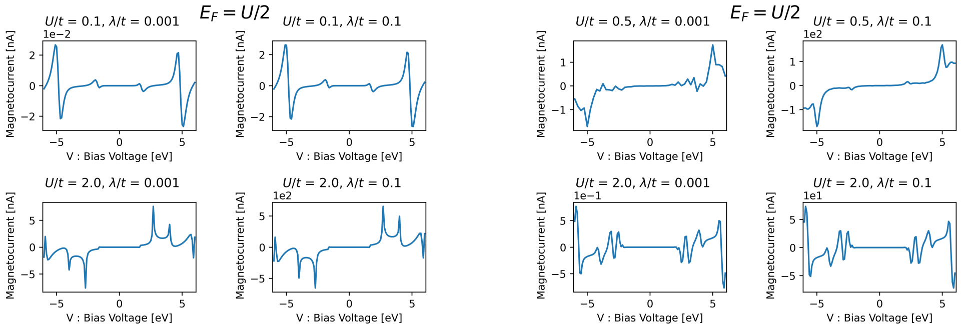

(c) HFA

(d) HIA

Figure 3.1: $\Delta I(m, V)$ for the the helical geometry. Asymmetric chemical potential **(a)** in the HFA, **(b)** in the HIA. Symmetric chemical potential: **(c)** in the HFA, **(d)** in the HIA.

consider the effects of magnetic stray field $\boldsymbol{B}$ that pierces the scattering region in the absence of spin-orbit coupling. The constant magnetic stray field either couples to the spin of the electron, yielding an on-site term or it induces a Peierls phase (see eq. (3.82)) in the hopping parameters due the Peierls substitution. We find that the coupling between the spin and the magnetic field alone yields a numerically vanishing magnetocurrent. The magnetocurrent due to a magnetic phase and nearest neighbour (rather than on-site) Coulomb interactions is negligibly small and of the order 10^{-4}%.

3.4. DISCUSSION

In this section we provide theoretical arguments to qualitatively explain our numerical results. We can expand the magnetocurrent (eq. (3.4)) in bias voltage as $\Delta I(m, V) = \Delta G_1(m)V + \Delta G_2(m)V^2 + \Delta G_3(m)V^3 + \ldots$, where:

$$\Delta G_n(m) = \frac{1}{n!}\left[\left(\frac{\partial}{\partial V}\right)^n \Delta I(m, V)\right]_{V=0}. \tag{3.5}$$

Onsager-Casimir reciprocity,[31,32] implies that $\Delta G_1(m) = 0$. To show that this relates back to time-reversal symmetry at equilibrium ($V = 0$ and equal temperatures for both leads[45]) we write $\Delta G_1(m)$ in terms of the transmission:

$$\begin{aligned}\Delta G_1(m) &= \frac{\partial \Delta I(m,V)}{\partial V}\Big|_{V=0},\\ &= \frac{e}{h}\int_{-\infty}^{\infty} f_0'\Big(T_{\mathrm{LR}}(m,V=0)-T_{\mathrm{LR}}(-m,V=0)\Big)dE.\end{aligned}\tag{3.6}$$

Here we adopted the notation: $f_0' = -\partial_E f(E, E_{\mathrm{F}}, \beta)$. Onsager requires that in equilibrium the system is time-reversal symmetric. This in combination with current conservation implies for the transmission that: $T_{\mathrm{LR}}(m, V = 0) = T_{\mathrm{LR}}(-m, V = 0)$ so that indeed $\Delta G_1(m) = 0$. As a consequence of this the magnetocurrent can only be non-linear in bias voltage $\Delta I(m,V) \propto \Delta G_2(m)V^2 + \Delta G_3(m)V^3 + \ldots$ in accordance with the conclusions of.[23,24] From our numerical calculations we indeed verify that the transmission satisfies $T_{\mathrm{LR}}(m, V = 0) = T_{\mathrm{LR}}(-m, V = 0)$ in the HFA and HIA, therefore Onsager-Casimir reciprocity is satisfied. The non linear-coefficients: $\Delta G_2(m), \Delta G_3(m), \ldots$ may however vanish. To show that $\Delta G_2(m)$ is finite, we analyse it via eq. (3.5). At equilibrium, time-reversal symmetry (TRS) implies that the occupation difference $\Delta n_{ks}(m,V) = \langle n_{ks}(m,V)\rangle - \langle n_{k\bar{s}}(-m,V)\rangle$ ($\bar{s}$ denotes that we flip spin s) is zero $\Delta n_{ks}(m, V = 0) = 0$. At nonzero bias, deviation from equilibrium manifests itself through $\Delta n_{ks}(m,V)$ which no longer vanishes when the bias voltage is finite. Therefore from (3.5) (Appendix 3.6.1) we have:

$$\Delta G_2(m) = \frac{1}{2}\frac{e}{h}\int_{-\infty}^{\infty} f_0' \sum_{k,s} \partial_{ks} T_{\mathrm{LR}}(m, V=0)\Big[\partial_V \Delta n_{ks}(m,V)\Big]_{V=0} dE, \tag{3.7}$$

where $\partial_{ks} = \partial_{\langle n_{ks}(m,V=0)\rangle}$. Eq. (3.7) can be understood as follows: the Green's function is time-reversal symmetric except for the electron densities. As the zeroth order term $\Delta n_{ks}(m, V = 0) = 0$, $\Delta G_2(m)$ can only scale with the first order derivative of $\Delta n_{ks}(m,V)$ at $V = 0$. Intuitively this makes sense: to what extent TRS is broken out of equilibrium ($V \neq 0$) scales with the occupation difference: $\Delta n_{ks}(m,V) = \langle n_{ks}(m,V)\rangle - \langle n_{k\bar{s}}(-m,V)\rangle$. Deviations from TRS thus manifest themselves through $\Delta n_{ks}(m,V)$. If this deviates from zero, $\Delta G_2(m)$ will too. If TRS is present out of equilibrium for every voltage ($\langle n_{ks}(m,V)\rangle = \langle n_{k\bar{s}}(-m,V)\rangle$) then $\Delta G_2(m) \propto \partial_V \Delta n_{ks}(m, V = 0) = 0$ and there is no magnetocurrent as expected due to Büttikers reciprocity theorem for two terminal systems.[25] Furthermore if $U = 0$ then $\Delta I(m,V) = 0$, since every derivative with respect to bias V yields an electron density multiplied by U. This shows the importance of going beyond the non-interacting particle picture. From eq. (3.5) (Appendix 3.6.1) we have for $\Delta G_3(m)$:

$$\begin{aligned}\Delta G_3(m) =& \frac{1}{4}\frac{e}{h}\int_{-\infty}^{\infty} f_0' \sum_{k,k',s,s'} \partial_{ks}\partial_{k's'} T_{\mathrm{LR}}(m, V=0)\\ &\times\Big[\partial_V\langle n_{ks}(m,V)\rangle\partial_V\langle n_{k's'}(m,V)\rangle - \partial_V\langle n_{k\bar{s}}(-m,V)\rangle\partial_V\langle n_{k'\bar{s}'}(-m,V)\rangle\Big]_{V=0} dE\\ &+\frac{1}{4}\frac{e}{h}\int_{-\infty}^{\infty} f_0' \sum_{k,s} \partial_{ks} T_{\mathrm{LR}}(m, V=0)\Big[\partial_V^2 \Delta n_{ks}(m, V=0)\Big] dE,\end{aligned}\tag{3.8}$$

for a symmetrically biased junction. For small V we expect that $\Delta n_{ks}(m,V)$ varies linearly with bias voltage V. It can then be shown that $\Delta G_3(m)/\Delta G_2(m) \propto U$ in the HFA and HIA (Appendix 3.6.1). This is consistent with figure 3.1a since $\Delta I(m,V)$ changes from even to odd with increasing U, and we see that for large U, the cubic term in the magnetocurrent tends to dominate. In the HIA we see similar behaviour only for much smaller U than considered in fig. 3.1b. The numerical results for $E_\mathrm{F} \neq \frac{U}{2}$ figs. 3.1a and 3.1b show that the even/odd behaviour of $\Delta I(m,V)$ can change a lot compared to $E_\mathrm{F} = \frac{U}{2}$. At $E_\mathrm{F} \neq \frac{U}{2}$ and $V = 0$ the system is not exactly half-filled which is more the rule than the exception in molecular junctions due to charge transfer to the molecule. Due to the large Coulomb interactions this will result in a magnetocurrent which is odd in bias voltage.

Here we comment on the Green's functions that are used to calculate the magnetocurrent. A derivation of the Green's functions is done in chapter 12 of Haug and Jauho.[42] Here we simply give the Green's functions for a system with spin-orbit coupling. The Hamiltonian without interactions ($U = 0$) is defined as: $\mathbf{H}_0 = \mathbf{H}_\mathrm{os} + \mathbf{H}_\mathrm{T} + \mathbf{H}_\mathrm{SOC}$. The retarded Green's function in the Hartree-Fock approximation is given by:

$$\mathbf{G}^+_\mathrm{HFA}(\epsilon) = \Big[\epsilon\mathbf{I} - \mathbf{H}_0 - U\mathbf{n} - \mathbf{\Sigma}\Big]^{-1}, \tag{3.9}$$

and the retarded Green's function in the Hubbard One approximation is given by:

$$\mathbf{G}^+_\mathrm{HIA}(\epsilon) = \frac{1}{(\epsilon\mathbf{I} - \mathbf{H}_\mathrm{os} - U\mathbf{I})(\epsilon\mathbf{I} - \mathbf{H}_0 - \mathbf{\Sigma}) - U\mathbf{n}(\mathbf{H}_\mathrm{T} + \mathbf{H}_\mathrm{SOC} + \mathbf{\Sigma})} \times \Big[\epsilon\mathbf{I} - \mathbf{H}_\mathrm{os} - U(\mathbf{I} - \mathbf{n})\Big]. \tag{3.10}$$

Where $\mathbf{\Sigma}$ is the retarded self-energy of the leads, which in the wide band limit for a magnetized left lead is given by $\mathbf{\Sigma} = -\frac{i}{2}\Big(\mathbf{\Gamma}_\mathrm{L}(m) + \mathbf{\Gamma}_\mathrm{R}\Big) = -\frac{i}{2}\mathbf{\Gamma}(m)$ and $\mathbf{n} = \sum_{ks}\langle n_{k\bar{s}}\rangle \hat{n}_{ks}$ is a diagonal matrix with the electron densities on the diagonal. For these Green's functions the density of states are symmetric around the Fermi energy $E_\mathrm{F} = \frac{U}{2}$ if the lattice is bipartite. The electron density for site k with spin s is given by:

$$\langle n_{ks}(m,V)\rangle = \int_{-\infty}^{\infty} \Big(\mathbf{G}^+\Big[\sum_{\alpha=\mathrm{L,R}} f_\alpha \mathbf{\Gamma}_\alpha\Big]\mathbf{G}^-\Big)_{ks,ks}\frac{d\epsilon}{2\pi}. \tag{3.11}$$

In eq. (3.9) the term $\sum_{k,s}\langle n_{k\bar{s}}\rangle \hat{n}_{ks}$ is the result of a Wick contraction of the term $n_{k\uparrow}n_{k\downarrow}$ in eq. (3.2). This contraction in principle also allows for the term:[46,47] $-\langle c^\dagger_{k\uparrow}c_{k\downarrow}\rangle c^\dagger_{k\downarrow}c_{k\uparrow} + h.c.$ which we will call the non-collinear Hubbard model. In that case we obtain (Appendix 3.6.2) the following non-collinear (NC) Hartree Fock Green's function:

$$\mathbf{G}^+_\mathrm{HFA,NC}(\epsilon) = \Big[\epsilon\mathbf{I} - \mathbf{H}_0 - U\mathbf{n} + U\boldsymbol{\rho} - \mathbf{\Sigma}\Big]^{-1} \tag{3.12}$$

and the the non-collinear Hubbard One Green's function:

$$\mathbf{G}^+_\mathrm{HFA,NC}(\epsilon) = \Big[(\epsilon\mathbf{I} - \mathbf{H}_\mathrm{os} - U\mathbf{I})(\epsilon\mathbf{I} - \mathbf{H}_0 - \mathbf{\Sigma}) - U(\mathbf{n} - \boldsymbol{\rho})(\mathbf{H}_\mathrm{T} + \mathbf{H}_\mathrm{SOC} + \mathbf{\Sigma})\Big]^{-1} \times \Big[\epsilon\mathbf{I} - \mathbf{H}_\mathrm{os} - U(\mathbf{I} - \mathbf{n} + \boldsymbol{\rho})\Big] \tag{3.13}$$

Where we defined: $\boldsymbol{\rho} = \sum_{ks}\langle c^{\dagger}_{k\bar{s}} c_{ks}\rangle c^{\dagger}_{ks} c_{k\bar{s}}$. The expectation value $\langle c^{\dagger}_{k\bar{s}} c_{ks}\rangle$ vanishes in the absence of spin-orbit coupling and it is expected that it does not change the result of our calculations. Indeed, when we include this term in our calculations the bias dependence of the magnetocurrent does not change with respect to $\langle c^{\dagger}_{k\bar{s}} c_{ks}\rangle = 0$ for all of the considered values of the spin-orbit coupling, Coulomb interaction strength and Fermi energy. Only in the HFA for $\frac{U}{t} = 2, \frac{\lambda}{t} = 0.1$ and $E_{\mathrm{F}} \neq \frac{U}{2}$ the size of the effect increases significantly to a few percent for low bias voltage. However this increase in the size of the effect happens for a particular choice Fermi energy and it is not clear to us why that happens however we suspect this is due to a numeric instability. Furthermore for large Coulomb interactions ($\frac{U}{t} > 1$) the non-collinear Hubbard One Green's function (eq. (3.13)) gives more accurate results and the size of the effect remains less than 1% while the magnetocurrent remains odd in bias voltage.

3.5. CONCLUSION

In this work we studied the voltage dependence of the magnetocurrent for system with Coulomb interactions (in the HFA and HIA). The system we studied has next-nearest neighbour, spin-dependent hopping that causes the lattice to be non-bipartite. Our numerical results show that the magnetocurrent is odd in bias voltage in both the HFA and HIA for strong Coulomb interactions $U > t$ in agreement with experiments.[9–16] Furthermore we verified that the Onsager-Casimir reciprocity is satisfied, as expected. For a large spin-orbit coupling parameter ($\frac{\lambda}{t} = 0.1$) we found that the size of the effect is of the order 0.1% which is of the same order as our previous work on Büttiker voltage probes.[20] How a bipartite lattice with spin-orbit coupling affects the voltage dependence of the magnetocurrent will be considered in a separate chapter.

3.6. APPENDIX

3.6.1. COULOMB INTERACTIONS: HIGHER ORDER DIFFERENTIAL CONDUCTANCE COEFFICIENTS

In section 3.6.1 the coefficients $\Delta G_2(m), \Delta G_3(m)$ will be calculated via equation (eq.) (3.5) and it will be shown that Onsager-Casimir reciprocity ($\Delta G_1(m) = 0$) follows from time-reversal symmetry in equilibrium. We then compare $\Delta G_2(m), \Delta G_3(m)$ for a system with Coulomb interactions in the Hartree-Fock approximation that satisfies Onsager-Casimir reciprocity.

HARTREE-FOCK: DIFFERENTIAL CONDUCTANCE COEFFICIENTS

Let us introduce the notation:

$$f_\alpha(E) = \left[\exp\!\big(\beta_\alpha(E-\mu_\alpha)\big)+1\right]^{-1}, \tag{3.14}$$

$$f'_\alpha \equiv \partial_{\mu_\alpha} f_\alpha, \quad f''_\alpha \equiv \partial^2_{\mu_\alpha} f_\alpha \tag{3.15}$$

Where μ_α is the the chemical potential of lead α and $\beta_\alpha = \frac{1}{k_{\mathrm{B}} T_\alpha}$ with T_α the temperature of lead α. We will only consider equal temperatures for the leads $\beta_{\mathrm{L,R}} = \frac{1}{k_{\mathrm{B}} T}$. The chemical potential of the left, right lead read given by:

$$\begin{aligned} \mu_{\mathrm{L}} = E_{\mathrm{F}} + \eta V, &\quad \mu_{\mathrm{R}} = E_{\mathrm{F}} - (1-\eta)V \\ \partial_V \mu_{\mathrm{L}} = \eta, &\quad \partial_V \mu_{\mathrm{R}} = -(1-\eta) \end{aligned} \tag{3.16}$$

Here η is the capacitive coupling. We define $f_0 = f_{\mathrm{L,R}}(E)|_{V=0} = [\exp\big(\beta(E-E_{\mathrm{F}})\big)+1]^{-1}$ and $f_0' = \partial_{\mu_{\mathrm{L,R}}} f_{\mathrm{L,R}}(E)|_{V=0}$.

ONSAGER-CASIMIR RECIPROCITY

Onsager demands that in equilibrium the system is time-reversal symmetric. To be unambiguous we define “equilibrium” as $V = 0$ (i.e. $\mu_{\mathrm{L}} = \mu_{\mathrm{R}}$) and equal temperatures for both leads (i.e. $T_{\mathrm{L}} = T_{\mathrm{R}}$) if one of these conditions is violated we say the system is “out of equilibrium”.[45] For the transmission time-reversal symmetry implies that $T_{\mathrm{LR}}(m, V = 0) = T_{\mathrm{RL}}(-m, V = 0)$. Also we have $T_{\mathrm{RL}}(m, V) = T_{\mathrm{LR}}(m, V)$, due to current conservation $I_{\mathrm{L}} + I_{\mathrm{R}} = 0$. Combining time-reversal symmetry and current conservation this implies for the transmission that:

$$T_{\mathrm{LR}}(m, V=0) = T_{\mathrm{LR}}(-m, V=0). \tag{3.17}$$

This implies that $\Delta G_1(m) = 0$ see eq. (3.6).

COEFFICIENT $\Delta G_2(m)$

From eq. (3.5) we obtain the following expression for $\Delta G_2(m)$ (invoking eq. (3.17)):

$$\begin{aligned} \Delta G_2(m) &= \frac{1}{2}\frac{\partial \Delta I(m, V=0)}{\partial V^2}, \\ &= \frac{1}{2}\frac{e}{h}\int_{-\infty}^{\infty} \Big[\partial_V T_{\mathrm{LR}}(m, V=0) - \partial_V T_{\mathrm{LR}}(-m, V=0)\Big] f_0' dE, \\ &= \frac{1}{2}\frac{e}{h}\int_{-\infty}^{\infty} \sum_{k,s} \partial_{ks} T_{\mathrm{LR}}(m, V=0)\Big[\partial_V \Delta n_{ks}(m, V=0)\Big] f_0' dE. \end{aligned} \tag{3.18}$$

Here we adopted the notation $\partial_{\langle n_{ks}(m,V=0)\rangle} \equiv \partial_{ks}$ and in the last line $\Delta n_{ks}(m, V) \equiv \langle n_{ks}(m, V)\rangle - \langle n_{k\bar{s}}(-m, V)\rangle$. Time-reversal symmetry at equilibrium implies that that the electron densities satisfy: $\langle n_{ks}(m, V=0)\rangle = \langle n_{k\bar{s}}(-m, V=0)\rangle$, meaning that the partial derivatives: $\partial_{\langle n_{ks}(m,V=0)\rangle} = \partial_{\langle n_{k\bar{s}}(-m,V=0)\rangle} \equiv \partial_{ks}$. Futhermore at equilibrium we have that $T_{\mathrm{LR}}(m, V = 0) = T_{\mathrm{LR}}(-m, V = 0)$ (see sec 3.6.1), we use this to write $\partial_{\langle n_{ks}(m,V=0)\rangle} T_{\mathrm{LR}}(m, V = 0) = \partial_{\langle n_{k\bar{s}}(-m,V=0)\rangle} T_{\mathrm{LR}}(-m, V = 0)$.

Coefficient $\Delta G_3(m)$

From eq. (3.5) we obtain the following expression for $\Delta G_3(m)$ (invoking eq. (3.17)):

$$\begin{aligned}
\Delta G_3(m) &= \frac{1}{6}\frac{\partial^3 \Delta I(m, V=0)}{\partial V^3} \\
&= \frac{1}{4}\frac{e}{h}\int_{-\infty}^{\infty} f_0''(2\eta-1)\sum_{k,s}\partial_{ks} T_{\mathrm{LR}}(m, V=0)\Big[\partial_V \Delta n_{ks}(m, V=0)\Big], \\
&+ \frac{1}{4}\frac{e}{h}\int_{-\infty}^{\infty} f_0' \sum_{k,k',ss'} \partial_{ks}\partial_{k's'} T_{\mathrm{LR}}(m, V=0) \\
&\times \Big[\partial_V \langle n_{ks}(m,V)\rangle \partial_V \langle n_{k's'}(m,V)\rangle - \partial_V \langle n_{k\bar{s}}(-m,V)\rangle \partial_V \langle n_{k'\bar{s}'}(-m,V)\rangle\Big]_{V=0} dE \\
&+ \frac{1}{4}\frac{e}{h}\int_{-\infty}^{\infty} f_0' \sum_{k,s}\partial_{ks} T_{\mathrm{LR}}(m, V=0)\Big[\partial_V^2 \Delta n_{ks}(m, V=0)\Big] dE.
\end{aligned} \tag{3.19}$$

To simplify the expression we used the expressions:

$$\begin{aligned}
\partial_{\langle n_{ks}(m,V=0)\rangle} T_{\mathrm{LR}}(m, V=0) &= \partial_{\langle n_{k\bar{s}}(-m,V=0)\rangle} T_{\mathrm{LR}}(-m, V=0), \\
\partial_{\langle n_{ks}(m,V=0)\rangle}\partial_{\langle n_{k's'}(m,V=0)\rangle} T_{\mathrm{LR}}(m, V=0) &= \partial_{\langle n_{k\bar{s}}(-m,V=0)\rangle}\partial_{\langle n_{k'\bar{s}'}(-m,V=0)\rangle} T_{\mathrm{LR}}(-m, V=0).
\end{aligned} \tag{3.20}$$

Furthermore we adopted the notation $\partial_{\langle n_{ks}(m,V=0)\rangle} \equiv \partial_{ks}$ and used that $\partial_{\langle n_{ks}(m,V=0)\rangle} = \partial_{\langle n_{k\bar{s}}(-m,V=0)\rangle}$ as discussed in sec. 3.6.1.

Comparing non-linear coefficients

In section 3.6.1 we show that: $\partial_{ks}\partial_{k's'} T_{\mathrm{LR}}(m, V=0) = U^2 T^{(2)}_{ks,k's'}(m) \propto U^2$ and $\partial_{ks} T_{\mathrm{LR}}(m, V=0) = U T^{(2)}_{ks}(m) \propto U$. For small bias we expect $\partial_V \langle n_{ks}(m, V=0)\rangle, \partial_V \langle n_{k\bar{s}}(-m, V=0)\rangle$ to vary approximately linear in bias voltage ($\partial_V^2 n_{ks}(\pm m) \propto 0$). Let us further assume symmetric capacitive coupling to the leads $\eta = 1/2$ then the ratio between $\Delta G_3(m)$ and $\Delta G_2(m)$ is given by;

$$\Delta G_3(m)/\Delta G_2(m) \propto U. \tag{3.21}$$

Transmission derivatives

In the previous section we encountered the derivatives: $\sum_{k,s}\partial_{ks} T_{\mathrm{LR}}(m, V=0)$ and $\sum_{k,k',s',s}\partial_{k's'}\partial_{ks} T_{\mathrm{LR}}(m, V=0)$, where we adopted the notation $\partial_{\langle n_{ks}(m,V=0)\rangle} = \partial_{ks}$. Here we investigate how the derivatives of the transmission scale with the interaction strength U in the HFA and HIA.

Hartree Fock

We use $\frac{\partial}{\partial x}\mathbf{A}^{-1} = -\mathbf{A}^{-1}\frac{\partial \mathbf{A}}{\partial x}\mathbf{A}^{-1}$ and that in the HFA Green's function (eq. (3.9)) at $V=0$ is given by: $\mathbf{G}_0^{\pm}(\epsilon, \mathbf{n}(m, V=0), m) = \Big[\mathbf{I}\epsilon - \mathbf{H}_0 - U\mathbf{n}(m, V=0) \pm \frac{i}{2}\boldsymbol{\Gamma}(m)\Big]^{-1}$. The derivative ∂_{ks} only acts on the electron densities:

$$\partial_{ks}\mathbf{G}_0^{\pm} = U\mathbf{G}_0^{\pm}\mathbf{X}^{ks}\mathbf{G}_0^{\pm}. \tag{3.22}$$

Where we define $\mathbf{X}^{ks} = \sum_{k',s'} \frac{\partial\langle n_{k'\bar{s}'}(m,V=0)\rangle}{\partial\langle n_{ks}(m,V=0)\rangle}\hat{n}_{k's'} = \hat{n}_{k\bar{s}}$. This is a diagonal matrix with only one non-zero element i.e. $\mathbf{X}^{k\uparrow} = \mathrm{diag}(0,0,..,1,0,...,0)$ and $\mathbf{X}^{k\downarrow} = \mathrm{diag}(0,0,..,0,1,...,0)$. The first derivative of the transmission then becomes:

$$\begin{aligned}\partial_{ks}T_{\mathrm{LR}}(m,V=0) &= U\mathrm{Tr}\Big[\mathbf{X}^{ks}\Big(\mathbf{G}_0^+\mathbf{\Gamma}_{\mathrm{R}}\mathbf{G}_0^-\mathbf{\Gamma}_{\mathrm{L}}(m)\mathbf{G}_0^+ + h.c.\Big)\Big]\\ &= UT^{(1)}_{ks}(m,V=0) \propto U.\end{aligned} \tag{3.23}$$

Now we continue with the second derivative using (3.22):

$$\begin{aligned}&\partial_{k's'}\partial_{ks}T_{\mathrm{LR}}(m,V=0)\\ &= U^2\mathrm{Tr}\Big[\mathbf{X}^{ks}\Big(\mathbf{G}_0^+\mathbf{X}^{k's'}\mathbf{G}_0^+\mathbf{\Gamma}_{\mathrm{R}}\mathbf{G}_0^-\mathbf{\Gamma}_{\mathrm{L}}(m)\mathbf{G}_0^+ + h.c.\Big)\Big]\\ &+ U^2\mathrm{Tr}\Big[\mathbf{X}^{ks}\Big(\mathbf{G}_0^+\mathbf{\Gamma}_{\mathrm{R}}\mathbf{G}_0^-\mathbf{X}^{k's'}\mathbf{G}_0^-\mathbf{\Gamma}_{\mathrm{L}}(m)\mathbf{G}_0^+ + h.c.\Big)\Big]\\ &+ U^2\mathrm{Tr}\Big[\mathbf{X}^{ks}\Big(\mathbf{G}_0^+\mathbf{\Gamma}_{\mathrm{R}}\mathbf{G}_0^-\mathbf{\Gamma}_{\mathrm{L}}(m)\mathbf{G}_0^+\mathbf{X}^{k's'}\mathbf{G}_0^+ + h.c.\Big)\Big]\\ &= U^2\,T^{(2)}_{k's',ks}(m,V=0) \propto U^2\end{aligned} \tag{3.24}$$

This thus shows that $\partial_{k's'}\partial_{ks}T_{\mathrm{LR}}(m) \propto U^2$.

HUBBARD ONE

In the Hubbard One Approximation the Green's function is given by eq. (3.10). We rewrite it as $\mathbf{G}^+_{\mathrm{HIA}} = \mathbf{A}^{-1}\mathbf{B}$ where $\mathbf{A},\mathbf{B}$ are given by: $\mathbf{A} = \Big[(\epsilon\mathbf{I}-\mathbf{H}_{\mathrm{os}}-U\mathbf{I})(\epsilon\mathbf{I}-\mathbf{H}_0-\mathbf{\Sigma})-U\mathbf{n}(\mathbf{H}_{\mathrm{T}}+\mathbf{H}_{\mathrm{SOC}}+\mathbf{\Sigma})\Big]$ and $\mathbf{B} = \epsilon\mathbf{I}-\mathbf{H}_{\mathrm{os}}-U(\mathbf{I}-\mathbf{n})$. Taking the derivative with respect to the electron density of $\mathbf{G}^+_{\mathrm{HIA}}$ gives:

$$\partial_{ks}\mathbf{G}^+_{\mathrm{HIA}} = U\mathbf{A}^{-1}\Big[\mathbf{X}^{ks}\Big(\mathbf{H}_{\mathrm{T}}+\mathbf{H}_{\mathrm{SOC}}+\mathbf{\Sigma}\Big)\mathbf{G}^+_{\mathrm{HIA}}+\mathbf{X}^{ks}\Big] \tag{3.25}$$

$$\begin{aligned}\partial_{k's'}\partial_{ks}\mathbf{G}^+_{\mathrm{HIA}} &= U^2\mathbf{A}^{-1}\mathbf{X}^{k's'}\Big(\mathbf{H}_{\mathrm{T}}+\mathbf{H}_{\mathrm{SOC}}+\mathbf{\Sigma})\mathbf{A}^{-1}\Big[\mathbf{X}^{ks}\Big(\mathbf{H}_{\mathrm{T}}+\mathbf{H}_{\mathrm{SOC}}+\mathbf{\Sigma}\Big)\mathbf{G}^+_{\mathrm{HIA}}+\mathbf{X}^{ks}\Big]\\ &+U^2\mathbf{A}^{-1}\mathbf{X}^{ks}\Big(\mathbf{H}_{\mathrm{T}}+\mathbf{H}_{\mathrm{SOC}}+\mathbf{\Sigma}\Big)\mathbf{A}^{-1}\Big[\mathbf{X}^{k's'}\Big(\mathbf{H}_{\mathrm{T}}+\mathbf{H}_{\mathrm{SOC}}+\mathbf{\Sigma}\Big)\mathbf{G}^+_{\mathrm{HIA}}+\mathbf{X}^{k's'}\Big]\end{aligned} \tag{3.26}$$

The first derive of the transmission with respect to the electron density is given by:

$$\partial_{ks}T_{\mathrm{LR}}(m,V=0) = \mathrm{Tr}\Big[\mathbf{\Gamma}_{\mathrm{L}}(m)\partial_{ks}\mathbf{G}^+_{\mathrm{HIA}}\mathbf{\Gamma}_{\mathrm{R}}\mathbf{G}^-_{\mathrm{HIA}}+\mathbf{\Gamma}_{\mathrm{L}}(m)\mathbf{G}^+_{\mathrm{HIA}}\mathbf{\Gamma}_{\mathrm{R}}\partial_{ks}\mathbf{G}^-_{\mathrm{HIA}}\Big] \propto U, \tag{3.27}$$

and with eq. (3.25) we see it is proportional to U. The second derivative of the transmission with respect to the electron density is given by:

$$\begin{aligned}\partial_{k's'}\partial_{ks}T_{\mathrm{LR}}(m,V=0) = \mathrm{Tr}\Big[&\mathbf{\Gamma}_{\mathrm{L}}(m)\partial_{k's'}\partial_{ks}\mathbf{G}^+_{\mathrm{HIA}}\mathbf{\Gamma}_{\mathrm{R}}\mathbf{G}^-_{\mathrm{HIA}}+\mathbf{\Gamma}_{\mathrm{L}}(m)\partial_{ks}\mathbf{G}^+_{\mathrm{HIA}}\mathbf{\Gamma}_{\mathrm{R}}\partial_{k's'}\mathbf{G}^-_{\mathrm{HIA}}\\ &+\mathbf{\Gamma}_{\mathrm{L}}(m)\partial_{k's'}\mathbf{G}^+_{\mathrm{HIA}}\mathbf{\Gamma}_{\mathrm{R}}\partial_{ks}\mathbf{G}^-_{\mathrm{HIA}}+\mathbf{\Gamma}_{\mathrm{L}}(m)\mathbf{G}^+_{\mathrm{HIA}}\mathbf{\Gamma}_{\mathrm{R}}\partial_{k's'}\partial_{ks}\mathbf{G}^-_{\mathrm{HIA}}\Big] \propto U^2,\end{aligned} \tag{3.28}$$

and with eqs. (3.25),(3.26) we see it is proportional to U^2.

3.6.2. DERIVATION OF ELECTRON GREEN'S FUNCTION

In this section the Green's function with Coulomb interactions will be derived in the Hartree-Fock and Hubbard One Approximation. A derivation of these Green's functions is done in the work of Haug and Jauho for a system *without* spin-orbit coupling while the novelty in this section is that we derive these Green's functions for a system *with* spin-orbit coupling.

This section is structured as follows, in 3.6.2 we will define conventions for our Fourier transforms, in 3.6.2 we will give a short introduction on Green's function, in 3.6.2 we will introduce the equation of motion technique, in 3.6.2 we will define the Hamiltonian, in 3.6.2 we will derive the equation of motion for the retarded Green's function, in sec. 3.6.2 we will solve the retarded Green's function in the Hartree-Fock approximation and in sec. 3.6.2 we will solve the retarded Green's function in the Hubbard One approximation.

DEFINITIONS

We define the Fourier transforms conventions:

$$\mathscr{F}(f(t)) \equiv f(\omega) = \int_{-\infty}^{\infty} e^{i\omega t} f(t)dt = \int_{-\infty}^{\infty} e^{i\frac{\epsilon}{\hbar}t} f(t)dt = f(\epsilon), \tag{3.29}$$

$$\mathscr{F}(f(\omega)) \equiv f(t) = \frac{1}{2\pi}\int_{-\infty}^{\infty} e^{-i\omega t} f(\omega)d\omega = \frac{1}{2\pi\hbar}\int_{-\infty}^{\infty} e^{-i\frac{\epsilon}{\hbar}t} f(\epsilon)d\epsilon. \tag{3.30}$$

Equation (3.30) implies that: $\mathscr{F}(i\hbar\dot{f}(t)) = \epsilon f(\epsilon)$. We define $[A,B]_{\pm} \equiv AB \pm BA$. From this definition we define the anti-commutator: $\{A,B\} \equiv [A,B]_{+}$ and the commutator: $[A,B] \equiv [A,B]_{-}$.

GREEN'S FUNCTION

The Green's function in the time domain is defined as the time ordered product of a creation and annihilation operator:

$$G_{\alpha s,\beta s'}(t-t') = -\frac{i}{\hbar}\langle T\{c_{\alpha s}(t)c^{\dagger}_{\beta s'}(t')\}\rangle. \tag{3.31}$$

Here $c^{\dagger}_{\alpha s}$ and $c_{\alpha s}$ are the creation and annihilation operators respectively, the Greek indices α,β label sites and roman labels s,s' label spin. Throughout this chapter we will only consider fermionic operators these satisfy anti-commutation relations:

$$\{c_{\alpha s}, c^{\dagger}_{\beta s'}\} = \delta_{\alpha\beta}\delta_{ss'}, \tag{3.32}$$

$$\{c_{\alpha s}, c_{\beta s'}\} = 0 = \{c^{\dagger}_{\alpha s}, c^{\dagger}_{\beta s'}\}. \tag{3.33}$$

We can write the Green's function as:

$$G(t-t') = \Theta(t-t')G^{>}(t-t') + \Theta(t-t')G^{<}(t-t'). \tag{3.34}$$

Here $G^{>}(t-t')$ and $G^{<}(t-t')$ are the greater and lesser green's function respectively and $\Theta(x)$ is the Heaviside step function. Here greater and lesser refer to the time difference $t-t'$ being greater or lesser than zero. We identify:

$$G^{>}_{\alpha s,\beta s'}(t-t') = -\frac{i}{\hbar}\langle c_{\alpha s}(t) c^{\dagger}_{\beta s'}(t')\rangle, \tag{3.35}$$

$$G^{<}_{\alpha s,\beta s'}(t-t') = \frac{i}{\hbar}\langle c^{\dagger}_{\beta s'}(t') c_{\alpha s}(t)\rangle. \tag{3.36}$$

We will work with retarded and advanced Green's functions respectively:

$$G^{+}_{\alpha s,\beta s'}(t-t') = -\frac{i}{\hbar}\Theta(t-t')\langle\{c_{\alpha s}(t), c^{\dagger}_{\beta s'}(t')\}\rangle, \tag{3.37}$$

$$G^{-}_{\alpha s,\beta s'}(t-t') = \frac{i}{\hbar}\Theta(t'-t)\langle\{c_{\alpha s}(t), c^{\dagger}_{\beta s'}(t')\}\rangle. \tag{3.38}$$

Here retarded and advanced refer to an event happening at time t that is before time t' ($t > t'$) or after time t' respectively ($t < t'$). In the Fourier domain it can be shown that: $\boldsymbol{G}^{-}(\epsilon) = (\boldsymbol{G}^{+}(\epsilon))^{\dagger}$. The Green's functions in eqs. (3.35) - (3.38) are by their definition related as : $\boldsymbol{G}^{+} - \boldsymbol{G}^{-} = \boldsymbol{G}^{>} - \boldsymbol{G}^{<}$.

EQUATION OF MOTION TECHNIQUE

In the equation of motion technique we try to get a closed expression for the retarded,advanced Green's function. We start from the definitions of the retarded Green's function (3.37) and take the derivative with respect to t:

$$\begin{aligned} i\hbar\dot{G}^{+}_{\kappa s'',\chi s'''}(t-t') &= \delta(t-t')\langle\{c_{\kappa s''}(t), c^{\dagger}_{\chi s'''}(t')\}\rangle, \\ &\quad + \Theta(t-t')\langle\{\dot{c}_{\kappa s''}(t), c^{\dagger}_{\chi s'''}(t')\}\rangle. \end{aligned} \tag{3.39}$$

This equation is central to the equation of motion technique. In the equation above $\dot{c}_{\kappa s''}(t)$ appears. We can calculate the time derivative in the Heisenberg picture. In that picture the operators evolve in time and the eigenstates are stationary. The time derivative works on an operator $\boldsymbol{A}$ as:

$$i\hbar\dot{\boldsymbol{A}}(t) = [\boldsymbol{A}(t), \boldsymbol{H}]. \tag{3.40}$$

with $\boldsymbol{H}$ the Hamiltonian of the system. Given a specific Hamiltonian we can calculate $\dot{c}_{\kappa s''}(t)$ in eq. (3.39) via eq. (3.40).

COUPLED, INTERACTING SYSTEM

In this section we define our Hamiltonian. For a molecule that is coupled to leads and has on-site Coulomb interactions between opposite spins, the Hamiltonian is given by:

$$\begin{aligned} \boldsymbol{H} = &\sum_{\alpha s}\epsilon_{\alpha s} n_{\alpha s} + \frac{U}{2}\sum_{\alpha s} n_{\alpha s} n_{\alpha\bar{s}} \\ &+ \sum_{\alpha,\beta,s,\alpha\neq\beta} t_{\alpha\beta} c^{\dagger}_{\alpha s} c_{\beta s} + \sum_{\alpha,\beta,s,s',\alpha\neq\beta} v_{\alpha\beta,ss'} c^{\dagger}_{\alpha,s} c_{\beta,s'} \\ &+ \sum_{K}\sum_{\alpha,\beta,s,s'} V^{K}_{\alpha s',\beta s} c^{\dagger}_{\alpha s'} d^{K}_{\beta s} + V^{\dagger K}_{\alpha s',\beta s} d^{\dagger K}_{\beta s} c_{\alpha s'} + \sum_{K,\beta,s}\epsilon^{K}_{\beta,s} d^{\dagger K}_{\beta s} d^{K}_{\beta s} \end{aligned} \tag{3.41}$$

Here $c^\dagger_{\alpha s}$ and $c_{\alpha s}$ are the creation and annihilation operators on the molecule respectively. The on-site Hamiltonian is given by: $\boldsymbol{H}_{\mathrm{os}} = \sum_{\alpha s} \epsilon_{\alpha s} n_{\alpha s}$ with $\epsilon_{\alpha s}$ the on-site energy for spin s and $n_{\alpha s} = c^\dagger_{\alpha s} c_{\alpha s}$ the number operator. The Coulomb interaction gives rise to on-site interactions between opposite spins which is described by the Hamiltonian $\boldsymbol{H}_U = \frac{U}{2} \sum_{\alpha s} n_{\alpha s} n_{\alpha \bar{s}}$ here $\bar{s}$ indicates that spin s is flipped and U is the Coulomb interactions strength. The spin-independent hopping Hamiltonian is given by $\boldsymbol{H}_{\mathrm{T}} = \sum_{\alpha,\beta,s,\alpha\neq\beta} t_{\alpha\beta} c^\dagger_{\alpha s} c_{\beta s}$ where $t_{\alpha\beta}$ describes hopping between different sites. For purely real NN hopping we have that: $t_{\alpha\beta} = t(\delta_{\alpha,\beta+1} + \delta_{\beta,\alpha+1})$. The spin-orbit coupling gives rise to a spin-dependent hopping $\boldsymbol{H}_{\mathrm{SOC}} = \sum_{\alpha,\beta,s,s',\alpha\neq\beta} v_{\alpha\beta,ss'} c^\dagger_{\alpha,s} c_{\beta,s'}$. The operators $d^{\dagger K}_{\beta s}$ and $d^K_{\beta s}$ are the creation and annihilation operators of electrons in lead K respectively. The term $\boldsymbol{H}_{\text{lead-molecule}} = \sum_K \sum_{\alpha,\beta,s,s'} V^K_{\alpha s',\beta s} c^\dagger_{\alpha s'} d^K_{\beta s} + h.c.$ describes the coupling between electrons on the different leads and on the molecule and $\boldsymbol{H}_{\text{lead}} = \sum_{\beta,s} \epsilon^K_{\beta s} d^{\dagger K}_{\beta s} d^K_{\beta s}$ is the Hamiltonian of the lead K and $\epsilon^K_{\beta s}$ its on-site energy. The Hamiltonian of the molecule without interactions ($U = 0$) is defined as: $\boldsymbol{H}_0 = \boldsymbol{H}_{\mathrm{os}} + \boldsymbol{H}_{\mathrm{T}} + \boldsymbol{H}_{\mathrm{SOC}}$.

RETARDED GREEN'S FUNCTION: EQUATION OF MOTION

Now that we have defined our Hamiltonian we first compute time-derivatives of the annihilation operators in the molecule and on the lead $\dot{c}_{\kappa s''}, \dot{d}^K_{\kappa s''}$ via (3.41) and (3.40), then we will obtain the equation of motion for the Green's functions.

Time - derivatives of operators

i) For electrons in the molecule we have:

$$i\hbar \dot{c}_{\kappa s''} = [c_{\kappa s''}, \boldsymbol{H}] = \left[\epsilon_{\kappa s''} + U n_{\kappa \bar{s}''}\right] c_{\kappa s''} + \sum_{\beta} t_{\kappa\beta} c_{\beta s''} + \sum_{\beta,s} v_{\kappa\beta,s''s} c_{\beta,s} + \sum_{K,\beta s} V^K_{\kappa s'',\beta s} d^K_{\beta s}. \tag{3.42}$$

ii) The time derivative of the operators in the lead are given by:

$$i\hbar \dot{d}^K_{\kappa s''} = [d^K_{\kappa s''}, \boldsymbol{H}] = \epsilon^K_{\kappa s''} d^K_{\kappa s''} + \sum_{\alpha,s'} (V^{\dagger K}_{\alpha s',\kappa s''}) c_{\alpha s'}. \tag{3.43}$$

Green's Functions

In the equation of motion of the retarded Green's function (eq. (3.39)) we replace $\dot{c}_{\kappa s''}$ by eq. (3.42) and we Fourier transform on both sides with respect to $t - t'$. This results in the following expression:

$$\begin{aligned} &\left[\epsilon - \epsilon_{\kappa s''}\right] G^+_{\kappa s'',\chi s'''}(\epsilon) - \sum_{K,\beta s} V^K_{\kappa s'',\beta s} G^{+,K}_{\beta s,\chi s'''}(\epsilon) - \sum_{\beta} t_{\kappa\beta} G^+_{\beta s'',\chi s'''}(\epsilon) - \sum_{\beta s} v_{\kappa\beta,s''s} G^+_{\beta s,\chi s'''}(\epsilon) \\ &= \delta_{\kappa\chi} \delta_{s''' s''} + U G^{+2}_{\kappa \bar{s}'',\kappa s'',\chi s'''}(\epsilon). \end{aligned} \tag{3.44}$$

Here we define:

$$G^{+2}_{\kappa \bar{s}'',\kappa s'',\chi s'''}(t - t') = -\frac{i}{\hbar} \Theta(t - t') \langle \{ n_{\kappa \bar{s}''}(t) c_{\kappa s''}(t), c^\dagger_{\chi s'''}(t') \} \rangle, \tag{3.45}$$

$$G^{+,K}_{ab,cd}(t - t') = -\frac{i}{\hbar} \Theta(t - t') \langle \{ d^K_{ab}(t), c^\dagger_{cd}(t') \} \rangle, \tag{3.46}$$

with $G^{+2}_{\kappa\bar{s}'',\kappa s'',\chi s'''}(\epsilon)$ and $G^{+,K}_{ab,cd}(\epsilon)$ the respective Fourier transforms.

To solve for $G^{+,K}_{ab,cd}(\epsilon)$ we first take a derivative with respect to t of eq. (3.46) and use eq. (3.43) for $\dot{d}^K_{ab}(t)$, then we Fourier transform and solve to to find: $G^{+,K}_{ab,cd}(\epsilon) = \sum_{ef} \frac{V^{K*}_{ef,ab}}{(\epsilon-\epsilon^K_{ab})} G^{+}_{ef,cd}(\epsilon)$. We then use this to obtain:

$$\sum_{K,\beta s} V^K_{\kappa s'',\beta s} G^{+,K}_{\beta s,\chi s'''}(\epsilon) = \sum_{K,ef} \Big(\sum_{\beta s} \frac{V^K_{\kappa s''\beta s} V^{K*}_{ef,\beta s}}{\epsilon - \epsilon^K_{\beta s}} \Big) G^{+}_{ef,\chi s'''}(\epsilon) = \sum_{K,ef} \Sigma^K_{\kappa s'',ef} G^{+}_{ef,\chi s'''}(\epsilon). \quad (3.47)$$

Where we define:

$$\Sigma^K_{ab,cd}(\epsilon) = \sum_{\chi\beta} \frac{V^K_{ab,\chi\beta} V^{K*}_{cd,\chi\beta}}{\epsilon - \epsilon^K_{\chi\beta}}, \quad (3.48)$$

as the retarded self-energy of lead K. It is common to split the retarded self energy into an imaginary and a real part:

$$\Sigma^K_{ab,cd}(\epsilon) = \Lambda_{ab,cd}(\epsilon) - \frac{i}{2}\Gamma_{ab,cd}(\epsilon), \quad (3.49)$$

where $\Lambda_{ab,cd}(\epsilon)$ and $\Gamma_{ab,cd}(\epsilon)$ are real numbers. Now eq. (3.44) becomes:

$$\Big[\epsilon - \epsilon_{\kappa s''}\Big] G^{+}_{\kappa s'',\chi s'''}(\epsilon) - \sum_{K,ef} \Sigma^K_{\kappa s'',ef} G^{+}_{ef',\chi s'''}(\epsilon) - \sum_{\beta} t_{\kappa\beta} G^{+}_{\beta s'',\chi s'''}(\epsilon) - \sum_{\beta s} v_{\kappa\beta,s''s} G^{+}_{\beta s,\chi s'''}(\epsilon)$$
$$= \delta_{\kappa\chi}\delta_{s'''s''} + U G^{+2}_{\kappa\bar{s}'',\kappa s'',\chi s'''}(\epsilon). \quad (3.50)$$

HARTREE - FOCK APPROXIMATION

Normally in the Hartree-Fock approximation the second order and first order Greens function are related as:

$$G^{+2}_{\kappa\bar{s}'',\kappa s'',\chi s'''}(\epsilon) = \langle n_{\kappa\bar{s}''}\rangle G^{+}_{\kappa s'',\chi s'''}(\epsilon). \quad (3.51)$$

We do this to cut of the hierarchy of the Green's function. Physically it means that you neglect correlations between all occupation numbers. Equation (3.51) is the result of considering the Wick contraction of the first two equal time operators: $c^\dagger_{\kappa\bar{s}''} c_{\kappa\bar{s}''} c_{\kappa s''}$ in eq. (3.45). However we can also consider the contraction of the first with the third (note that $\langle c_{ab} c_{ef}\rangle = 0$) resulting in:

$$c^\dagger_{\kappa\bar{s}''} c_{\kappa\bar{s}''} c_{\kappa s''} = \langle n_{\kappa\bar{s}''}\rangle c_{\kappa s''} - \langle c^\dagger_{\kappa\bar{s}''} c_{\kappa s''}\rangle c_{\kappa\bar{s}''}. \quad (3.52)$$

The expectation value $\langle c^\dagger_{\kappa\bar{s}''} c_{\kappa s''}\rangle$ is nonzero in the presence of spin-orbit coupling (but vanishes if the spin-orbit coupling is set to zero). Thus we can approximate the second order Green's function as:

$$G^{+2}_{\kappa\bar{s}'',\kappa s'',\chi s'''}(\epsilon) = \langle n_{\kappa\bar{s}''}\rangle G^{+}_{\kappa s'',\chi s'''}(\epsilon) - \langle c^\dagger_{\kappa\bar{s}''} c_{\kappa s''}\rangle G^{+}_{\kappa\bar{s}'',\chi s'''}(\epsilon). \quad (3.53)$$

for a system with spin-orbit coupling. We now substitute eq. (3.53) into eq. (3.50) to find the equation of motion:

$$\begin{aligned}&\Big[\epsilon-\epsilon_{\kappa s''}\Big]G^{+}_{\kappa s'',\chi s'''}(\epsilon)-U\langle n_{\kappa\bar{s}''}\rangle G^{+}_{\kappa s'',\chi s'''}(\epsilon)+U\langle c^{\dagger}_{\kappa\bar{s}''}c_{\kappa s''}\rangle G^{+}_{\kappa\bar{s}'',\chi s'''}(\epsilon)\\&+\sum_{K,e,f}\Sigma^{K}_{\kappa s'',ef}G^{+}_{ef,\chi s'''}(\epsilon)-\sum_{\beta}t_{\kappa\beta s''}G^{+}_{\beta s',\chi s'''}(\epsilon)-\sum_{\beta s}v_{\kappa\beta s''s}G^{+}_{\beta s,\chi s'''}(\epsilon)=\delta_{\kappa\chi}\delta_{s'''s''}.\end{aligned}\tag{3.54}$$

We can now solve this equation for $\mathbf{G}^{+}$. The retarded Green's function in matrix notation is given by:

$$\mathbf{G}^{+}_{\mathrm{HFA}}(\epsilon)=\Big[\epsilon\mathbf{1}-\boldsymbol{H}_0-U\boldsymbol{n}+U\boldsymbol{\rho}-\boldsymbol{\Sigma}\Big]^{-1}.\tag{3.55}$$

Here $\boldsymbol{\Sigma}=\sum_K\boldsymbol{\Sigma}^K$ is the sum of all retarded self-energies of the leads, $\boldsymbol{n}=\sum_{\kappa s}\langle n_{\kappa\bar{s}}\rangle n_{\kappa s}$ is a diagonal matrix with the electron densities on the diagonal and $\boldsymbol{\rho}=\sum_{\kappa s}\langle c^{\dagger}_{\kappa\bar{s}}c_{\kappa s}\rangle c^{\dagger}_{\kappa s}c_{\kappa\bar{s}}$ is an off-diagonal matrix.

The term $\boldsymbol{\rho}$ describes hopping between up and down electrons on the same site, therefore it can have an imaginary and a real part: $\langle c^{\dagger}_{\kappa\bar{s}''}c_{\kappa s''}\rangle=a+ib$ and its complex conjugate $a-ib$ which makes that $\boldsymbol{\rho}$ is proportional to the Pauli matrices: $a\sigma_x+b\sigma_y$. Thus we can interpret this term as an on-site spin in the x and y direction. That is why some references call this the non-collinear Hubbard model,[47] since the spin is not parallel to z direction. Therefore we call the Green's function in eq. (3.55) the non-collinear Hartree Fock Green's function.

The Hartree Fock Green's function is usually made particle-hole symmetric by subtracting a factor of 1/2 from the electron densities: $U\Big(\langle n_{\kappa\bar{s}}\rangle-\frac{1}{2}\Big)n_{\kappa s}$. For a bipartite lattice the density of states are symmetric around the energy $E=0$. When the factor of 1/2 is omitted the density of states are symmetric around the energy $E=\frac{U}{2}$.

HUBBARD ONE APPROXIMATION

In the Hubbard One approximation we solve for $G^{+2}_{\kappa\bar{s}'',\kappa s'',\chi s'''}(\epsilon)$ instead of approximating it (via eq. (3.53)). A solution is sought via the equation of motion of $G^{+2}_{\kappa\bar{s}'',\kappa s'',\chi s'''}(\epsilon)$, which is obtained by taking the time derivative of eq. (3.45) with respect to t:

$$\begin{aligned}\dot{G}^{+2}_{\kappa\bar{s}'',\kappa s'',\chi s'''}(t-t')=&-\frac{i}{\hbar}\delta(t-t')\langle\{n_{\kappa\bar{s}''}(t)c_{\kappa s''}(t),c^{\dagger}_{\chi s'''}(t')\}\rangle\\&-\frac{i}{\hbar}\Theta(t-t')\langle\{\dot{n}_{\kappa\bar{s}''}(t)c_{\kappa s''}(t),c^{\dagger}_{\chi s'''}(t')\}\rangle\\&-\frac{i}{\hbar}\Theta(t-t')\langle\{n_{\kappa\bar{s}''}(t)\dot{c}_{\kappa s''}(t),c^{\dagger}_{\chi s'''}(t')\}\rangle.\end{aligned}\tag{3.56}$$

In eq. (3.56) the time derivative of the number operator $\dot{n}_{\kappa\bar{s}''}(t)$ is given by:

$$\begin{aligned}\dot{n}_{\kappa\bar{s}''}(t) &= [n_{\kappa\bar{s}''}, \boldsymbol{H}]\\ &= \sum_{\beta} t_{\kappa\beta} c^{\dagger}_{\kappa\bar{s}''} c_{\beta\bar{s}''} - t_{\beta\kappa} c^{\dagger}_{\beta\bar{s}''} c_{\kappa\bar{s}''}\\ &+ \sum_{\beta,s'} v_{\kappa\beta,\bar{s}''s'} c^{\dagger}_{\kappa\bar{s}''} c_{\beta s'} - v_{\beta\kappa,s'\bar{s}''} c^{\dagger}_{\beta s'} c_{\kappa\bar{s}''}\\ &+ \sum_{K}\sum_{\beta,s} V^{K}_{\kappa\bar{s}'',\beta s} c^{\dagger}_{\kappa\bar{s}''} d^{K}_{\beta s} - V^{\dagger K}_{\kappa\bar{s}'',\beta s} d^{\dagger K}_{\beta s} c_{\kappa\bar{s}''}.\end{aligned} \tag{3.57}$$

In the original work of Hubbard[48] the time derivative of the number operator is set to zero ($\dot{n}_{\kappa\bar{s}''}(t) = 0$). We will not put that into eq. (3.56) directly (for reasons that will become clear later). In eq. (3.56) we substitute eqs. (3.42) for $\dot{c}_{\kappa s''}(t)$ and eq. (3.57) for $\dot{n}_{\kappa\bar{s}''}(t)$ and Fourier transform the resulting equation with respect to $t - t'$:

$$\begin{aligned}(\epsilon - \epsilon_{\kappa s''}) G^{+2}_{\kappa\bar{s}'',\kappa s'',\chi s'''} &= \delta_{\kappa\chi}\delta_{s''s'''}\langle n_{\kappa\bar{s}''}\rangle - \delta_{\kappa\chi}\delta_{\bar{s}''s'''}\langle c^{\dagger}_{\kappa\bar{s}''} c_{\kappa s''}\rangle\\ &+ U G^{+3}_{\kappa s''\chi s'''}(\epsilon)\\ &+ \sum_{\beta} t_{\kappa\beta} G^{+2}_{\kappa\bar{s}'',\beta s'',\chi s'''} + \sum_{\beta s} v_{\kappa\beta,ss''} G^{+2}_{\kappa\bar{s}'',\beta s,\chi s'''}\\ &+ \sum_{K,\beta s'} V^{K}_{\kappa s'',\beta s'} G^{+2,K}_{\kappa\bar{s}'',\beta s',\chi s'''}\\ &+ \sum_{\beta} t_{\kappa\beta} \overline{G}^{+2}_{\kappa\bar{s}'',\beta\bar{s}'',\kappa s'',\chi s'''} - t_{\beta\kappa} \overline{G}^{+2}_{\beta\bar{s}'',\kappa\bar{s}'',\kappa s'',\chi s'''}\\ &+ \sum_{\beta,s'} v_{\kappa\beta,\bar{s}''s'} \overline{G}^{+2}_{\kappa\bar{s}'',\beta s',\kappa s'',\chi s'''} - v_{\beta\kappa,s'\bar{s}''} \overline{G}^{+2}_{\beta s',\kappa\bar{s}'',\kappa s'',\chi s'''}\\ &+ \sum_{K}\sum_{\beta,s} V^{K}_{\kappa\bar{s}'',\beta s} \overline{G}^{+2,K}_{\kappa\bar{s}'',\beta s,\kappa s'',\chi s'''} - (V^{K}_{\kappa\bar{s}'',\beta s})^{\dagger} \overline{G}^{-2,K}_{\beta s,\kappa\bar{s}'',\kappa s'',\chi s'''}.\end{aligned} \tag{3.58}$$

Note the appearance of $\langle c^{\dagger}_{\kappa\bar{s}''} c_{\kappa s''}\rangle$ which usually is set to zero[42,48] but not here (due to spin-orbit coupling). Furthermore we define:

$$G^{+2}_{\kappa s'',ef,\chi s'''}(t-t') = -\frac{i}{\hbar}\Theta(t-t')\langle\{n_{\kappa\bar{s}''}(t) c_{ef}(t), c^{\dagger}_{\chi s'''}(t')\}\rangle, \tag{3.59}$$

$$G^{+2,K}_{\kappa\bar{s}'',\beta s',\chi s'''}(t-t') = -\frac{i}{\hbar}\Theta(t-t')\langle\{n_{\kappa\bar{s}''}(t) d^{K}_{\beta s'}(t), c^{\dagger}_{\chi s'''}(t')\}\rangle, \tag{3.60}$$

$$\overline{G}^{+2}_{ab,cd,ef,gh}(t-t') = -\frac{i}{\hbar}\Theta(t-t')\langle\{c^{\dagger}_{ab}(t) c_{cd}(t) c_{ef}(t), c^{\dagger}_{gh}(t')\}\rangle, \tag{3.61}$$

$$\overline{G}^{+2,K}_{ab,cd,ef,gh}(t-t') = -\frac{i}{\hbar}\Theta(t-t')\langle\{c^{\dagger}_{ab}(t) d^{K}_{cd}(t) c_{ef}(t), c^{\dagger}_{gh}(t')\}\rangle, \tag{3.62}$$

$$\overline{G}^{-2,K}_{ab,cd,ef,gh}(t-t') = -\frac{i}{\hbar}\Theta(t-t')\langle\{d^{\dagger K}_{ab}(t) c_{cd}(t) c_{ef}(t), c^{\dagger}_{gh}(t')\}\rangle, \tag{3.63}$$

with $G^{+2}_{\kappa\bar{s}'',ef,\chi s'''}(\epsilon)$, $G^{+2,K}_{\kappa\bar{s}'',\beta s',\chi s'''}(\epsilon)$,$\overline{G}^{+2}_{ab,cd,ef,gh}(\epsilon)$, $\overline{G}^{+2,K}_{ab,cd,ef,gh}(\epsilon)$ and $\overline{G}^{-2,K}_{ab,cd,ef,gh}(\epsilon)$ as the respective Fourier transforms. The third order Green's function is defined as:

$$G^{3+}_{\kappa s'',\chi s'''}(t-t') = -\frac{i}{\hbar}\Theta(t-t')\langle\{n_{\kappa\bar{s}''}(t)n_{\kappa\bar{s}''}(t)c_{\kappa s''}(t), c(t')^{\dagger}_{\chi s'''}\}\rangle, \tag{3.64}$$

and $G^{3+}_{\kappa s'',\chi s'''}(\epsilon)$ its Fourier transform. For fermions working on a number state we have that $n^2_{\kappa\bar{s}''} = n_{\kappa\bar{s}''}$, thus we conclude $G^{3+}_{\kappa s'',\chi s'''}(\epsilon) = G^{+2}_{\kappa\bar{s}'',\kappa s'',\chi s'''}(\epsilon)$. Now in order to solve eq. 3.58 in terms of $G^{+2}_{\kappa\bar{s}'',\kappa s'',\chi s'''}$ we need to approximate.

Approximations

As an approximation we will consider all non-zero possible Wick contractions of the equal time operators in eqs. (3.59) -(3.63):

$$G^{+2}_{\kappa\bar{s}'',\alpha s,\chi s'''} = \langle n_{\kappa\bar{s}''}\rangle G^{+}_{\alpha s,\chi s'''} - \langle c^{\dagger}_{\kappa\bar{s}''}c_{\alpha s}\rangle G^{+}_{\kappa\bar{s}'',\chi s'''}, \tag{3.65}$$

$$G^{+2,K}_{\kappa\bar{s}'',\beta s',\chi s'''} = \langle n_{\kappa\bar{s}''}\rangle G^{+,K}_{\beta s',\chi s'''} - \langle c^{\dagger}_{k\bar{s}''}d^{K}_{\beta s'}\rangle G^{+}_{\kappa\bar{s}'',\chi s'''}, \tag{3.66}$$

$$\overline{G}^{+2}_{ab,cd,ef,gh} = \langle c^{\dagger}_{ab}c_{cd}\rangle G^{+}_{ef,gh} - \langle c^{\dagger}_{ab}c_{ef}\rangle G^{+}_{cd,gh}, \tag{3.67}$$

$$\overline{G}^{+2,K}_{ab,cd,ef,gh} = -\langle c^{\dagger}_{ab}c_{ef}\rangle G^{+,K}_{cd,gh} + \langle c^{\dagger}_{ab}d_{cd}\rangle G^{+}_{ef,gh}, \tag{3.68}$$

$$\overline{G}^{-2,K}_{ab,cd,ef,gh} = \langle d^{\dagger}_{ab}c_{cd}\rangle G^{+}_{ef,gh} - \langle d^{\dagger}_{ab}c_{ef}\rangle G^{+}_{cd,gh}. \tag{3.69}$$

Putting the approximations eqs. (3.65)-(3.69) into eq. (3.58) we obtain after some rearrangement:

$$\begin{aligned}
(\epsilon-\epsilon_{\kappa s''}-U)G^{+2}_{\kappa\bar{s}'',\kappa s'',\chi s'''} &= \delta_{\kappa\chi}\delta_{s''s'''}\langle n_{\kappa\bar{s}''}\rangle - \delta_{\kappa\chi}\delta_{\bar{s}''s'''}\langle c^{\dagger}_{\kappa\bar{s}''}c_{\kappa s''}\rangle \\
&+ \langle n_{\kappa\bar{s}''}\rangle\Big(\sum_{\beta} t_{\kappa\beta}G^{+}_{\beta s'',\chi s'''} + \sum_{\beta s} v_{\kappa\beta,ss''}G^{+}_{\beta s,\chi s'''} + \sum_{K,\beta s'} V^{K}_{\kappa s'',\beta s'}G^{+,K}_{\beta s',\chi s'''}\Big) \\
&- \langle c^{\dagger}_{\kappa\bar{s}''}c_{\kappa s''}\rangle\Big(\sum_{\beta} t_{\kappa\beta}G^{+}_{\beta\bar{s}'',\chi s'''} + \sum_{\beta,s'} v_{\kappa\beta,\bar{s}''s'}G^{+}_{\beta s',\chi s'''} + \sum_{K}\sum_{\beta s} V^{K}_{\kappa\bar{s}'',\beta s}G^{K}_{\beta s,\chi s'''}\Big) \\
&+ \Big[\sum_{\beta} t_{\beta\kappa}\langle c^{\dagger}_{\beta\bar{s}''}c_{\kappa s''}\rangle - t_{\kappa\beta}\langle c^{\dagger}_{\kappa\bar{s}''}c_{\beta s''}\rangle \\
&+ \sum_{\beta,s} v_{\beta\kappa,s\bar{s}''}\langle c^{\dagger}_{\beta s}c_{\kappa s''}\rangle - v_{\kappa\beta,ss''}\langle c^{\dagger}_{\kappa\bar{s}''}c_{\beta s}\rangle \\
&+ \sum_{K}\sum_{\beta,s}(V^{K}_{\kappa\bar{s}'',\beta s})^{\dagger}\langle d^{\dagger K}_{\beta s}c_{\kappa s''}\rangle - V^{K}_{\kappa s'',\beta s'}\langle c^{\dagger}_{k\bar{s}''}d^{K}_{\beta s'}\rangle\Big]G^{+}_{\kappa\bar{s}'',\chi s'''} \\
&+ \Big[\sum_{\beta} t_{\kappa\beta}\langle c^{\dagger}_{\kappa\bar{s}''}c_{\beta\bar{s}''}\rangle - t_{\beta\kappa}\langle c^{\dagger}_{\beta\bar{s}''}c_{\kappa\bar{s}''}\rangle \\
&+ \sum_{\beta,s}\langle c^{\dagger}_{\kappa\bar{s}''}c_{\beta s'}\rangle v_{\kappa\beta,\bar{s}''s} - v_{\beta\kappa,s\bar{s}''}\langle c^{\dagger}_{\beta s}c_{\kappa\bar{s}''}\rangle \\
&+ \sum_{K}\sum_{\beta,s} V^{K}_{\kappa\bar{s}'',\beta s}\langle c^{\dagger}_{\kappa\bar{s}''}d^{K}_{\beta s}\rangle - V^{\dagger K}_{\kappa\bar{s}'',\beta s}\langle d^{\dagger K}_{\beta s}c_{\kappa\bar{s}''}\rangle\Big]G^{+}_{\kappa s'',\chi s'''}.
\end{aligned} \tag{3.70}$$

The term in front of $G^{+}_{\kappa s'',\chi s'''}$ in eq. (3.70) is recognized as the expectation value of the time derivative of the number operator: $\langle\dot{n}_{\kappa s''}(t)\rangle$ (via eq. (3.57)). We set this expectation value to zero since in steady state the electron density is constant.

To show that the term in front of $G^{+}_{\kappa\bar{s}'',\chi s'''}$ in eq. (3.70) is zero we first calculate the time derivative of $c^{\dagger}_{\kappa\bar{s}''}(t)c_{\kappa s''}(t)$:

$$\begin{aligned}\frac{d}{dt}c^{\dagger}_{\kappa\bar{s}''}(t)c_{\kappa s''}(t) &= [c^{\dagger}_{\kappa\bar{s}''}c_{\kappa s''}, \boldsymbol{H}]\\ &= \sum_{\beta} t_{\kappa\beta}c^{\dagger}_{\kappa\bar{s}''}c_{\beta s''} - t_{\beta\kappa}c^{\dagger}_{\beta\bar{s}''}c_{\kappa s''}\\ &+ \sum_{\beta s} v_{\kappa\beta,ss''}c^{\dagger}_{\kappa\bar{s}''}c_{\beta s''} - v_{\beta\kappa,s\bar{s}''}c^{\dagger}_{\beta\bar{s}''}c_{\kappa s''}\\ &+ \sum_{K,\beta s} V^{K}_{\kappa s'',\beta s}c^{\dagger}_{\kappa\bar{s}''}d^{K}_{\beta s} - V^{\dagger K}_{\kappa\bar{s}'',\beta s}d^{K}_{\beta s}c_{\kappa s''},\end{aligned} \tag{3.71}$$

where we used that $\epsilon_{\alpha s} = \epsilon_{\alpha\bar{s}}$ (no magnetic field in the molecule). With the result in eq. (3.71) we see that the term in front of $G^{+}_{\kappa\bar{s}'',\chi s'''}$ in eq. (3.70) is equal to :$-\langle\frac{d}{dt}c^{\dagger}_{\kappa\bar{s}''}c_{\kappa s''}\rangle$. We set this term to zero as well since the average spin in the x, y direction will be fixed in steady state. Given these approximations we obtain the following equation of motion:

$$\begin{aligned}(\epsilon - \epsilon_{\kappa s''} - U)G^{+2}_{\kappa\bar{s}'',\kappa s'',\chi s'''} &= \langle n_{\kappa\bar{s}''}\rangle\delta_{\kappa\chi}\delta_{s''' s''} - \delta_{\kappa\chi}\delta_{\bar{s}'' s'''}\langle c^{\dagger}_{\kappa\bar{s}''}c_{\kappa s''}\rangle\\ &+ \langle n_{\kappa\bar{s}''}\rangle\Big(\sum_{\beta} t_{\kappa\beta}G^{+}_{\beta s'',\chi s'''} + \sum_{\beta s} v_{\kappa\beta,ss''}G^{+}_{\beta s,\chi s'''} + \sum_{K,ef}\Sigma^{K}_{\kappa s'',ef}G^{+}_{ef,\chi s'''}\Big)\\ &- \langle c^{\dagger}_{\kappa\bar{s}''}c_{\kappa s''}\rangle\Big(\sum_{\beta} t_{\kappa\beta}G^{+}_{\beta\bar{s}'',\chi s'''} + \sum_{\beta,s'} v_{\kappa\beta,\bar{s}'' s'}G^{+}_{\beta s',\chi s'''} + \sum_{K}\sum_{ef}\Sigma^{K}_{\kappa\bar{s}'',ef}G^{+}_{ef,\chi s'''}\Big).\end{aligned} \tag{3.72}$$

Where we also used eq. (3.47) and the definition of the retarded self energy (eq. (3.48)). Now we come back to reason why we did not put the approximation $\dot{n}_{\kappa\bar{s}''} = 0$ directly in (3.56). Had we done that, then the terms in front of $G^{+}_{\kappa s'',\chi s'''}$ and $G^{+}_{\kappa\bar{s}'',\chi s'''}$ could not have been recognized as $\langle\dot{n}_{\kappa s''}(t)\rangle$ and $-\langle\frac{d}{dt}c^{\dagger}_{\kappa\bar{s}''}c_{\kappa s''}\rangle$ respectively, because there would be correlators missing that otherwise would have come from $\dot{n}_{\kappa\bar{s}''}(t)$. Usually the relation: $\dot{n}_{\kappa\bar{s}''}(t) = 0$ is used directly and then (after some Wick contractions) individual correlators are set to zero. We point out that this 'usual' procedure results in the same equation of motion for G^{+2} if $\langle c^{\dagger}_{\kappa\bar{s}''}c_{\kappa s''}\rangle = 0$. We now solve for the retarded Green's function by via eqs. (3.50) and (3.72) which in matrix notation become:

$$(\epsilon\boldsymbol{I} - \boldsymbol{H}_0 - \boldsymbol{\Sigma})\boldsymbol{G}^{+} - U\boldsymbol{G}^{+2} = \boldsymbol{I}, \tag{3.73}$$

and:

$$\boldsymbol{G}^{+2} = \Big[(\epsilon\boldsymbol{I} - \boldsymbol{H}_{\text{os}} - U\boldsymbol{I})\Big]^{-1}\Big[(\boldsymbol{n} - \boldsymbol{\rho})\Big(\boldsymbol{I} + (\boldsymbol{H}_{\text{T}} + \boldsymbol{H}_{\text{SOC}} + \boldsymbol{\Sigma})\boldsymbol{G}^{+}\Big)\Big], \tag{3.74}$$

respectively. Substituting (3.74) into (3.73) and solving for $\boldsymbol{G}^{+}$ gives:

$$\begin{aligned}\boldsymbol{G}^{+}_{\text{HIA}}(\epsilon) = &\frac{1}{\Big[(\epsilon\boldsymbol{I} - \boldsymbol{H}_{\text{os}} - U\boldsymbol{I})(\boldsymbol{E} - \boldsymbol{H}_{\text{os}}) - \Big(\epsilon\boldsymbol{I} - \boldsymbol{H}_{\text{os}} - U(\boldsymbol{I} - \boldsymbol{n} + \boldsymbol{\rho})\Big)\Big(\boldsymbol{H}_{\text{T}} + \boldsymbol{H}_{\text{SOC}} + \boldsymbol{\Sigma}\Big)\Big]}\\ &\times\Big[\epsilon\boldsymbol{I} - \boldsymbol{H}_{\text{os}} - U(\boldsymbol{I} - \boldsymbol{n} + \boldsymbol{\rho})\Big].\end{aligned} \tag{3.75}$$

Which we will call the non-collinear Hubbard One Green's function. If the spin-orbit coupling is small we can set $\boldsymbol{\rho} = 0$ and the Green's function reduces to its well-known form [42].

Now follow some sanity checks. It is common to write the lesser, greater Green's function in the Fourier domain as:

$$\boldsymbol{G}^{<} = \boldsymbol{G}^{+}\Big[\sum_K \boldsymbol{\Gamma}^K f_K\Big]\boldsymbol{G}^{-}, \quad \boldsymbol{G}^{>} = \boldsymbol{G}^{+}\Big[\sum_K \boldsymbol{\Gamma}^K (1-f_K)\Big]\boldsymbol{G}^{-}, \tag{3.76}$$

with $\boldsymbol{\Gamma}^K = 2\mathrm{Im}[(\boldsymbol{\Sigma}^K)^{\dagger}]$ and f_K the Fermi-Dirac distribution of lead K. This implies that $\boldsymbol{G}^{>} - \boldsymbol{G}^{<} = \boldsymbol{i}\boldsymbol{G}^{+}\boldsymbol{\Gamma}\boldsymbol{G}^{-}$. By definition of the Green's function we should then find $\boldsymbol{G}^{>} - \boldsymbol{G}^{<} \equiv \boldsymbol{G}^{+} - \boldsymbol{G}^{-} = \boldsymbol{i}\boldsymbol{G}^{+}\sum_K \boldsymbol{\Gamma}^K \boldsymbol{G}^{-}$. To show that this we first rewrite the Green's function as:

$$\boldsymbol{G}^{+} = [\boldsymbol{g}_0^{-1} - \boldsymbol{\Sigma}]^{-1}, \tag{3.77}$$

with $\boldsymbol{g}_0^{-1} = \Big[\epsilon\boldsymbol{I} - \boldsymbol{H}_{\mathrm{os}} - U(\boldsymbol{I} - \boldsymbol{n} + \boldsymbol{\rho})\Big]^{-1}\Big[(\epsilon\boldsymbol{I} - \boldsymbol{H}_{\mathrm{os}} - U\boldsymbol{I})(\boldsymbol{E} - \boldsymbol{H}_{\mathrm{os}})\Big] - (\boldsymbol{H}_{\mathrm{T}} + \boldsymbol{H}_{\mathrm{SOC}})$. From the fact that $\epsilon\boldsymbol{I}, U\boldsymbol{I}, \boldsymbol{H}_{\mathrm{os}}$ are diagonal and $\boldsymbol{H}_{\mathrm{T}}, \boldsymbol{H}_{\mathrm{SOC}}$ are hermitian it follows that $\boldsymbol{g}_0^{-1} = (\boldsymbol{g}_0^{-1})^{\dagger}$. From this we can easily verify that: $\boldsymbol{G}^{+} - \boldsymbol{G}^{-} = \boldsymbol{i}\boldsymbol{G}^{+}\sum_K \boldsymbol{\Gamma}^K \boldsymbol{G}^{-}$ is satisfied. For small U we should retrieve the Hartree-Fock Green's function. We can expand $\boldsymbol{g}_0^{-1}$ to first order in U:

$$\boldsymbol{g}_0^{-1} = \boldsymbol{g}_0^{-1}|_{U=0} + U\partial_U \boldsymbol{g}_0^{-1}{}_{U=0} = \boldsymbol{E} - \boldsymbol{H}_{\mathrm{os}} - U(\boldsymbol{n} - \boldsymbol{\rho})_{U=0} - \boldsymbol{H}_{\mathrm{T}} - \boldsymbol{H}_{\mathrm{SOC}}. \tag{3.78}$$

Here we used $\frac{d\boldsymbol{A}^{-1}}{dx} = \boldsymbol{A}^{-1}\frac{d\boldsymbol{A}}{dx}\boldsymbol{A}^{-1}$ .Plugging the equation above back into eq. (3.77) $\boldsymbol{G}^{+} = \Big[\boldsymbol{E} - \boldsymbol{H}_{\mathrm{os}} - U(\boldsymbol{n} - \boldsymbol{\rho})_{U=0} - \boldsymbol{H}_{\mathrm{T}} - \boldsymbol{H}_{\mathrm{SOC}} - \boldsymbol{\Sigma}\Big]^{-1}$ which is identical to the non collinear Hartree Fock Green's function (eq. (3.55)) when $\boldsymbol{n}, \boldsymbol{\rho}$ are expanded to zeroth order in U. These two sanity checks support that the Green's function found eq. (3.75) is correct.

3.6.3. EVENNESS OR ODDNESS OF MAGNETOCURRENT

In this section we will present the results regarding the odd or even behaviour of $\Delta I(m, V)$. In order to quantify the degree to which a function is odd or even, we define the quantity $P(V)$:

$$P(V) = \frac{\int_0^V O[\Delta I(m, V')]^2 - E[\Delta I(m, V')]^2 dV'}{\int_0^V O[\Delta I(m, V')]^2 + E[\Delta I(m, V')]^2 dV'}. \tag{3.79}$$

Here $O[\Delta I(m, V')], E[\Delta I(m, V')]$ are the odd and even part of $\Delta I(m, V')$ in bias voltage respectively. For functions that are purely odd or even we have $P(V) = 1$ and $P(V) = -1$ respectively. If $P(V) > 1/4$ we say that $\Delta I(m, V)$ is odd, if $P(V) < -1/4$, $\Delta I(m, V)$ is even and if $|P(y)| \leq \frac{1}{4}$, then we say that $\Delta I(m, V)$ is neither odd nor even. For small V the errors on $\Delta I(m, V)$ are relatively large, therefore $P(V)$ is sensitive to these errors for small bias. Therefore we neglect $|\Delta I(m, V)| < 10^{-8}$. In fig. 3.2 we see the $P(V)$ parameter for the helical geometry in the HFA and HIA approximation. In fig. 3.2a $P(V)$ is plotted for $E_{\mathrm{F}} \neq \frac{U}{2}$ in the HFA. For $\frac{U}{t} = 0.1$ and for $\frac{U}{t} = 2$ the magnetocurrent is even for small bias and odd for large bias respectively. In fig. 3.2b) $P(V)$ is plotted for $E_{\mathrm{F}} \neq \frac{U}{2}$ in the HIA. Here the magnetocurrent is and odd function. The unclear symmetry of the magnetocurrent for $U/t = \frac{1}{2}$ and small bias we attribute to the relatively large numerical errors present in that range (especially for $\lambda = 10^{-3}$ where the signal is very weak). Since both $U/t, \lambda/t$ are small the magnetocurrent is expected to be small and its behaviour sensitive to numerical errors. In fig. 3.2c $P(V)$ is plotted for $E_\text{F} = \frac{U}{2}$ in the HFA and $\Delta I(m,V)$ is perfectly odd function of bias voltage for small U/t and dominantly odd for large U/t. In fig. 3.2d) $P(V)$ is plotted for $E_\text{F} = \frac{U}{2}$ in the HIA. We see that $\Delta I(m,V)$ is a pure odd function of bias voltage for large U/t and a dominantly odd function for small U/t. From fig. 3.2 we can conclude that the magnetocurrent is an odd function of bias voltage.

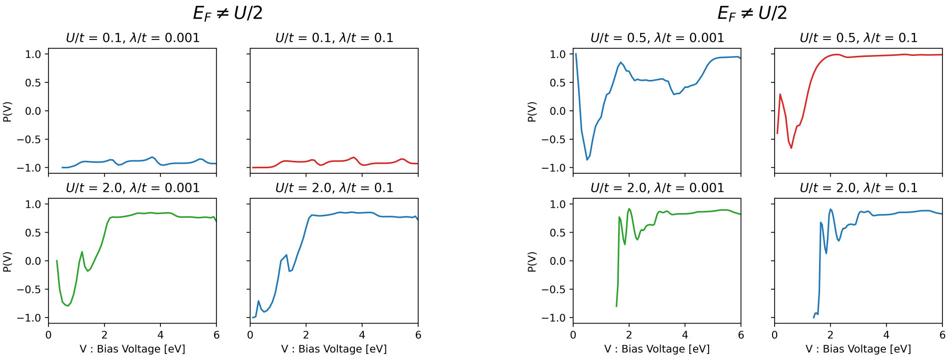

(a) HFA

(b) HIA

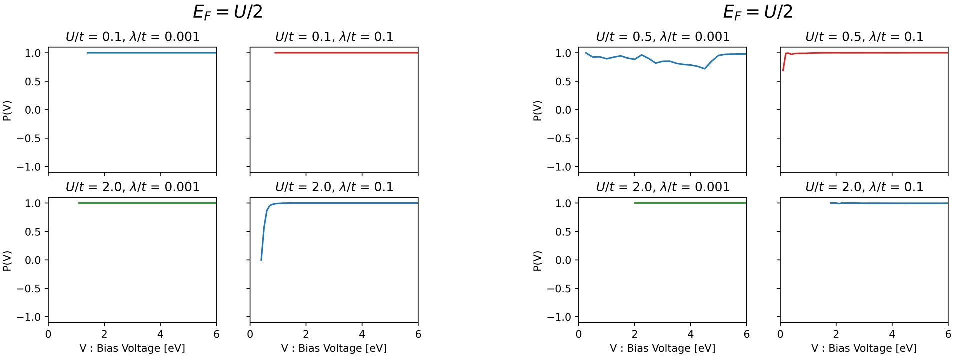

(c) HFA

(d) HIA

Figure 3.2: $P(V)$ for the the helical geometry. Asymmetric chemical potential **(a)** in the HFA, **(b)** in the HIA. Symmetric chemical potential: **(c)** in the HFA, **(d)** in the HIA.

3.6.4. Magnetic Stray fields

Theoretical work aimed at obtaining a finite magnetocurrent through on-site Coulomb interactions[1,28,49] or via the addition of Büttiker voltage probes[20] relies on the spin-orbit coupling of the molecules or the substrate. The work of our group indicates that that, for large values of the spin-orbit coupling parameter, the size of the effect is of the order of 0.1 %,[1,20,49] well below the size of the effect in experiments. The odd bias dependence found in experiment was reproduced by a model with NNN spin-orbit coupling and on-site Coulomb repulsion in the wide-band limit[1] and a model with NN spin-orbit coupling and on-site Coulomb repulsion for semi-infinite leads.[49] The spin-orbit coupling of the leads is often considered as the mechanism behind the CISS effect. However in the photo-emission experiments[50] the effect has been observed for aluminium substrates which have a small spin-orbit coupling. Therefore it is useful to search for another mechanism to obtain a magnetocurrent without relying on the spin-orbit coupling. We now evaluate the role of magnetic stray fields in this context.

In the work of Bedkihal and Segal [51] two models of a double-dot Aharonov-Bohm interferometer were studied. In Model I a magnetocurrent was generated by a phase-shift in the hybridization matrix[52] (due to a magnetic flux piercing the scattering region) combined with an asymmetry in the on-site energies $\epsilon_1 \neq \epsilon_2$ and nearest neighbour Coulomb interactions. In Model II the interactions were modeled only using Büttiker probes.[51] It was found that both Coulomb interactions (Model I) and Büttiker probes (Model II) capture the relevant transport properties, thereby implying a correspondence them. The point of interest here is that a magnetocurrent was obtained through a magnetic phase and nearest-neighbour Coulomb interactions. In other words no spin-orbit coupling was required.

In a different study on a triple dot Aharonov-Bohm interferometer [53], three sites in a triangle configuration were considered and a magnetic flux piercing the scattering region generated a phase in the hopping parameters between the sites. Interactions were modeled via Büttiker voltage probes and a finite magnetocurrent was obtained. Site 1 and 2 were couple to the left and right lead respectively and the hybridization matrix did not obtain a magnetic phase in this case. A finite magnetocurrent was found by introducing an asymmetry in one of the on-site energies of the triangle.[53] Given the correspondence between the probe method and Coulomb repulsion, as was demonstrated by Bedkihal and Segal [51] the magnetocurrent of the triangle configuration could also have been obtained by modeling interactions via nearest neighbour Coulomb interactions.

In most CISS experiments the magnetic field applied to the leads pierces the region with the molecules as well for example due to stray fields. However, in the work of Pramanik et al. [54] the magnetic field was orientated orthogonal to the direction of the current to exclude the electrical magnetochiral anisotropy effects, which originates from the parallel components of current and magnetic field .[55] The presence of this magnetic field makes it is possible that the hopping parameters in the molecules obtain a phase shift due the Peierls substitution. Furthermore most molecules in CISS experiments have a large Coulomb interaction. Take for example carbon atoms inside a helicene molecule. The nearest neighbour Coulomb repulsion W in the Ohno-parametrization[56] for two Carbon atoms separated by 1.3 Å and an on-site Coulomb repulsion term for isolated Carbon of $U_C = 10$ eV[40] gives $W = 7.4$ eV. In reality the on-site repulsion term U is lowered due to the image-charge effect[39] and to what extent depends on the molecule-lead separation. However we expect the on-site repulsion to still be large when compared the to the hopping parameter of Carbon $t = 2.4$ eV,[38] for example $U_C = 2t \approx 5$ eV results in $W = 4.5$ eV. We conclude that the nearest-neighbour Coulomb interactions are non-negligible.

In this section we will investigate the bias dependence of the magnetocurrent and the size of the effect due to magnetic stray fields and nearest neighbour Coulomb interactions. To that end we model a molecule as a tight binding chain where the sites lie on a helix connected to leads that are modeled in the wide-band limit. We will also verify Onsager reciprocity.

THE MODEL

The total Hamiltonian is given by:

$$\boldsymbol{H} = \boldsymbol{H}_U + \boldsymbol{H}_W + \boldsymbol{H}_{\text{os}} + \boldsymbol{H}_{\text{hop}} + \boldsymbol{H}_{\text{leads-molecule}} + \boldsymbol{H}_{\text{leads}}, \tag{3.80}$$

where $\boldsymbol{H}_U, \boldsymbol{H}_W$ describe the Coulomb interactions, $\boldsymbol{H}_{\text{os}}$ is the on-site Hamiltonian, $\boldsymbol{H}_{\text{hop}}$ the hopping Hamiltonian, $\boldsymbol{H}_{\text{lead-molecule}}$ describes the coupling of the molecule to the leads and $\boldsymbol{H}_{\text{leads}}$ describes the Hamiltonian of the leads. We consider Coulomb interaction between electrons on the same site between opposite spins : $\boldsymbol{H}_U = U\sum_m (n_{m\uparrow} - \frac{1}{2})(n_{m\downarrow} - \frac{1}{2})$ and between neighbouring sites: $\boldsymbol{H}_W = W\sum_{\langle nm\rangle}(\hat{n}_m - 1)(\hat{n}_n - 1)$. Here $\hat{n}_{m\sigma} = \hat{c}^\dagger_{m\sigma}\hat{c}_{m\sigma}$, where $\hat{c}^\dagger_{m\sigma}$ and $\hat{c}_{m\sigma}$ are fermionic creation and annihilation operators respectively for site m and spin σ and $\hat{n}_m \equiv \hat{n}_{m\uparrow} + \hat{n}_{m\downarrow}$. We then approximate the Coulomb interaction in a mean field theory: $\boldsymbol{H}^{MF}_U \rightarrow U\sum_{m,\sigma}\left(\langle n_{m\bar{\sigma}}\rangle - \frac{1}{2}\right)\hat{n}_{m\sigma}$ and $\boldsymbol{H}^{MF}_W \rightarrow W\sum_{\langle nm\rangle}(\langle \hat{n}_n\rangle - 1)\hat{n}_m$ which is the result of considering the Wick contractions of the full operator. Here $\langle n_{m\bar{\sigma}}\rangle$ is the average electron density on site m with spin $\bar{\sigma}$.

A constant, magnetic stray field $\boldsymbol{B}$ pierces the scattering region and couples to the spin $\boldsymbol{\sigma}$ of the electron, which causes a shift in the on-site energy. The on-site Hamiltonian is given by $\boldsymbol{H}_{\text{os}}(\boldsymbol{B}) = \sum_{m,\sigma,\sigma'} c^\dagger_{m\sigma}\left(\epsilon_m\delta_{\sigma\sigma'} + \mu_{\text{B}}(\boldsymbol{B}\cdot\boldsymbol{\sigma})_{\sigma\sigma'}\right)\hat{c}_{m\sigma'}$, with $\epsilon_m = \epsilon_{\text{os}}$ the on-site energy, $\boldsymbol{\sigma}$ a vector of Pauli-matrices $\boldsymbol{\sigma} = [\sigma_{\text{x}}, \sigma_{\text{y}}, \sigma_{\text{z}}]$, the Bohr magneton $\mu_{\text{B}} = 5.8\cdot 10^{-5}\,\text{eV}\,\text{T}^{-1}$.

The hopping Hamiltonian is given by: $\boldsymbol{H}_{\text{hop}}(\boldsymbol{B}) = \sum_{mn\sigma} t_{mn} e^{i\phi_{mn}(\boldsymbol{B})}\hat{c}^\dagger_{m\sigma}\hat{c}_{n\sigma} + \text{h.c.}$ where h.c. denotes hermitian conjugate, t_{mn} is the hopping parameter between site m and n and the phase $\phi_{mn}(\boldsymbol{B})$ is generated by the constant, magnetic stray field $\boldsymbol{B}$. This phase is determined as follows. All sites lie on a helix with radius a and pitch c. N is the number of sites within one winding and M is the number of windings such that MN is the total number of sites in the molecule. The position of site k is given by:

$$\boldsymbol{R}_k = [a\cos(\varphi_k), a\sin(\varphi_k), c\frac{\varphi_k}{2\pi}\frac{N}{NM-1}], \tag{3.81}$$

with $\varphi_k = \frac{2\pi(k-1)}{N}$, $\quad k \in MN$. Here the constant stray field is chosen orthogonal to the helical axis $\hat{z}$: $\boldsymbol{B} = B\hat{x}$, this generates the phase ϕ_{mn} which is calculated via:[57]

$$\phi_{mn}(\boldsymbol{B}) = \frac{2\pi}{\Phi_0}\left[\frac{1}{2}\boldsymbol{B}\cdot\left(\boldsymbol{R}_m \times \boldsymbol{R}_n\right) + \chi(\boldsymbol{R}_n) - \chi(\boldsymbol{R}_m)\right]. \tag{3.82}$$

with $\Phi_0 = \frac{h}{e} \approx 4.136\cdot 10^{-15}$ Wb, the magnetic flux quantum and $\chi(\boldsymbol{r})$ a scalar gauge field. We use the helical coordinates given by eq. (3.81) to calculate the phase in eq. (3.82). Now we fix our choice of the gauge field $\chi(\boldsymbol{r})$ by demanding that the phase ϕ_{mn} should be invariant with one rotation of 2π around the helical axis. This leads to the gauge choice:[57] $\chi(\boldsymbol{r}) = \frac{1}{2}(\boldsymbol{r}\cdot\boldsymbol{t})(\boldsymbol{r}\cdot(\boldsymbol{t}\times\boldsymbol{B}))$, with $\boldsymbol{t} = \hat{z}$.

MAGNETOCURRENT STRAY FIELDS

The magnetocurrent depends not only on the magnetisation of the leads but also on the stray field $\boldsymbol{B}$ and it is given by (using eq. (3.4)):

$$\begin{aligned}\Delta I(m,\boldsymbol{B},V) &\equiv I(m,\boldsymbol{B},V) - I(-m,-\boldsymbol{B},V)\\ &= \frac{e}{h}\int_{-\infty}^{\infty}\Big[T_{\mathrm{LR}}(m,\boldsymbol{B},V) - T_{\mathrm{LR}}(-m,-\boldsymbol{B},V)\Big](f_{\mathrm{L}}-f_{\mathrm{R}})dE. \end{aligned} \tag{3.83}$$

The transmission depends on the electron densities via the retarded and advanced Green's functions. The densities are determined self-consistently for every voltage via:

$$\langle n_k(m,\boldsymbol{B},V)\rangle = \int_{-\infty}^{\infty}\Big(\mathbf{G}^{+}\Big[\sum_{\alpha=\mathrm{L,R}} f_\alpha \boldsymbol{\Gamma}_\alpha\Big]\mathbf{G}^{-}\Big)_{k,k}\frac{d\epsilon}{2\pi}. \tag{3.84}$$

Here the mean field Green's function is given by:

$$\mathbf{G}^{\pm}(\epsilon,\langle n_k\rangle,m,\boldsymbol{B}) = \Big[\epsilon\mathbf{1} - \boldsymbol{H}_U^{\mathrm{MF}}(\boldsymbol{B}) - \boldsymbol{H}_W^{\mathrm{MF}}(\boldsymbol{B}) - \boldsymbol{H}_{\mathrm{hop}}(\boldsymbol{B}) \mp \boldsymbol{\Sigma}(m,\epsilon)\Big]^{-1}, \tag{3.85}$$

where $\boldsymbol{\Sigma}(m,\epsilon) = \boldsymbol{\Sigma}^{\mathrm{L}}(m,\epsilon) + \boldsymbol{\Sigma}^{\mathrm{R}}(\epsilon)$ and $\boldsymbol{\Sigma}^{\alpha}$ the retarded self energy of the lead α. In the wide-band limit the retarded self energies are purely imaginary and independent of energy $\boldsymbol{\Sigma}^{\alpha} = -\frac{i}{2}\boldsymbol{\Gamma}^{\alpha}$.

RESULTS

We then calculate the magnetocurrent (eq. (3.83)) arising from the stray field $\boldsymbol{B}$. First of all we find that the magnetocurrent vanishes numerically (10^{-15}) if the magnetic phase is set to zero, (as expected) independent of the value of μ_{B}. We conclude that in the presence of interactions an on-site term arising from the coupling between the spin and the magnetic field cannot cause a finite magnetocurrent. That is why we set $\mu_{\mathrm{B}} = 0$ in the rest of this section. A magnetocurrent can then be caused only by the magnetic phase ϕ_{mn}.

We then consider two distinct scenarios. In the first scenario we set the on-site repulsion between opposite spins to zero: $U = 0$, but not the interaction between neighbouring electrons $W \neq 0$, the leads are not magnetically polarized $p_z^{\alpha} = 0$ and the stray fields are non-zero $\boldsymbol{B} \neq \boldsymbol{0}$. In the second scenario we consider $U = W \neq 0$ and we only magnetically polarize the left lead $p_z^{\mathrm{L}} = 0.5$ which changes sign with the magnetic stray field. The main difference with our model in section 3.2 is that the spin-orbit coupling here is zero. The stray field $\boldsymbol{B}$ is always oriented orthogonal to the transport direction. The nearest neighbour Coulomb interaction strengths are taken as $W \leq t$ as is typical for a mean field theory. For large values of the nearest neighbour Coulomb interaction strength Extended Dynamical Mean-Field Theory[58,59] are more accurate.

We consider a model consisting of 4 sites $N = 4$ and one winding $M = 1$ and the radius and pitch of the helix are chosen as $a = 1.4$ Å and $c = 3.6$ Å respectively.[18] The hopping between the sites is NN and NNN and corresponding hopping parameters are given by : $t_{NN} = 2.4$ eV, $t_{NNN} = 0.4t_{NN}$. The on-site energy is taken as $\epsilon_0 = 0$. The coupling to the left and right lead is taken to be $\gamma = 0.5$ eV.[41] We choose the Fermi level such that the system is approximately half filled. We take the size of orthogonal magnetic field $|\boldsymbol{B}| = 1$ T, comparable to the orthogonal field of ref. [54].

In fig. 3.3 the magnetocurrent is plotted for $E_F = 0.44$ eV in fig. 3.3a and for $E_F = -0.37$ eV in fig. 3.3b. In both figures the finite interaction strength $U = 0$ and W is varied between $0.5t$ and t. The figures show that the magnetocurrent is dominantly even for small values of W and dominantly odd for larger values of W. This is the general trend we find for different Fermi levels. Note that we do not magnetize the left lead in this case $m = 0$, the signal that is found is purely due to the stray field $\boldsymbol{B}$.

In fig. 3.3c the magnetocurrent is plotted for $E_F = 0.44$ eV and in in fig. 3.3d for $E_F = -0.37$ eV. In both figures the finite interaction strengths U, W are varied between $0.5t$ and t. The figures show that the magnetocurrent is dominantly even for small values of U, W and dominantly odd for larger values of U, W. This is the general trend we find for different Fermi levels.

The size of the effect corresponding to the magnetocurrents in fig. 3.3 is of the order 10^{-4}%. This result makes sense, since the magnetic flux enclosed by the molecule is very small (in eq. (3.82): $|\phi_{mn}| \approx \frac{BR^2}{\Phi_0} \approx 10^{-6}$ where $R \approx 10^{-10} m$ and $B = 1$ Tesla). Further note that the magnetocurrent vanishes if the next-nearest neighbour hopping is set to zero. In equilibrium (i.e. $\mu_L = \mu_R = E_F$ and $T_L = T_R = T$) we find that the transmissions satisfies time-reversal symmetry, thereby confirming that Onsager-reciprocity is satisfied. Our code can be found on `https://github.com/khhuisman/Nearest_Neigbour_Coulomb`. The Hamiltonian $\boldsymbol{H}_{\text{mol.}} = \boldsymbol{H}_{\text{os}} + \boldsymbol{H}_{\text{hop}}$ is constructed with the Kwant code[43] and the Qsymm code.[44]

Conclusion

We modelled a chiral chain with on-site and nearest neighbour Coulomb interactions, where a magnetic stray field induced a magnetic phase in the hopping due to the Peierls substitution and an on-site coupling between the spin of the electron. The coupling between the spin of the electron and the magnetic stray fields yields a numerically vanishing magnetocurrent. When a phase shift due to the Peierls substitution was taken into account the effect was of the order 10^{-4}% for realistic parameters. We conclude that magnetic stray fields have a negligibly small effect. To improve this study one could consider investigate the effect of stronger Coulomb interactions. In that case the Extended Dynamical Mean-Field Theory[58,59] might be give more accurate results than a mean field theory.

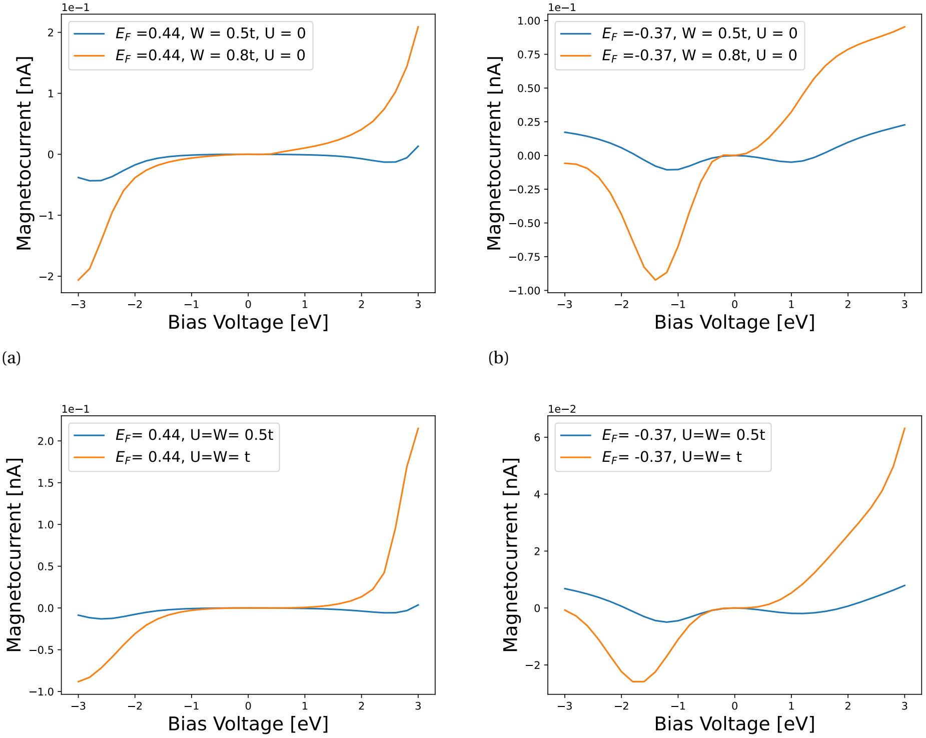

(a) (b)

(c) (d)

Figure 3.3: The magnetocurrent for different values of the Fermi level and Coulomb interactions strength. (a) $E_\mathrm{F} = 0.44$ eV and $U = 0, W = 0.5t, 0.8t$ eV (b) $E_\mathrm{F} = -0.37$ eV and $U = 0, W = 0.5t, 0.8t$. (c) $E_\mathrm{F} = 0.44$ eV and $U = W = 0.5t, t$ eV (d) $E_\mathrm{F} = -0.37$ eV and $U = W = 0.5t, t$. The size of the orthogonal stray field is $|\boldsymbol{B}| = 1$ Tesla.

REFERENCES

(1) Huisman, K. H.; Heinisch, J.-B. M.-Y.; Thijssen, J. M. Chirality-Induced Spin Selectivity (CISS) Effect: Magnetocurrent–Voltage Characteristics with Coulomb Interactions I. *The Journal of Physical Chemistry C* **2023**, *127*, 6900–6905.

(2) Ray, K.; Ananthavel, S. P.; Waldeck, D. H.; Naaman, R. Asymmetric Scattering of Polarized Electrons by Organized Organic Films of Chiral Molecules. *Science* **1999**, *283*, 814–816.

(3) Göhler, B.; Hamelbeck, V.; Markus, T. Z.; Kettner, M.; Hanne, G. F.; Vager, Z.; Naaman, R.; Zacharias, H. Spin Selectivity in Electron Transmission Through Self-Assembled Monolayers of Double-Stranded DNA. *Science* **2011**, *331*, 894–897.

(4) Kettner, M.; Maslyuk, V. V.; Nürenberg, D.; Seibel, J.; Gutierrez, R.; Cuniberti, G.; Ernst, K.-H.; Zacharias, H. Chirality-Dependent Electron Spin Filtering by Molecular Monolayers of Helicenes. *The Journal of Physical Chemistry Letters* **2018**, *9*, PMID: 29618210, 2025–2030.

(5) Kettner, M.; Göhler, B.; Zacharias, H.; Mishra, D.; Kiran, V.; Naaman, R.; Waldeck, D. H.; Sęk, S.; Pawłowski, J.; Juhaniewicz, J. Spin Filtering in Electron Transport Through Chiral Oligopeptides. *The Journal of Physical Chemistry C* **2015**, *119*, 14542–14547.

(6) Ben Dor, O.; Yochelis, S.; Radko, A.; Vankayala, K.; Capua, E.; Capua, A.; Yang, S.-H.; Baczewski, L.; Parkin, S. Magnetization Switching in Ferromagnets by Adsorbed Chiral Molecules Without Current or External Magnetic Field. *Nature Communications* **2017**, *8*, 14567.

(7) Meirzada, I.; Sukenik, N.; Haim, G.; Yochelis, S.; Baczewski, L. T.; Paltiel, Y.; Bar-Gill, N. Long-Time-Scale Magnetization Ordering Induced by an Adsorbed Chiral Monolayer on Ferromagnets. *ACS Nano* **2021**, *15*, PMID: 33591720, 5574–5579.

(8) Liu, T.; Wang, X.; Wang, H.; Shi, G.; Gao, F.; Feng, H.; Deng, H.; Hu, L.; Lochner, E.; Schlottmann, P., et al. Linear and Nonlinear Two-Terminal Spin-Valve Effect from Chirality-Induced Spin Selectivity. *ACS Nano* **2020**, *14*, PMID: 33136367, 15983–15991.

(9) Rahman, M. W.; Firouzeh, S.; Pramanik, S. Carrier localization and magnetoresistance in DNA-functionalized carbon nanotubes. *Nanotechnology* **2021**, *32*, 455001.

(10) Kulkarni, C.; Mondal, A.; Das, T.; Grinbom, G.; Tassinari, F.; Mabesoone, M.; Meijer, E.; Naaman, R. Highly Efficient and Tunable Filtering of Electrons' Spin by Supramolecular Chirality of Nanofiber-Based Materials. *Advanced Materials* **2020**, *32*, DOI: `10.1002/adma.201904965`.

(11) Kiran, V.; Mathew, S.; Cohen, S.; Hernandez Delgado, I.; Lacour, J.; Naaman, R. Helicenes-A New Class of Organic Spin Filter. *Advanced materials (Deerfield Beach, Fla.)* **2016**, *28*, DOI: `10.1002/adma.201504725`.

(12) Xie, Z.; Markus, T. Z.; Cohen, S. R.; Vager, Z.; Gutierrez, R.; Naaman, R. Correction to Spin Specific Electron Conduction through DNA Oligomers. *Nano Letters* **2012**, *12*, PMID: 22132798, 523–523.

(13) Al Bustami, H.; Koplovitz, G.; Primc, D.; Yochelis, S.; Capua, E.; Porath, D.; Naaman, R.; Paltiel, Y. Single Nanoparticle Magnetic Spin Memristor. *Small* **2018**, *14*, 1801249.

(14) Bullard, G.; Tassinari, F.; Ko, C.-H.; Mondal, A. K.; Wang, R.; Mishra, S.; Naaman, R.; Therien, M. J. Low-Resistance Molecular Wires Propagate Spin-Polarized Currents. *Journal of the American Chemical Society* **2019**, *141*, PMID: 31411873, 14707–14711.

(15) Tassinari, F.; Jayarathna, D.; Kantor-Uriel, N.; Davis, K.; Varade, V.; Achim, C.; Naaman, R. Chirality Dependent Charge Transfer Rate in Oligopeptides. *Advanced Materials* **2018**, *30*, 1706423.

(16) Bloom, B. P.; Kiran, V.; Varade, V.; Naaman, R.; Waldeck, D. H. Spin Selective Charge Transport Through Cysteine Capped Cdse Quantum Dots. *Nano Letters* **2016**, *16*, PMID: 27336320, 4583–4589.

(17) Aiello, C. D.; Abendroth, J. M.; Abbas, M.; Afanasev, A.; Agarwal, S.; Banerjee, A. S.; Beratan, D. N.; Belling, J. N.; Berche, B.; Botana, A., et al. A Chirality-Based Quantum Leap. *ACS Nano* **2022**, *16*, PMID: 35318848, 4989–5035.

(18) Geyer, M.; Gutierrez, R.; Mujica, V.; Cuniberti, G. Chirality-Induced Spin Selectivity in a Coarse-Grained Tight-Binding Model for Helicene. *The Journal of Physical Chemistry C* **2019**, *123*, 27230–27241.

(19) Zöllner, M. S.; Varela, S.; Medina, E.; Mujica, V.; Herrmann, C. Insight Into the Origin of Chiral-Induced Spin Selectivity From a Symmetry Analysis of Electronic Transmission. *Journal of Chemical Theory and Computation* **2020**, *16*, PMID: 32271568, 2914–2929.

(20) Huisman, K. H.; Thijssen, J. M. CISS Effect: A Magnetoresistance Through Inelastic Scattering. *The Journal of Physical Chemistry. C, Nanomaterials and Interfaces* **2021**, *125*, 23364–23369.

(21) Medina, E.; López, F.; Ratner, M. A.; Mujica, V. Chiral molecular films as electron polarizers and polarization modulators. *Europhysics Letters* **2012**, *99*, 17006.

(22) Ghazaryan, A.; Paltiel, Y.; Lemeshko, M. Analytic Model of Chiral-Induced Spin Selectivity. *The Journal of Physical Chemistry C* **2020**, *124*, PMID: 32499842, 11716–11721.

(23) Yang, X.; van der Wal, C. H.; van Wees, B. J. Spin-Dependent Electron Transmission Model for Chiral Molecules in Mesoscopic Devices. *Phys. Rev. B* **2019**, *99*, 024418.

(24) Yang, X.; van der Wal, C. H.; van Wees, B. J. Detecting Chirality in Two-Terminal Electronic Nanodevices. *Nano Letters* **2020**, *20*, PMID: 32672980, 6148–6154.

(25) Büttiker, M. Symmetry of Electrical Conduction. *IBM Journal of Research and Development* **1988**, *32*, 317–334.

(26) Spivak, B.; Zyuzin, A. Signature of the Electron-Electron Interaction in the Magnetic-Field Dependence of Nonlinear I-V Characteristics in Mesoscopic Systems. *Physical Review Letters* **2004**, *93*, DOI: `10.1103/physrevlett.93.226801`.

(27) Fransson, J. Vibrational Origin of Exchange Splitting and Chirality Induced Spin Selectivity. *Physical Review B* **2020**, DOI: 10.1103/PhysRevB.102.235416.

(28) Fransson, J. Chirality-Induced Spin Selectivity: The Role of Electron Correlations. *The Journal of Physical Chemistry Letters* **2019**, *10*, PMID: 31657931, 7126–7132.

(29) Alwan, S.; Dubi, Y. Spinterface Origin for the Chirality-Induced Spin-Selectivity Effect. *Journal of the American Chemical Society* **2021**, *143*, PMID: 34460242, 14235–14241.

(30) Dalum, S.; Hedegård, P. Theory of Chiral Induced Spin Selectivity. *Nano Letters* **2019**, *19*, PMID: 31265313, 5253–5259.

(31) Onsager, L. Reciprocal Relations in Irreversible Processes. I. *Phys. Rev.* **1931**, *37*, 405–426.

(32) Onsager, L. Reciprocal Relations in Irreversible Processes. II. *Phys. Rev.* **1931**, *38*, 2265–2279.

(33) Casimir, H. B. G. On Onsager's Principle of Microscopic Reversibility. *Rev. Mod. Phys.* **1945**, *17*, 343–350.

(34) Evers, F.; Aharony, A.; Bar-Gill, N.; Entin-Wohlman, O.; Hedegård, P.; Hod, O.; Jelinek, P.; Kamieniarz, G.; Lemeshko, M.; Michaeli, K., et al. Theory of Chirality Induced Spin Selectivity: Progress and Challenges. *Advanced Materials* **2022**, *34*, 2106629.

(35) Sánchez, D.; Büttiker, M. Magnetic-Field Asymmetry of Nonlinear Mesoscopic Transport. *Physical Review Letters* **2004**, *93*, DOI: 10.1103/physrevlett.93.106802.

(36) Das, T. K.; Tassinari, F.; Naaman, R.; Fransson, J. Temperature-Dependent Chiral-Induced Spin Selectivity Effect: Experiments and Theory. *The Journal of Physical Chemistry C* **2022**, *126*, 3257–3264.

(37) Fransson, J. The Chiral Induced Spin Selectivity Effect What It Is, What It Is Not, And Why It Matters. *Israel Journal of Chemistry* **2022**, *62*, e202200046.

(38) Ramasesha, S.; Sinha, B.; Albert, I. Nature of exchange interactions in stacked radicals/radical-ions of cyclic polyenes. *Journal of Molecular Structure* **1994**, *327*, 173–180.

(39) Verzijl, C. J. O.; Gil, J. A. C.; Perrin, M. L.; Dulić, D.; van der Zant, H. S. J.; Thijssen, J. M. Image effects in transport at metal-molecule interfaces. *The Journal of Chemical Physics* **2015**, *143*, 174106.

(40) Bursill, R. J.; Castleton, C.; Barford, W. Optimal parametrisation of the Pariser–Parr–Pople Model for benzene and biphenyl. *Chemical Physics Letters* **1998**, *294*, 305–313.

(41) Verzijl, C. J. O.; Seldenthuis, J. S.; Thijssen, J. M. Applicability of the wide-band limit in DFT-based molecular transport calculations. *The Journal of Chemical Physics* **2013**, *138*, 094102.

(42) Haug, H. J. W.; Jauho, A. P., *Quantum Kinetics in Transport and Optics of Semiconductors*; Springer: 2008.

(43) Groth, C. W.; Wimmer, M.; Akhmerov, A. R.; Waintal, X. Kwant: A Software Package for Quantum Transport. *New Journal of Physics* **2014**, *16*, 063065.

(44) Varjas, D.; Rosdahl, T.; Akhmerov, A. Qsymm: Algorithmic symmetry finding and symmetric Hamiltonian generation. *New Journal of Physics* **2018**, *20*, DOI: `10.1088/1367-2630/aadf67`.

(45) Jacquet, P. A. ThermoElectric Transport Properties of a Chain of Quantum Dots with Self-Consistent Reservoirs. *Journal of Statistical Physics* **2009**, *134*, 709–748.

(46) Penn, D. R. Stability Theory of the Magnetic Phases for a Simple Model of the Transition Metals. *Phys. Rev.* **1966**, *142*, 350–365.

(47) Pasrija, K.; Kumar, S. Noncollinear and noncoplanar magnetic order in the extended Hubbard model on anisotropic triangular lattice. *Physical Review B* **2016**, *93*, DOI: `10.1103/physrevb.93.195110`.

(48) Hubbard, J. Electron Correlations in Narrow Energy Bands. *Proceedings of the Royal Society of London. Series A, Mathematical and Physical Sciences* **1963**, *276*, 238–257.

(49) Huisman, K. H.; Heinisch, J. B. M. Y.; Thijssen, J. M. CISS effect: Magnetocurrent–voltage characteristics with Coulomb interactions. II. *The Journal of Chemical Physics* **2023**, *158*, 174108, DOI: `10.1063/5.0148748`.

(50) Mishra, D.; Markus, T. Z.; Naaman, R.; Kettner, M.; Göhler, B.; Zacharias, H.; Friedman, N.; Sheves, M.; Fontanesi, C. Spin-dependent electron transmission through bacteriorhodopsin embedded in purple membrane. *Proceedings of the National Academy of Sciences* **2013**, *110*, 14872–14876.

(51) Bedkihal, S.; Segal, D. Magnetotransport in Aharonov-Bohm interferometers: Exact numerical simulations. *Phys. Rev. B* **2014**, *90*, 235411.

(52) Bedkihal, S.; Bandyopadhyay, M.; Segal, D. Flux-dependent occupations and occupation difference in geometrically symmetric and energy degenerate double-dot Aharonov-Bohm interferometers. *Phys. Rev. B* **2013**, *87*, 045418.

(53) Bandyopadhyay, M.; Ghosh, S.; Dubey, A.; Bedkihal, S. Flux dependent current rectification in geometrically symmetric interconnected triple-dot Aharanov-Bohm interferometer. *Physica E: Low-dimensional Systems and Nanostructures* **2021**, *133*, 114786.

(54) Hossain, M. A.; Illescas-Lopez, S.; Nair, R.; Cuerva, J. M.; Álvarez de Cienfuegos, L.; Pramanik, S. Transverse magnetoconductance in two-terminal chiral spin-selective devices. *Nanoscale Horiz.* **2023**, *8*, 320–330.

(55) Rikken, G.; Fölling, J.; Wyder, P. Electrical Magnetochiral Anisotropy. *Physical review letters* **2002**, *87*, 236602.

(56) Ohno, K. Some remarks on the Pariser-Parr-Pople method. *Theoretica chimica acta* **1964**, *2*, 219–227.

(57) Cresti, A. Convenient Peierls phase choice for periodic atomistic systems under magnetic field. *Phys. Rev. B* **2021**, *103*, 045402.

(58) Chitra, R.; Kotliar, G. Effect of Long Range Coulomb Interactions on the Mott Transition. *Phys. Rev. Lett.* **2000**, *84*, 3678–3681.

(59) Smith, J. L.; Si, Q. Spatial correlations in dynamical mean-field theory. *Phys. Rev. B* **2000**, *61*, 5184–5193.

4

BIPARTICE STRUCTURES WITH COULOMB INTERACTIONS

"I am not afraid of the Great Gray Wolf"

Artorias

One of the manifestations of chirality-induced spin selectivity (CISS) is the appearance of a magnetocurrent. Magnetocurrent is defined as the difference between the charge currents at finite bias in a two terminal device for opposite magnetizations of one of the leads. In experiments on chiral molecules assembled in monolayers the magnetocurrent is dominantly odd in bias voltage, while theory often yields an even one. From theory it is known that the spin-orbit coupling and chirality of the molecule can only generate a finite magnetocurrent in the presence of interactions, either of the electrons with vibrational modes or among themselves, through the Coulomb interaction. Here we analytically show that the magnetocurrent in bipartite-chiral structures mediated through Coulomb interactions is exactly even in the wide band limit and exactly odd for semi-infinite leads due to the bipartite lattice symmetry of the Green's function. Our numerical results confirm these analytical findings.

Part of this chapter has been published in the *Journal of Chemical Physics* **2023**, *158*, 174108 [1].

4.1. INTRODUCTION

One of the manifestations of chirality-induced spin selectivity (CISS) is the appearance of a magnetocurrent. Magnetocurrent is defined as the difference between the charge currents at finite bias in a two terminal device for opposite magnetizations of one of the leads. Onsager-Casimir reciprocity[2–4] prohibits a magnetocurrent from being observed in two-terminal junctions in the linear regime. In fully coherent two terminal transport, this absence of a magnetocurrent extends to the nonlinear regime as well, this is called Büttiker reciprocity.[5] In order to see a magnetocurrent in the nonlinear regime, coherence must be broken; this is done through interactions of the electrons with vibrational modes or among themselves, through the Coulomb interaction. It should be noted that several experiments[6–10] seem to show violation of Onsager-Casimir reciprocity for reasons that are not yet known. In some of these experiments the currents for positive and negative magnetization show a plateau of zero current around zero bias voltage such that the demonstration of Onsager-Casimir reciprocity is not really convincing.

In this paper we focus on the symmetry of the magnetocurrent versus bias voltage. In two terminal transport experiments on chiral molecules the magnetocurrent is dominantly odd in bias voltage[6–18] (for an extensive overview see ref [19]). In theory an even magnetocurrent is found by introducing a decoherence node[20] or via the Büttiker voltage probe method.[21] A model including spin-dependent electron-phonon coupling[22] yields an odd magnetocurrent. However the seemingly linear magnetocurrent found in ref [22] violates Onsager-Casimir reciprocity. In our previous paper on Coulomb interactions[23] we found that Onsager-Casimir reciprocity is satisfied and the odd magnetocurrent is mediated by the strong Coulomb interactions in combination with the next nearest-neighbor spin-orbit coupling, making the lattice non-bipartite. We found, in the wide-band limit (WBL), that the magnetocurrent was nearly perfectly odd in the bias voltage, when the Fermi level was aligned with the energy around which the spectrum is approximately particle hole symmetric. In this paper we study the bias dependence of the magnetocurrent for a bipartite lattice when the Fermi level is aligned with the energy around which the spectrum is exactly particle hole symmetric. We show that, close to this symmetry point, there is a difference between the bias dependence of the magnetocurrent for bipartite and non-bipartite lattices.

In most work done on two-terminal transport through molecular junctions the leads are modelled using the wide-band limit (see e.g.[20–23]), however, for some metals, semi-infinite (SIF) leads may be more realistic. We will analyse the magnetocurrent analytically for WBL and SIF leads by exploiting the bipartite lattice symmetry and the time reversal property of the Green's function. To confirm our analytical findings we analyze a chiral model system with a nearest-neighbor spin-orbit coupling and Coulomb interactions numerically.

In sec. 4.2 we define our model. In sec. 4.3 the magnetocurrent is analysed analytically for WBL and SIF leads. In sec. 4.3.1 we define the magnetocurrent, in sec. 4.3.2 we define the Green's functions in the Hartree-Fock (HFA) and Hubbard One approximation (HIA) and in sec. 4.3.3 it is specified how these Green's functions transform under bipartite lattice symmetry and the time-reversal operator. In sec. 4.3.4 and sec. 4.3.5 the bias dependence of the magnetocurrent is analysed for WBL and SIF leads respectively, in sec. 4.4 the numerical results are presented and we conclude our work in sec 4.5.

4.2. MODEL DESCRIPTION

The Hamiltonian of a molecular transport junction is given by:

$$\mathbf{H} = \mathbf{H}_{\text{os}} + \mathbf{H}_{\text{T}} + \mathbf{H}_{\text{SOC}} + \mathbf{H}_{\text{U}} + \mathbf{H}_{\text{lead-molecule}} + \mathbf{H}_{\text{leads}}, \tag{4.1}$$

where $\mathbf{H}_{\text{os}}$ is the on-site Hamiltonian, $\mathbf{H}_{\text{T}}$ is the hopping Hamiltonian, $\mathbf{H}_{\text{SOC}}$ is the hopping Hamiltonian due to spin-orbit coupling, $\mathbf{H}_{\text{U}}$ describes the Coulomb interactions, $\mathbf{H}_{\text{lead-molecule}}$ describes the coupling of the molecule to the leads and $\mathbf{H}_{\text{leads}}$ describes the Hamiltonian of the leads. The on-site Hamiltonian is given by $\mathbf{H}_{\text{os}} = \sum_m \epsilon_m \hat{n}_m$, we set this to zero ($\epsilon_m = 0$) throughout this paper. The hopping Hamiltonian is given by: $\mathbf{H}_{\text{T}} = -\sum_m t\, \hat{c}^\dagger_{m+1}\hat{c}_m +$ h.c., where t is the hopping parameter and h.c. denotes the hermitian conjugate. In order to see the effect of the effect of bipartite lattice symmetry, we consider an S-shaped structure,[24] see fig. 4.1. The spin-dependent hopping Hamiltonian acting between nearest neighbor sites is given by:

$$\mathbf{H}_{\text{SOC}} = -i\lambda \sum_k \sum_{\langle m,n\rangle} \hat{c}^\dagger_m \sigma \cdot (\boldsymbol{e} \times \boldsymbol{d}_k)\hat{c}_n + h.c., \tag{4.2}$$

with λ the spin-orbit coupling parameter. A constant electric field pointing in the out of plane direction generates this nearest neighbor spin-dependent hopping and the components of $\vec{\sigma}$ are the Pauli-matrices. Here $\boldsymbol{d}_k$ is the hopping vector and k indicates its direction (longitudinal and transverse), $\boldsymbol{e}$ indicates the direction of the electric field. This model is defined on a $2D$ lattice where the indices m, n label the sites. $\mathbf{H}_{\text{U}}$ contains the Coulomb interactions, we take those to be on-site:

$$\mathbf{H}_{\text{U}} = U \sum_m (\hat{n}_{m\uparrow} - \frac{1}{2})(\hat{n}_{m\downarrow} - \frac{1}{2}). \tag{4.3}$$

Here U is the Coulomb interaction strength. The factors of $\frac{1}{2}$ are included to make the spectrum of the Hamiltonian particle hole symmetric around the energy $\epsilon = 0$. The S-shape in fig. 4.1 has a C_2 symmetry around the out of plane direction p, leading to a difference between the (non-spin flip) spin-up and down transmissions.[24] Here $\mathbf{H}^\alpha_{\text{lead-molecule}} = \sum_{k,m,s,s'} V^\alpha_{ms,ks'} c^\dagger_{ms} d^K_{ks'} + h.c.$ where $V^\alpha_{ms,ks'}$ the coupling parameter between electrons on the molecule and lead α. The Hamiltonian of the non-interacting lead α is $\mathbf{H}^\alpha_{\text{lead}} = \sum_{k,s} \epsilon^\alpha_{ks} d^{\dagger\alpha}_{ks} d^\alpha_{ks}$.

4.3. THEORY

4.3.1. MAGNETOCURRENT DEFINITION

The transmission for a 2-terminal system with Coulomb interactions depends on the bias voltage V through the electron densities: $T_{\text{LR}}(\epsilon, m) \rightarrow T_{\text{LR}}(\epsilon, m, V) = T_{\text{LR}}(\epsilon, m, \langle n_{ks}(m, V)\rangle)$, where $\langle n_{ks}(m, V)\rangle$ is the average electron density for site k with spin s given by eq. (4.14) and m is the magnetization of the left lead. The current into the left lead is then given by (see Appendix 4.6.6):

$$I(m, V) = \frac{e}{h} \int_{-\infty}^{\infty} T_{\text{LR}}(\epsilon, m, V)\Big(f(\epsilon, \mu_{\text{L}}) - f(\epsilon, \mu_{\text{R}})\Big) d\epsilon, \tag{4.4}$$

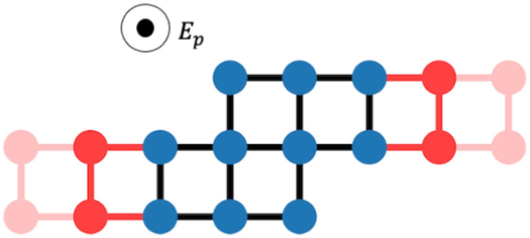

Figure 4.1: Schematic of the S geometry. Blue dots are sites of the scattering region and the red dots are sites on the lead. The black and red links between the sites represent hopping. E_p is the component of the electric field pointing in the out of plane direction.

where $f(\epsilon,\mu_\alpha) = [\exp\big(\beta_\alpha(\epsilon-\mu_\alpha)\big)+1]^{-1}$, μ_α is the the chemical potential of lead α and $\beta_\alpha = \frac{1}{k_\mathrm{B}T_\alpha}$ with T_α the temperature of lead α. We will restrict ourselves to equal temperatures for the leads $\beta_{\mathrm{L,R}} = \frac{1}{k_\mathrm{B}T} = \beta$. The chemical potential of the left, right lead read are given by $\mu_\mathrm{L} = E_\mathrm{F} + \frac{1}{2}V, \quad \mu_\mathrm{R} = E_\mathrm{F} - \frac{1}{2}V$ (assuming symmetric capacitive coupling). The transmission is given by

$$T_{\mathrm{LR}}(\epsilon,m,V) = \mathrm{Tr}\big[\mathbf{\Gamma}_\mathrm{L}(\epsilon,m)\mathbf{G}^+\mathbf{\Gamma}_\mathrm{R}(\epsilon)\mathbf{G}^-(\epsilon,\langle n_{ks}(m,V)\rangle,m)\big]. \tag{4.5}$$

Note that from now on, whenever a product of operators occurs, the arguments of the Green's functions are written at the end of the product, so in eq. (4.5) the retarded and advanced Green's functions depend on the same argument $(\epsilon,\langle n_{ks}(m,V)\rangle,m)$. It can be seen that we only magnetize the left lead with magnetization m. Using eq. (4.4) we can write the magnetocurrent as:

$$\begin{aligned}\Delta I(m,V) &\equiv I(m,V) - I(-m,V)\\ &= \int_{-\infty}^{\infty}\Big[T_{\mathrm{LR}}(\epsilon,m,V) - T_{\mathrm{LR}}(\epsilon,-m,V)\Big]\Big(f(\epsilon,\mu_\mathrm{L}) - f(\epsilon,\mu_\mathrm{R})\Big)d\epsilon.\end{aligned} \tag{4.6}$$

It is our goal to determine the bias dependence of the magnetocurrent $\Delta I(m,V)$. If the Coulomb interactions are absent, $(U=0)$ the magnetocurrent vanishes due to Büttiker's reciprocity theorem for two terminal systems. Thus we should go beyond the non-interacting particle picture $(U \neq 0)$ in order to find a finite magnetocurrent in the presence of spin-orbit coupling.[21,23,25] This magnetocurrent can only be non-linear in the bias voltage, since linear terms vanish due to the Onsager-Casimir reciprocity[2–4] theorem. Due to the absence of vibrational modes in our description, only the Coulomb interactions can be responsible for the occurrence of a non zero magnetocurrent and these interactions manifest themselves through the electron densities. The bias dependence of the magnetocurrent therefore has its origin in the bias dependence of the electron densities. We study the bias dependence of the electron densities in detail by exploiting the bipartite lattice symmetry and time-reversal property of the Green's function.

4.3.2. ELECTRON GREEN'S FUNCTION

The retarded Green's function of the scattering region, coupled to leads, in the Hartree-Fock approximation is given by:

$$\mathbf{G}^{+}_{\mathrm{HFA}}(\epsilon, \langle n_{ks}(m,V)\rangle, m) = \left[\left(\epsilon + \frac{U}{2}\right)\mathbf{I} - \mathbf{H}_{\mathrm{T}} - \mathbf{H}_{\mathrm{SOC}} - U\mathbf{n}(\langle n_{ks}(m,V)\rangle) - \boldsymbol{\Sigma}(\epsilon, m)\right]^{-1}, \quad (4.7)$$

and in the Hubbard One approximation the retarded Green's function is given by (see e.g. chapter 12 of Haug and Jauho[26]):

$$\mathbf{G}^{+}_{\mathrm{HIA}}(\epsilon, \langle n_{ks}(m,V)\rangle, m) = \left[\left[(\epsilon - \frac{U}{2})\mathbf{I} + U\mathbf{n}(\langle n_{ks}(m,V)\rangle)\right]^{-1}(\epsilon - \frac{U}{2})(\epsilon + \frac{U}{2})\mathbf{I} - \mathbf{H}_{\mathrm{T}} - \mathbf{H}_{\mathrm{SOC}} - \boldsymbol{\Sigma}(\epsilon, m)\right]^{-1}, \quad (4.8)$$

For our analyses of the WBL and SIF leads we will only magnetize the left lead with magnetization m. Here the retarded self energy is defined as the sum of retarded self-energies for the left and right lead $\boldsymbol{\Sigma}(\epsilon, m) = \boldsymbol{\Sigma}^{\mathrm{L}}(\epsilon, m) + \boldsymbol{\Sigma}^{\mathrm{R}}(\epsilon)$ and the diagonal matrix $\mathbf{n}(\langle n_{ks}(m,V)\rangle)$ has elements $n_{ks,k's'} = \langle n_{k\bar{s}}(m,V)\rangle \delta_{kk'}\delta_{ss'}$ (where $\bar{s}$ denotes that spin s is flipped).

In the WBL, the retarded self energy is purely imaginary and energy-independent, it is given by: $\boldsymbol{\Sigma}_{\mathrm{WBL}}(\epsilon, m) = -\frac{i}{2}\left(\boldsymbol{\Gamma}_{\mathrm{L}}(m) + \boldsymbol{\Gamma}_{\mathrm{R}}\right)$. Only the diagonal matrix elements of lead α that are coupled to the molecule are nonzero and they are given by $\gamma_\alpha(\mathbf{I} + p_z^\alpha \sigma_z)$. Here γ_α is the coupling strength and $p_z^\alpha \in [-1,1]$ is the magnetic polarization of lead α.
For SIF leads with on-site energy ϵ_0 and nearest neighbour hopping t_{lead}, the retarded self energy is given by $\Sigma(\epsilon) = \Lambda(\epsilon) - \frac{i}{2}\Gamma(\epsilon)$. Here $\Lambda(\epsilon), \Gamma(\epsilon)$ are both real and for $|\epsilon - \epsilon_0| < 2t_{\mathrm{lead}}$ they are given by:[27] $\Gamma(\epsilon, \epsilon_0, t_{\mathrm{lead}}) = \sqrt{(2t_{\mathrm{lead}})^2 - (\epsilon - \epsilon_0)^2}$, $\Lambda(\epsilon, \epsilon_0, t) = \frac{\epsilon - \epsilon_0}{2}$ and for $|\epsilon - \epsilon_0| \geq 2t_{\mathrm{lead}}$ they are given by $\Gamma(\epsilon, \epsilon_0, t_{\mathrm{lead}}) = 0$, $\Lambda(\epsilon, \epsilon_0, t_{\mathrm{lead}}) = \frac{\epsilon - \epsilon_0}{2} - \mathrm{sign}(\epsilon - \epsilon_0)\frac{1}{2}\sqrt{(\epsilon - \epsilon_0)^2 - (2t_{\mathrm{lead}})^2}$.

For semi infinite leads we take the coupling parameter between electrons on the molecule and the lead to be a constant real number: t_{c}, and as a consequence, the retarded self energy is given by $\Sigma(\epsilon, \epsilon_0, t_{\mathrm{lead}}) \rightarrow \tilde{\Sigma}(\epsilon, \epsilon_0, t_{\mathrm{lead}}, t_{\mathrm{c}}) = \left|\frac{t_c}{t_{\mathrm{lead}}}\right|^2 \left[\Lambda(\epsilon, \epsilon_0, t_{\mathrm{lead}}) - \frac{i}{2}\Gamma(\epsilon, \epsilon_0, t_{\mathrm{lead}})\right]$. When lead α is magnetically polarized with $p_z^\alpha \in [-1,1]$ the bands for up and down spin electron split such that for the spin - up bands: $\epsilon_0 \rightarrow \epsilon_u = \epsilon_0 + m^\alpha$ and for the spin-down bands $\epsilon_0 \rightarrow \epsilon_d = \epsilon_0 - m^\alpha$, where the magnetization of lead α is defined as $m^\alpha = 2t_{\mathrm{lead}} p_z^\alpha$. For a SIF lead magnetized with magnetization m and $\epsilon_0 = 0$, Γ and Λ satisfy:

$$\Gamma(\epsilon, m) = \Gamma(-\epsilon, -m), \quad (4.9)$$

$$\Lambda(\epsilon, m) = -\Lambda(-\epsilon, -m). \quad (4.10)$$

Throughout our analyses for SIF leads we take the on-site energies of the left and right lead to be zero $\epsilon_0 = 0$.

4.3.3. GREEN'S FUNCTION: TRANSFORMATION UNDER TIME-REVERSAL - AND SUBLATTICE SYMMETRY

The time reversal operator is given by $\mathbf{T} = i\sigma_y\mathbf{K}$, where $\mathbf{K}$ is the conjugation operator. Under $\mathbf{T}$ the retarded and advanced Green's functions (indicated with a plus and minus respectively) transform as follows:

$$\mathbf{T}\mathbf{G}^{\pm}(\epsilon,\langle n_{ks}(m,V)\rangle,m)\mathbf{T}^{-1} = \mathbf{G}^{\mp}(\epsilon,\langle n_{k\bar{s}}(m,V)\rangle,-m). \tag{4.11}$$

We emphasize that in eq. (4.11) the magnetization m in the argument of the electron densities does not change sign because the real valued electron densities transform under $\mathbf{T}$ as: $\mathbf{T}\langle n_{ks}(m,V)\rangle\mathbf{T}^{-1} = \langle n_{k\bar{s}}(m,V)\rangle$.

If the lattice of the system can be separated into sublattices A and B such that there is only hopping possible from site A to site B and vice versa, then the system is bipartite. In that case the Green's function (HFA eq. (4.7) and HIA eq. (4.8)) in the wide-band limit and for semi-infinite leads (SIF) satisfy:

$$\mathbf{G}^{\pm}_{\mathrm{WBL}}(\epsilon,\langle n_{ks}(m,V)\rangle,m) = -\mathbf{M}\mathbf{G}^{\mp}_{\mathrm{WBL}}(-\epsilon,1-\langle n_{ks}(m,V)\rangle,m)\mathbf{M}, \tag{4.12}$$

$$\mathbf{G}^{\pm}_{\mathrm{SIF}}(\epsilon,\langle n_{ks}(m,V)\rangle,m) = -\mathbf{M}\mathbf{G}^{\mp}_{\mathrm{SIF}}(-\epsilon,1-\langle n_{ks}(m,V)\rangle,-m)\mathbf{M}. \tag{4.13}$$

Here $\mathbf{M}$ is a diagonal matrix which takes the values $+1$ for sites on sublattice A and -1 for sites on sublattice B. Here the diagonal matrices $\mathbf{I},\mathbf{n},\mathbf{\Sigma}$ are invariant under $\mathbf{M}$ and nearest neighbor hopping matrices change sign under $\mathbf{M}$: $\mathbf{M}\mathbf{H}_{\mathrm{T,SOC}}\mathbf{M} = -\mathbf{H}_{\mathrm{T,SOC}}$. Note that particles and holes are interchanged: $\langle n_{ks}(m,V)\rangle \to 1-\langle n_{ks}(m,V)\rangle$ and note that (contrary to WBL leads) for SIF leads the magnetization m changes sign under this transformation due to properties of the self energies in eqs. (4.9), (4.10) (see Appendix 4.6.1).

The electron density for site k with spin s is given by:

$$\langle n_{ks}(m,V)\rangle = \int \Big(\mathbf{G}^{+}\mathbf{\Gamma}^{<}(\epsilon,m,V)\mathbf{G}^{-}(\epsilon,\langle n_{ks}(m,V)\rangle,m)\Big)_{ks,ks}\frac{d\epsilon}{2\pi}, \tag{4.14}$$

where (with $E_{\mathrm{F}} = 0$):

$$\mathbf{\Gamma}^{<}(\epsilon,m,V) = \mathbf{\Gamma}_{\mathrm{L}}(\epsilon,m)f(\epsilon,\frac{V}{2}) + \mathbf{\Gamma}_{\mathrm{R}}(\epsilon)f(\epsilon,-\frac{V}{2}). \tag{4.15}$$

Note that in eq. (4.14) both the retarded and advanced Green's functions depend on the same argument $(\epsilon,\langle n_{ks}(m,V)\rangle,m)$ written at the end of the expression, while $\mathbf{\Gamma}^{<}$ depends on (ϵ,m,V). Note the the Fermi level E_{F} is precisely aligned with the energy $\epsilon = 0$ around which the density of states, corresponding to these systems, is particle hole symmetric. This alignment forms one of the cornerstones of our analyses the other one being that the capacitive coupling to the left and right lead is symmetric.

4.3.4. WIDE BAND LIMIT

The wide band limit is representative for a gold lead with its flat density of states around the Fermi level.[28] In this section we analyse the electron density in eq. (4.14) and the magnetocurrent (4.6) using the time-reversal and bipartite lattice transformations of the Green's functions in eqs. (4.11), (4.12). From the time-reversal transformation of the

Green's function (4.11) and $\mathbf{T}\langle n_{ks}(m,V)\rangle\mathbf{T}^{-1} = \langle n_{k\bar{s}}(m,V)\rangle$ (note that m does not change sign, since $\mathbf{T}$ only flips the spin index of the matrix) follows the identity: $\mathbf{G}^{+}\mathbf{\Gamma}^{<}(\epsilon,m,V)\mathbf{G}^{-}(\epsilon,\langle n_{ks}(m,V)\rangle,m) = \mathbf{T}^{-1}\mathbf{G}^{-}\mathbf{\Gamma}^{<}(\epsilon,-m,V)\mathbf{G}^{+}(\epsilon,\langle n_{k\bar{s}}(m,V)\rangle,-m)\mathbf{T}$ which we use to rewrite the RHS of eq. (4.14). We then multiply both sides from the left with $\mathbf{T}$ and from the right with $\mathbf{T}^{-1}$ which flips the spin on the LHS and cancels the time-reversal operators on the RHS. Equation (4.14) then becomes:

$$\langle n_{k\bar{s}}(m,V)\rangle = \int_{-\infty}^{\infty}\Big(\mathbf{G}^{-}\mathbf{\Gamma}^{<}(\epsilon,-m,V)\mathbf{G}^{+}(\epsilon,\langle n_{k\bar{s}}(m,V)\rangle,-m)\Big)_{ks,ks}\frac{d\epsilon}{2\pi}. \tag{4.16}$$

For the WBL, we can rewrite $\mathbf{\Gamma}^{<}(\epsilon,-m,V)$ using the fact that $f(\epsilon,\mu)+f(-\epsilon,-\mu)=1$. The electron density in eq. (4.16) can thus be expressed as:

$$\begin{aligned}\langle n_{k\bar{s}}(m,V)\rangle = &\int_{-\infty}^{\infty}\Big(\mathbf{G}^{-}\Big[\mathbf{\Gamma}_{\mathrm{L}}(-m)+\mathbf{\Gamma}_{\mathrm{R}}\Big]\mathbf{G}^{+}(\epsilon,\langle n_{k\bar{s}}(m,V)\rangle,-m)\Big)_{ks,ks}\frac{d\epsilon}{2\pi}\\ &-\int_{-\infty}^{\infty}\Big(\mathbf{G}^{-}\mathbf{\Gamma}^{<}_{\mathrm{WBL}}(-\epsilon,-m,-V)\mathbf{G}^{+}(\epsilon,\langle n_{k\bar{s}}(m,V),-m)\Big)_{ks,ks}\frac{d\epsilon}{2\pi}.\end{aligned} \tag{4.17}$$

From the properties of the HFA and HIA Green's functions, defined in eqs. (4.7) & (4.8), it follows that they satisfy the identity: $\mathbf{G}^{-}\Big[\mathbf{\Gamma}_{\mathrm{L}}+\mathbf{\Gamma}_{\mathrm{R}}\Big]\mathbf{G}^{+} = \mathbf{G}^{+}\Big[\mathbf{\Gamma}_{L}+\mathbf{\Gamma}_{R}\Big]\mathbf{G}^{-}$. This identity is used to rewrite the first term on the RHS, which is recognized to be equal to 1, because it can be interpreted as an electron density on site k with spin s, where the chemical potentials of the left and right lead are at infinity ($f(\epsilon,\mu\to\infty)=1$) yielding a filled level. Thus this expression can be rewritten as:

$$1-\langle n_{k\bar{s}}(m,V)\rangle = \int_{-\infty}^{\infty}\Big(\mathbf{G}^{-}\mathbf{\Gamma}^{<}_{\mathrm{WBL}}(-\epsilon,-m,-V)\mathbf{G}^{+}(\epsilon,\langle n_{k\bar{s}}(m,V)\rangle,-m)\Big)_{ks,ks}\frac{d\epsilon}{2\pi}. \tag{4.18}$$

Next we use the bipartite lattice symmetry. First we multiply the LHS and the RHS from the left and right with the matrix $\mathbf{M}$. The LHS does not change. On the RHS we insert the identity matrix $\mathbf{I}=\mathbf{MM}$ between the matrices of the product and finally use eq. (4.12) to transform the Green's functions. The integration variable is changed as $\epsilon\to-\epsilon$ to obtain:

$$1-\langle n_{k\bar{s}}(m,V)\rangle = \int_{-\infty}^{\infty}\Big(\mathbf{G}^{+}\mathbf{\Gamma}^{<}_{\mathrm{WBL}}(\epsilon,-m,-V)\mathbf{G}^{-}(\epsilon,1-\langle n_{k\bar{s}}(m,V)\rangle,-m)\Big)_{ks,ks}\frac{d\epsilon}{2\pi}. \tag{4.19}$$

Note that eq. (4.19) is, except for the density dependence of the Green's functions, almost the same as the expression for the densities $\langle n_{ks}(-m,-V)\rangle$:

$$\langle n_{ks}(-m,-V)\rangle = \int_{-\infty}^{\infty}\Big(\mathbf{G}^{+}\mathbf{\Gamma}^{<}_{\mathrm{WBL}}(\epsilon,-m,-V)\mathbf{G}^{-}(\epsilon,\langle n_{ks}(-m,-V)\rangle,-m)\Big)_{ks,ks}\frac{d\epsilon}{2\pi}. \tag{4.20}$$

Equations (4.19) and (4.20) describe self-consistency equations for the respective densities. Self-consistent solutions of eq. (4.20) are by definition solutions of eq. (4.19) and vice-versa. From this we conclude:

$$1-\langle n_{k\bar{s}}(m,V)\rangle = \langle n_{ks}(-m,-V)\rangle. \tag{4.21}$$

Now we turn to the magnetocurrent. The transmission is given by eq. (4.5) and for WBL leads the $\mathbf{\Gamma}_{\mathrm{L,R}}$ are energy-independent. The time-reversal operator allows us to rewrite this expression as:

$$T_{\mathrm{LR}}(\epsilon,m,V)=\mathrm{Tr}\big[\mathbf{\Gamma}_{\mathrm{L}}(m)\mathbf{G}^{-}\mathbf{\Gamma}_{\mathrm{R}}\mathbf{G}^{+}\big(\epsilon,\langle n_{k\bar{s}}(m,V)\rangle,-m\big)\big], \tag{4.22}$$

since $\mathbf{T}\langle n_{ks}(m,V)\rangle\mathbf{T}^{-1}=\langle n_{k\bar{s}}(m,V)\rangle$. The bipartite symmetry of the Green's function (eq. (4.12)) in combination with $\langle n_{k\bar{s}}(m,V)\rangle = 1-\langle n_{ks}(-m,-V)\rangle$ (eq. (4.21)) implies:

$$T_{\mathrm{LR}}(\epsilon,m,V)=\mathrm{Tr}[\mathbf{\Gamma}_{\mathrm{L}}(-m)\mathbf{G}^{+}\mathbf{\Gamma}_{\mathrm{R}}\mathbf{G}^{-}\big(-\epsilon,\langle n_{ks}(-m,-V)\rangle,-m\big)\big]. \tag{4.23}$$

The expression on the RHS is recognized as the transmission for a negative magnetization and negative bias voltage and negative energy: $T_{\mathrm{LR}}(-\epsilon,-m,-V)$. Provided the bias window is centered around the symmetric point $\epsilon=0$ it follows from the definition of the current (eq. (4.4)) and this property of the transmission that:

$$I(-m,-V)=-I(m,V). \tag{4.24}$$

Then the magnetocurrent satisfies $\Delta I(m,V)=I(m,V)-I(-m,V)=I(m,-V)-I(-m,-V)=\Delta I(m,-V)$. Therefore, the magnetocurrent is a purely even function of the bias voltage $\Delta I_{\mathrm{WBL}}(m,V)=\Delta I_{\mathrm{WBL}}(m,-V)$.

4.3.5. SEMI - INFINITE LEADS

Here we analyse the electron densities for SIF leads. First we rewrite $\mathbf{\Gamma}^{<}(\epsilon,m,V)$ by using that $f(\epsilon,\mu)+f(-\epsilon,-\mu)=1$ and by using eq. (4.9) to rewrite $\mathbf{\Gamma}_{\mathrm{L}}(\epsilon,m)$ and $\mathbf{\Gamma}_{\mathrm{R}}(\epsilon)$. The electron density in eq. (4.16) is then rewritten as:

$$1-\langle n_{k\bar{s}}(m,V)\rangle=\int_{-\infty}^{\infty}\Big(\mathbf{G}^{-}\mathbf{\Gamma}^{<}_{\mathrm{SIF}}(-\epsilon,m,-V)\mathbf{G}^{+}(\epsilon,\langle n_{k\bar{s}}(m,V)\rangle,-m)\Big)_{ks,ks}\frac{d\epsilon}{2\pi}. \tag{4.25}$$

Note the opposite sign of the magnetization m in $\mathbf{\Gamma}^{<}_{\mathrm{SIF}}$ in eq. (4.25) with respect to that occurring in eq. (4.18). Again we apply the matrix $\mathbf{M}$ to both sides and insert the identity matrix $\mathbf{I}=\mathbf{MM}$ between the matrices of this product and use eq. (4.13) to transform the Green's functions. Changing the integration variable as $\epsilon\rightarrow-\epsilon$ gives:

$$1-\langle n_{k\bar{s}}(m,V)\rangle=\int_{-\infty}^{\infty}\Big(\mathbf{G}^{+}\mathbf{\Gamma}^{<}_{\mathrm{SIF}}(\epsilon,m,-V)\mathbf{G}^{-}(\epsilon,1-\langle n_{k\bar{s}}(m,V)\rangle,m)\Big)_{ks,ks}\frac{d\epsilon}{2\pi}. \tag{4.26}$$

The RHS of this self-consistency equation has the same form as the one for $\langle n_{ks}(+m,-V)\rangle$. From this we conclude:

$$1-\langle n_{k\bar{s}}(m,V)\rangle=\langle n_{ks}(m,-V)\rangle. \tag{4.27}$$

We now turn to the transmission, which is given by eq. (4.5). For SIF leads the $\mathbf{\Gamma}_{\mathrm{L,R}}$ are energy dependent. The Green's functions transform under time-reversal symmetry according to eq. (4.11) and the transformation under bipartite lattice symmetry for semi-infinite leads according to eq. (4.13). Combining these two transformations we obtain for the transmission:

$$\begin{aligned} T_{\mathrm{LR}}(\epsilon, m, V) &= \mathrm{Tr}\Big[\boldsymbol{\Gamma}_{\mathrm{L}}(\epsilon, -m)\mathbf{G}^{+}\boldsymbol{\Gamma}_{\mathrm{R}}(\epsilon)\mathbf{G}^{-}\big(-\epsilon, 1-\langle n_{k\bar{s}}(m, V)\rangle, m\big)\Big], \\ &= \mathrm{Tr}\Big[\boldsymbol{\Gamma}_{\mathrm{L}}(-\epsilon, m)\mathbf{G}^{+}\boldsymbol{\Gamma}_{\mathrm{R}}(-\epsilon)\mathbf{G}^{-}\big(-\epsilon, \langle n_{ks}(m, -V)\rangle, m\big)\Big], \\ &= T_{\mathrm{LR}}(-\epsilon, m, -V). \end{aligned} \tag{4.28}$$

In the last step we rewrite $\boldsymbol{\Gamma}_{\mathrm{L}}(\epsilon, -m)$ and $\boldsymbol{\Gamma}_{\mathrm{R}}(\epsilon)$ using eq. (4.9) and we use that the electron density satisfies eq. (4.27). The RHS of eq. (4.28) is recognized as the transmission for negative bias and negative energy. If the bias window is centered around the symmetric point $\epsilon = 0$ then from the definition of the current eq. (4.4) and eq. (4.28) it follows that $I(m, V) = -I(m, -V)$ and thus that the magnetocurrent is an odd function of bias voltage $\Delta I_{\mathrm{SIF}}(m, V) = -\Delta I_{\mathrm{SIF}}(m, -V)$. In Appendix 4.6.2 we show that if the on-site energies of the left and right leads are equal to the chemical potential of the respective leads ($\epsilon_{0,\mathrm{L}} \to \mu_{\mathrm{L}} = E_{\mathrm{F}} + \frac{V}{2}$ & $\epsilon_{0,\mathrm{R}} \to \mu_{\mathrm{R}} = E_{\mathrm{F}} - \frac{V}{2}$) then still the magnetocurrent is an exactly odd function of bias voltage for SIF leads.

4.4. NUMERICAL RESULTS

We use parameters corresponding to a molecule consisting of sp^2- hybridized carbon atoms, to resemble that we have 1 electron per site. The hopping parameter then is $t = 2.4$ eV[29] and the on-site Coulomb interaction parameter $U_C = 10.06$ eV.[30] However due to the image-charge effect[31] the Coulomb interaction strength will be lowered to an extent which sensitively depends on the molecule-lead separation. In our case it is not known what the exact value of U will be due to the image-charge effect, probably we are in the regime where $U/t > 1$ making the HIA more appropriate. However to show that our analytical result is independent of the approximation we perform a numerical calculation for both the HFA and the HIA. We vary U between $0.5t$ and $3t$, where for small values of the Coulomb interaction strength ($U/t \leq 1$) the HFA is used and for large values ($U/t > 1$) the HIA is used. Furthermore we take $T = 300$ K. The spin-orbit coupling parameter is taken to be $\lambda/t = 0.1$, this is rather large, however we found that symmetry of the bias dependence of the magnetocurrent is not affected by the size λ. The magnitude of the magnetocurrent of course scales directly with λ. In the WBL the coupling parameter to the leads is taken to be $\gamma_{\mathrm{L,R}} = 0.5$ eV[28] and $p_z^{\mathrm{L}} = 0.5$. For SIF leads the hopping parameter of the left and right lead is take to be $t_{\mathrm{lead}} = 3t$, the coupling parameter $t_{coup} = \frac{1}{2}\sqrt{t_{\mathrm{lead}}}$, the magnetic polarization of the left lead is taken to be $p_z^{\mathrm{L}} = 0.8$ and the on-site energies of the left and right lead are equal to the chemical potential of the respective leads ($\epsilon_{0,\mathrm{L}} \to \mu_{\mathrm{L}} = \frac{V}{2}$ & $\epsilon_{0,\mathrm{R}} \to \mu_{\mathrm{R}} = -\frac{V}{2}$). We always take the Fermi level $E_{\mathrm{F}} = 0$. We have implemented a non-equilibrium transport code which can be found in `https://github.com/khhuisman/Coulomb_Bipartite.git` and for details regarding the calculation of the electron densities see Appendix 4.6.5.

In fig. 4.2 the magnetocurrent is plotted as function of bias voltage for leads in the WBL and Green's function in the HFA (fig. 4.2a) and the HIA (fig. 4.2b). Both figures show that the magnetocurrent is an even function of the bias voltage. This is explained as follows. We have found that the electron densities in the WBL satisfy eq. (4.21), which we rewrite in the form:

$$1 - \langle n_{k\bar{s}}(m, V)\rangle - \langle n_{ks}(-m, -V)\rangle = 0. \tag{4.29}$$

In our numerical calculations we find that the LHS of this equation vanishes indeed (except for numerical errors that can be made small), which is due to the bipartite lattice symmetry of the Green's functions with WBL leads. In sec. 4.3.4 we showed the magnetocurrent then is an even function of the bias voltage. We varied the value of U/t for both the HFA and HIA and found that the magnetocurrent remained dominantly even. When an asymmetry between the coupling parameter to the left and right lead $\gamma_\mathrm{L} \neq \gamma_\mathrm{R}$ is introduced the magnetocurrent remains a dominantly even function of bias voltage as expected (see Appendix 4.6.3).

In fig. 4.3 the magnetocurrent for SIF leads $\Delta I_\mathrm{SIF}(m, V)$ is plotted as a function of bias voltage for the HFA (fig. 4.3a) and the HIA (fig. 4.3b). In both cases the magnetocurrent is a dominantly odd function of bias voltage. We have found that the electron densities for SIF leads satisfy eq. (4.27), which we rewrite in the form:

$$1 - \langle n_{k\bar{s}}(m, V)\rangle - \langle n_{ks}(m, -V)\rangle = 0. \tag{4.30}$$

Again we find in our numerical calculations that the LHS of this equation vanishes. This is a consequence of the bipartite lattice symmetry of the Green's function with SIF leads and it explains why we find an odd magnetocurrent as discussed in sec. 4.3.5. Again when an asymmetry in the coupling parameter t_c is introduced between the left and the right lead we find that the magnetocurrent remains and odd function for SIF leads (see Appendix 4.6.3).

Finally, we demonstrate time-reversibility for the densities in equilibrium. As in our previous work on Coulomb interactions,[23] our numerical results show that in equilibrium the electron densities satisfy time-reversal symmetry: $\langle n_{ks}(m, V = 0)\rangle = \langle n_{k\bar{s}}(-m, V = 0)\rangle$, which is attributed to the Onsager-Casimir reciprocity. In Appendix 4.6.4 we analytically show that the electron densities always satisfy time-reversal symmetry in equilibrium. Furthermore we find that the magnetocurrent vanishes if the spin-orbit coupling parameter is set to zero and that the largest size of the effect, defined as $P_C = \frac{I(m)-I(-m)}{I(m)+I(-m)}$, is of the order 0.1 %. A more minimal model of the S-shape (in fig. 4.1), consisting of a chain with 4 sites and with a 'kink' present between the second and the third site, also shows a finite magnetocurrent that satisfies the same symmetries.

4.5. CONCLUSION

In this work we studied the voltage dependence of the magnetocurrent for systems with Coulomb interactions (in the HFA and HIA) and a nearest neighbour spin-orbit coupling. We showed analytically that for a Fermi level that is aligned with energy around which the density of states is particle hole symmetric and a capacitive coupling of the molecule to the lead that is symmetric, the magnetocurrent is exactly even in the WBL and exactly odd for SIF leads by exploiting the bipartite lattice symmetry of the Green's function. Our numerical calculations support this result. To test the predicted behaviour of the magnetocurrent experimentally, a gate voltage can be used to align the energy around which the density of states is particle hole symmetric with the Fermi-level. The WBL is appropriate for gold electrodes near the Fermi-level, thus provided that the molecule is approximately particle-hole symmetric an even magnetocurrent is expected. An asymmetry in the coupling from the molecule to right and left lead ($\gamma_L \neq \gamma_R$) does not affect symmetry properties either, as shown in appendix 4.6.3. In our previous work on Coulomb interactions[23] we modelled leads in the WBL and we had a next-nearest neighbor spin-orbit coupling mechanism which destroys the bipartite lattice symmetry. When the Fermi level was aligned with the energy around which the density of states is approximately particle hole symmetric and the capacitive coupling of the molecule to the lead that was symmetric, we found a nearly perfect odd magnetocurrent. The absence of bipartite lattice symmetry in our previous work is the reason why we find a different behaviour of the magnetocurrent than in this paper, where ΔI_{WBL} is even in bias voltage.

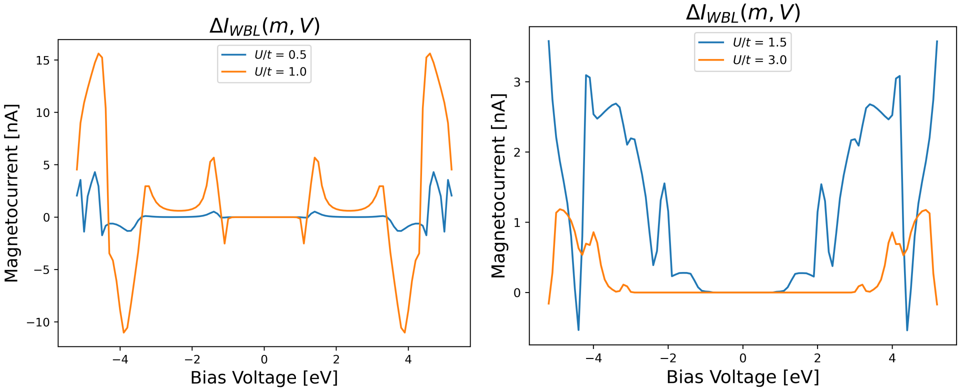

(a) (b)

Figure 4.2: The WBL magnetocurrent, $\Delta I_{\text{WBL}}(m,V)$, is plotted as a function of bias voltage in the HFA (fig. 4.2a) and HIA (fig. 4.2b).

4.6. APPENDIX

4.6.1. GREEN'S FUNCTION : PARTICLE HOLE TRANSFORMATION

In this section we will show that the Hartree-Fock Green's function in eq. (4.7) transforms as in eqs. (4.12) and (4.13). In eq. (4.7) the hopping matrices change sign under particle hole transformation: $\mathbf{M}\mathbf{H}_{\text{T,SOC}}\mathbf{M} = -\mathbf{H}_{\text{T,SOC}}$ while the self energy $\mathbf{\Sigma}(\epsilon,m)$ and the electron density matrix $\mathbf{n}$ do not, because they are diagonal matrices: $\mathbf{M}\mathbf{\Sigma}(\epsilon,m)\mathbf{M} = \mathbf{\Sigma}(\epsilon,m)$ and $\mathbf{M}\mathbf{n}\mathbf{M} = \mathbf{n}$. Therefore in general the HFA Green's function transforms as:

$$\begin{aligned} -\mathbf{M}\mathbf{G}^{+}_{\text{HFA}}(\epsilon,\langle n_{is}(m,V)\rangle,m)\mathbf{M} &= -\left[\epsilon\mathbf{I}+\mathbf{H}_{\text{T}}+\mathbf{H}_{\text{SOC}}-U\mathbf{n}+\frac{U}{2}\mathbf{I}-\mathbf{\Sigma}(\epsilon,m)\right]^{-1}, \\ &= \left[-\epsilon\mathbf{I}-\mathbf{H}_{\text{T}}-\mathbf{H}_{\text{SOC}}-U\Big(\mathbf{I}-\mathbf{n}\Big)+\frac{U}{2}\mathbf{I}+\mathbf{\Sigma}(\epsilon,m)\right]^{-1}. \end{aligned} \tag{4.31}$$

In the WBL the retarded self-energy is purely imaginary and does not depend on energy $\mathbf{\Sigma}(\epsilon,m) = -\frac{i}{2}\mathbf{\Gamma}(m)$ therefore $\mathbf{\Sigma}(\epsilon,m) = -\mathbf{\Sigma}^{\dagger}(-\epsilon,m)$. From this we obtain:

$$-\mathbf{M}\mathbf{G}^{+}_{\text{HFA,WBL}}(\epsilon,\langle n_{is}(m,V)\rangle,m)\mathbf{M} = \mathbf{G}^{-}_{\text{HFA,WBL}}(-\epsilon,1-\langle n_{is}(m,V)\rangle,m). \tag{4.32}$$

For SIF leads the retarded self-energy is given by: $\Sigma(\epsilon,m) = \Lambda(\epsilon,m) - \frac{i}{2}\Gamma(\epsilon,m)$. In the region $|\epsilon-m| < 2t_{\text{lead}}$ Λ,Γ satisfy: $\Lambda(\epsilon,m) = \frac{\epsilon-m}{2} = -\frac{-\epsilon-(-m)}{2} = -\Lambda(-\epsilon,-m)$ and $\Gamma(\epsilon,m) = \sqrt{(2t_{\text{lead}})^2-(\epsilon-m)^2} = \Gamma(-\epsilon,-m)$. From this is follows that $\Sigma(\epsilon,m) = -\Big[\Lambda(-\epsilon,-m)+\frac{i}{2}\Gamma(-\epsilon,-m)\Big] = -\Sigma^{\dagger}(-\epsilon,-m)$. In the region $|\epsilon-m| \geq 2t_{\text{lead}}$, $\Gamma(\epsilon,m) = 0$, therefore $\Sigma(\epsilon,m) = \frac{\epsilon-m}{2} - \text{sign}(\epsilon-m)\sqrt{(\epsilon-m)^2-(2t_{\text{lead}})^2} = -\Lambda(-\epsilon,-m)^{\dagger} = -\Sigma^{\dagger}(-\epsilon,-m)$. In conclusion, for SIF leads the reversal of the energy sign in the retarded self energy is accompanied by a reversal of the magnetization and hermitian conjugation: $\mathbf{\Sigma}(\epsilon,m) = \mathbf{\Sigma}^{\dagger}(-\epsilon,-m)$, which leads to the relation $-\mathbf{M}\mathbf{G}^{+}_{\text{HFA,SIF}}(\epsilon,\langle n_{is}(m,V)\rangle,m)\mathbf{M} = \mathbf{G}^{-}_{\text{HFA,SIF}}(-\epsilon,1-\langle n_{is}(m,V)\rangle,-m)$. One can also show these relations for the Green's function in the Hubbard One Approximation.

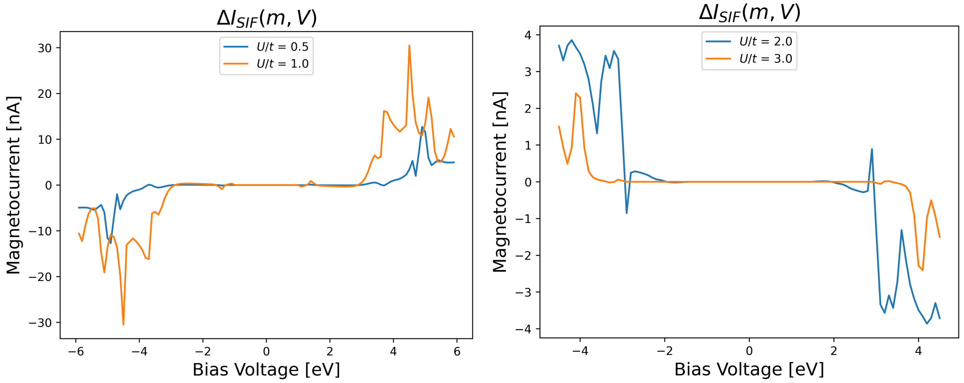

(a)

(b)

Figure 4.3: The SIF magnetocurrent, $\Delta I_{\mathrm{SIF}}(m,V)$, is plotted as a function of bias voltage in the the HFA (fig. 4.3a) and HIA (fig. 4.3b).

4.6.2. SEMI - INFINITE LEADS: VOLTAGE DEPENDENCE OF THE ONSITE ENERGY

In order to keep leads charge-neutral the onsite energy of the lead shift with the bias voltage such that: $\epsilon_{0,\mathrm{L}} = E_{\mathrm{F}} + \frac{V}{2}$ and $\epsilon_{0,\mathrm{R}} = E_{\mathrm{F}} - \frac{V}{2}$. The retarded Green's function becomes explicitly voltage dependent via the retarded self energy : $\mathbf{\Sigma}(\epsilon,m) \rightarrow \mathbf{\Sigma}(\epsilon,m,V)$. Since we use the convention that $E_{\mathrm{F}} = 0$ it follows from the properties of SIF leads (see sec. 4.3.2) that Γ, Λ now satisfy:

$$\Gamma(\epsilon,V,m) = \Gamma(-\epsilon,-V,-m), \tag{4.33}$$

$$\Lambda(\epsilon,V,m) = -\Lambda(-\epsilon,-V,-m). \tag{4.34}$$

where $\Gamma(\epsilon,V,m) = \sqrt{(2t_{\mathrm{lead}})^2 - (\epsilon - m - \frac{V}{2})^2}$ and $\Lambda(\epsilon,V,m) = \frac{\epsilon - m - \frac{V}{2}}{2}$ for $|\epsilon - m - \frac{V}{2}| < 2t_{\mathrm{lead}}$ and $\Gamma(\epsilon,V,m) = 0$, $\Lambda(\epsilon,V,m) = \frac{\epsilon - m - \frac{V}{2}}{2} - \frac{1}{2}\mathrm{sign}(\epsilon - m - \frac{V}{2})\sqrt{(\epsilon - m - \frac{V}{2})^2 - (2t_{\mathrm{lead}})^2}$ for $|\epsilon - m - \frac{V}{2}| \geq 2t_{\mathrm{lead}}$. Due to the properties in eqs. (4.33), (4.34) the bipartite lattice transformation for Green's functions now becomes:

$$\mathbf{G}^{\pm}_{\mathrm{SIF}}(\epsilon,\langle n_{ks}(m,V)\rangle,m,V) = -\mathbf{M}\mathbf{G}^{\mp}_{\mathrm{SIF}}(-\epsilon,1-\langle n_{ks}(m,V)\rangle,-m,-V)\mathbf{M}. \tag{4.35}$$

Note that in eq. (4.35) we added an explicit argument for the bias voltage V to indicate that the self-energy is voltage dependent.

The electron densities eq. (4.14) are now given by:

$$\langle n_{ks}(m,V)\rangle = \int \left(\mathbf{G}^{+}\overline{\mathbf{\Gamma}}^{<}_{\mathrm{SIF}}(\epsilon,m,V)\mathbf{G}^{-}(\epsilon,\langle n_{ks}(m,V)\rangle,m,V)\right)_{ks,ks}\frac{d\epsilon}{2\pi}, \tag{4.36}$$

where (for $E_{\mathrm{F}} = 0$),

$$\overline{\mathbf{\Gamma}}^{<}_{\mathrm{SIF}}(\epsilon,m,V) = \mathbf{\Gamma}_{\mathrm{L}}(\epsilon,V,m)f(\epsilon,\frac{V}{2}) + \mathbf{\Gamma}_{\mathrm{R}}(\epsilon,V)f(\epsilon,-\frac{V}{2}). \tag{4.37}$$

Note that $\mathbf{\Gamma}_{\mathrm{L,R}}$ are voltage dependent quantities here. We use the time-reversal operator to rewrite eq. (4.36) as:

$$\langle n_{k\bar{s}}(m,V)\rangle = \int_{-\infty}^{\infty}\Big(\mathbf{G}^{-}\overline{\mathbf{\Gamma}}^{<}(\epsilon,-m,V)\mathbf{G}^{+}(\epsilon,\langle n_{k\bar{s}}(m,V),-m,V)\Big)_{ks,ks}\frac{d\epsilon}{2\pi}. \tag{4.38}$$

Now we rewrite $\overline{\mathbf{\Gamma}}^{<}(\epsilon,-m,V)$ by using the fact that $f(\epsilon,\mu)+f(-\epsilon,-\mu)=1$ and that $\mathbf{\Gamma}_{\mathrm{L}}(\epsilon,m,V)$, $\mathbf{\Gamma}_{\mathrm{R}}(\epsilon,V)$ transform as in eq. (4.33). Analogously to sec. 4.3.5, the electron density in eq. (4.38) is then rewritten as:

$$1-\langle n_{k\bar{s}}(m,V)\rangle = \int_{-\infty}^{\infty}\Big(\mathbf{G}^{-}\overline{\mathbf{\Gamma}}^{<}_{\mathrm{SIF}}(-\epsilon,m,-V)\mathbf{G}^{+}(\epsilon,\langle n_{k\bar{s}}(m,V)\rangle,-m,V)\Big)_{ks,ks}\frac{d\epsilon}{2\pi}. \tag{4.39}$$

We then use the bipartite lattice symmetry. First we multiply the LHS and the RHS from the left and right with the matrix **M**. The LHS does not change. On the RHS we insert the identity matrix $\mathbf{I}=\mathbf{MM}$ between the matrices of this product and use eq. (4.35) to transform the Green's functions. The integration variable is changes as $\epsilon\to-\epsilon$ to obtain:

$$1-\langle n_{k\bar{s}}(m,V)\rangle = \int_{-\infty}^{\infty}\Big(\mathbf{G}^{+}\overline{\mathbf{\Gamma}}^{<}_{\mathrm{SIF}}(\epsilon,m,-V)\mathbf{G}^{-}(\epsilon,1-\langle n_{k\bar{s}}(m,V)\rangle,m,-V)\Big)_{ks,ks}\frac{d\epsilon}{2\pi}. \tag{4.40}$$

Equation (4.40) is identical to the self-consistency equation of $\langle n_{ks}(+m,-V)\rangle$. From this we conclude:

$$1-\langle n_{k\bar{s}}(m,V)\rangle = \langle n_{ks}(m,-V)\rangle. \tag{4.41}$$

We now turn to the transmission which is given by eq. (4.5) and for SIF leads $\mathbf{\Gamma}_{\mathrm{L,R}}$ are energy dependent. The Green's functions transforms under time-reversal symmetry as in eq. (4.11) and the transformation under particle hole-symmetry for semi-infinite leads as in eq. (4.13) . Combining these two transformations on the transmission we obtain:

$$T_{\mathrm{LR}}(\epsilon,m,V) = \mathrm{Tr}\Big[\mathbf{\Gamma}_{\mathrm{L}}(\epsilon,-m,V)\mathbf{G}^{+}\mathbf{\Gamma}_{\mathrm{R}}(\epsilon,V)\mathbf{G}^{-}\big(-\epsilon,1-\langle n_{k\bar{s}}(m,V)\rangle,m,-V\big)\Big]. \tag{4.42}$$

We then use eq. (4.33) to rewrite $\mathbf{\Gamma}_{\mathrm{L}}(\epsilon,-m,V)$ and $\mathbf{\Gamma}_{\mathrm{R}}(\epsilon,V)$ and that the electron density satisfies eq. (4.41) to obtain: $\mathrm{Tr}\Big[\mathbf{\Gamma}_{\mathrm{L}}(-\epsilon,m,-V)\mathbf{G}^{+}\mathbf{\Gamma}_{\mathrm{R}}(-\epsilon,-V)\mathbf{G}^{-}\big(-\epsilon,\langle n_{ks}(m,-V)\rangle,m,-V\big)\Big]$, which is recognized as the transmission for negative bias negative energy. Thus we conclude:

$$T_{\mathrm{LR}}(\epsilon,m,V) = T_{\mathrm{LR}}(-\epsilon,m,-V). \tag{4.43}$$

If the bias window is centered around the energy $\epsilon=0$ from the definition of the current eq. (2.3) and eq. (4.43) it follows that $I(m,V)=-I(m,-V)$ and thus that the magnetocurrent is an odd function of bias voltage $\Delta I_{\mathrm{SIF}}(m,V)=-\Delta I_{\mathrm{SIF}}(m,-V)$.

4.6.3. ASYMMETRIC COUPLING

In molecular junction there is often an asymmetry in the coupling of the molecule to the left and right lead i.e. $\gamma_{\mathrm{L}} \neq \gamma_{\mathrm{R}}$. In the wide-band limit we quantify this asymmetry by introducing the dimensionless parameter $\chi = \frac{\gamma_{\mathrm{L}} - \gamma_{\mathrm{R}}}{\gamma_{\mathrm{L}} + \gamma_{\mathrm{R}}}$. In fig. 4.4a the wide-band limit magnetocurrent is plotted as a function of bias voltage for different values of this parameters $\chi = -0.6, 0, 0.6$ (corresponding to $(\gamma_{\mathrm{L}}, \gamma_{\mathrm{R}}) = (0.5, 2), (0.5, 0.5), (2, 0.5)$ respectively) in the HFA for $U = 2t, p_{\mathrm{z}} = 0.5$. It clearly shows that for the magnetocurrent is in an even function of bias voltage independent of the value of χ.

For SIF leads we quantify this asymmetry by introducing the dimensionless parameter $\chi_2 = \frac{t_{\mathrm{c}}^{\mathrm{L}} - t_{\mathrm{c}}^{\mathrm{R}}}{t_{\mathrm{c}}^{\mathrm{L}} + t_{\mathrm{c}}^{\mathrm{R}}}$, where t_{c}^{α} is the coupling parameter for electrons on the molecule on electrons on lead α. In fig. 4.4b the SIF magnetocurrent is plotted as a function of bias voltage for $p_{\mathrm{z}} = 0.8$, $t_{\mathrm{lead}}^{\mathrm{L,R}} = 2t$, $t_c^{\mathrm{R}} = \frac{1}{2}\sqrt{t_{\mathrm{lead}}^{\mathrm{R}}}$, $t_c^{\mathrm{L}} = 2\sqrt{t_{\mathrm{lead}}^{\mathrm{L}}}$ and $\frac{U}{t} = 0.5, 1$ in the HFA. The figure shows that the magnetocurrent remains an odd function of voltage. For the HIA the magnetocurrent remains even function of bias voltage in the WBL and an odd function of bias voltage for SIF leads, when an asymmetry in the coupling constant is introduced.

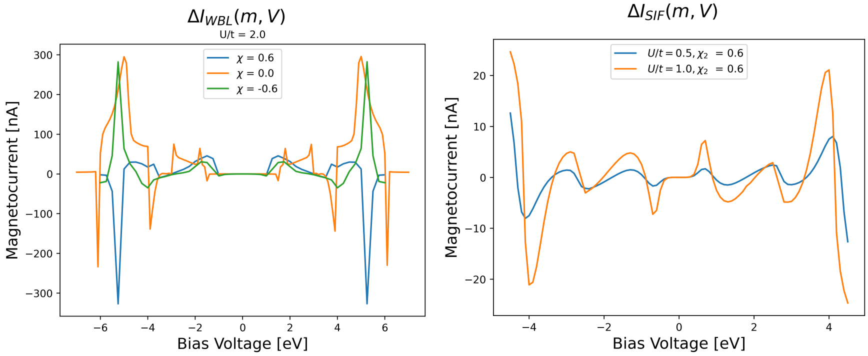

(a) (b)

Figure 4.4: (a) The magnetocurrent in the HFA is plotted as a function of bias voltage when an asymmetry between the coupling in the left and right lead is introduced for WBL leads. (b) The magnetocurrent in the HFA is plotted as a function of bias voltage when an asymmetry between the coupling in the left and right lead is introduced for and SIF leads.

4.6.4. TIME REVERSAL SYMMETRY IN EQUILIBRIUM

Here we show analytically that in equilibrium the electron densities satisfy time-reversal symmetry. To be unambiguous we define equilibrium as $V = 0$ (i.e. $\mu_L = \mu_R$) and take equal temperatures for both leads (i.e. $T_L = T_R$) if one of these conditions is violated we say the system is out of equilibrium.[32] In equilibrium the electron density (eq. (4.14)) is given by:

$$\langle n_{ks}(m, V=0)\rangle = \int_{-\infty}^{\infty} f_0\Big(\mathbf{G}^{+}\Big[\mathbf{\Gamma}_{\mathrm{L}} + \mathbf{\Gamma}_{\mathrm{R}}\Big]\mathbf{G}^{-}(\epsilon, \langle n_{ks}(m, V=0)\rangle, m)\Big)_{ks,ks}\frac{d\epsilon}{2\pi}, \tag{4.44}$$

where $f_0 = f_{\mathrm{L,R}}(E)|_{V=0} = [\exp\big(\beta(E-E_\mathrm{F})\big)+1]^{-1}$. From the time-reversal property of the Green's function eq. (4.11) and $\mathbf{T}\langle n_{ks}(m,V=0)\rangle\mathbf{T}^{-1} = \langle n_{k\bar{s}}(m,V=0)\rangle$ follows the identity: $\mathbf{G}^+[\mathbf{\Gamma}_\mathrm{L}+\mathbf{\Gamma}_\mathrm{R}]\mathbf{G}^-(\epsilon,\mathbf{n}_s(m,V=0),m) = \mathbf{T}^{-1}\mathbf{G}^-[\mathbf{\Gamma}_\mathrm{L}+\mathbf{\Gamma}_\mathrm{R}]\mathbf{G}^+(\epsilon,\mathbf{n}_{\bar{s}}(m,V=0),-m)\mathbf{T}$ which we use to rewrite the RHS of eq. (4.44). We then multiply both sides from the left with $\mathbf{T}$ and from the right with $\mathbf{T}^{-1}$ which flips the spin on the LHS and cancels the time-reversal operators on the RHS. We then use the identity $\mathbf{G}^-\Big[\mathbf{\Gamma}_L+\mathbf{\Gamma}_R\Big]\mathbf{G}^+ = \mathbf{G}^+\Big[\mathbf{\Gamma}_L+\mathbf{\Gamma}_R\Big]\mathbf{G}^-$, which follows from the definition of the Green's functions in eqs. (4.7) & (4.8)), to rewrite the RHS and we obtain:

$$\langle n_{k\bar{s}}(m,V=0)\rangle = \int_{-\infty}^{\infty} f_0\Big(\mathbf{G}^+\Big[\mathbf{\Gamma}_\mathrm{L}+\mathbf{\Gamma}_\mathrm{R}\Big]\mathbf{G}^-(\epsilon,\langle n_{k\bar{s}}(m,V=0)\rangle,-m)\Big)_{ks,ks}\frac{d\epsilon}{2\pi}. \tag{4.45}$$

The self-consistency equation above in eq. (4.45) is the same as for the self-consistency equation of $\langle n_{ks}(-m,V=0)\rangle$. Therefore we obtain the relation:

$$\langle n_{ks}(m,V=0)\rangle = \langle n_{k\bar{s}}(-m,V=0)\rangle. \tag{4.46}$$

Which is recognized as the time reversal symmetry in equilibrium since both spin and magnetization change sign. In our previous work on Coulomb interactions[23] we showed that time-reversal symmetry in equilibrium leads to the fulfillment of Onsager-Casimir reciprocity. Note that this conclusion holds for bipartite and non-bipartite lattices and also holds for any value of Fermi level E_F.

Perhaps it seems like a circular argument is presented here, since we use the time-reversal operator to prove that time-reversal symmetry is satisfied in equilibrium. However no such circular argument is presented. If the temperatures in the left,right lead are unequal (i.e. out of equilibrium) the electron densities after applying the time-reversal operator left and right become:

$$\langle n_{k\bar{s}}(m,V=0)\rangle = \int_{-\infty}^{\infty}\Big(\mathbf{G}^-\Big[\mathbf{\Gamma}_\mathrm{L}f_\mathrm{L}+\mathbf{\Gamma}_\mathrm{R}f_\mathrm{R}\Big]\mathbf{G}^+(\epsilon,\langle n_{k\bar{s}}(m,V=0)\rangle,-m)\Big)_{ks,ks}\frac{d\epsilon}{2\pi}. \tag{4.47}$$

Note that the Green's functions here are reversed with respect to the ones in eq. (4.44). Before we could use the identity $\mathbf{G}^-\Big[\mathbf{\Gamma}_L+\mathbf{\Gamma}_R\Big]\mathbf{G}^+ = \mathbf{G}^+\Big[\mathbf{\Gamma}_L+\mathbf{\Gamma}_R\Big]\mathbf{G}^-$. However in this case we cannot reverse the Green's functions since $\mathbf{G}^-\Big[\mathbf{\Gamma}_\mathrm{L}f_\mathrm{L}+\mathbf{\Gamma}_\mathrm{R}f_\mathrm{R}\Big]\mathbf{G}^+ \neq \mathbf{G}^+\Big[\mathbf{\Gamma}_\mathrm{L}f_\mathrm{L}+\mathbf{\Gamma}_\mathrm{R}f_\mathrm{R}\Big]\mathbf{G}^-$ and therefore $\langle n_{k\bar{s}}(m,V=0)\rangle \neq \langle n_{ks}(-m,V=0)\rangle$. Therefore we conclude that for unequal temperatures in the left,right lead (i.e. "out of equilibrium") the electron densities do not satisfy this time reversal property, consistent with our numerical calculations which show a very small deviation from TRS in that case and a linear magnetocurrent in that case.

4.6.5. SELF CONSISTENT DETERMINATION OF THE ELECTRON DENSITIES

In our transport code we determine the electron density as follows. Suppose we want to calculate the electron density for the decreasing or increasing bias voltages $\{0,V_1,V_2,\ldots\}$, ($|V_{i+1}| > |V_i|$). First of all we start our self-consistent calculation at zero bias voltage where we expect that every site is approximately half filled , therefore we take this as an initial guess ($\langle n_{ks}^{in,m=0}(V=0)\rangle = \frac{1}{2}$). Then we self-consistently determine the electron densities for $V=0$ and obtain the converged result $\langle n_{ks}^{converged}(V=0)\rangle$. We then use these values as an initial guess for the next bias voltage V_1: $\langle n_{ks}^{in,m=0}(V=V_1)\rangle = \langle n_{ks}^{converged}(V=0)\rangle$. We always use the output of a self-consistent calculation as initial guess for the next bias voltage: $\langle n_{ks}^{in,m=0}(V=V_{i+1})\rangle = \langle n_{ks}^{converged}(V=V_i)\rangle$ to adiabatically connect the two solutions. This procedure is done separately for positive and negative bias and both times we start in $V=0$.

Now follows a description of a self-consistent loop for bias voltage V_i. Given an initial guess for bias voltage V_i we iterate over eq. (4.14), $m_{\max}$ times. Every iteration m has an input and an output electron density and as convergence criterion for the m-th iteration we use: $|\langle n_{ks}^{in,m}\rangle - \langle n_{ks}^{out,m}\rangle| < 10^{-4}$. If a density did not converge within the maximum number of iterations $m_{\max}$, we discard it. Furthermore we employ linear mixing of the electron densities meaning that the input for iteration $m+1$ is a linear combination of the input and output of iteration m: $\langle n_{ks}^{in,m+1}(V_i)\rangle = (1-\alpha)\langle n_{ks}^{out,m}(V_i)\rangle + \alpha\langle n_{ks}^{in,m}(V_i)\rangle$ characterized by the parameter $\alpha \in [0,1)$.

The Hamiltonian of the isolated molecule, without interactions ($U=0$) is defined as: $\mathbf{H}_0 = \mathbf{H}_\mathrm{T} + \mathbf{H}_\mathrm{SOC}$ and is constructed with the Kwant code[33] and the Qsymm code.[34]

4.6.6. FORMULA FOR THE CURRENT

In the work of Meir and Wingreen[35] the current into the left lead is given by their eq. 5:

$$I_\mathrm{L} = \frac{ie}{h}\int \mathrm{Tr}\Big[\boldsymbol{\Gamma}_\mathrm{L}(\epsilon)[f(\epsilon,\mu_\mathrm{L})(\boldsymbol{G}^+(\epsilon)-\boldsymbol{G}^-(\epsilon))+\boldsymbol{G}^<(\epsilon)]\Big]d\epsilon. \tag{4.48}$$

We now show that $\mathbf{G}^+(\epsilon)-\mathbf{G}^-(\epsilon) = -i\mathbf{G}^+(\epsilon)\Big(\boldsymbol{\Gamma}_\mathrm{L}(\epsilon)+\boldsymbol{\Gamma}_\mathrm{R}(\epsilon)\Big)\mathbf{G}^-(\epsilon)$ in the HIA. Let us first rewrite $\mathbf{G}^\pm(\epsilon)$ in eq. (4.8):

$$\mathbf{G}^+(\epsilon) = \frac{1}{\mathbf{g}_0(\epsilon)^{-1}-\boldsymbol{\Sigma}(\epsilon)}, \quad \mathbf{G}^-(\epsilon) = \frac{1}{(\mathbf{g}_0(\epsilon)^\dagger)^{-1}-\boldsymbol{\Sigma}^\dagger(\epsilon)}, \tag{4.49}$$

where we define: $\mathbf{g}_0(\epsilon)^{-1} = \left[(\epsilon-\frac{U}{2})\mathbf{I}+U\mathbf{n}\right]^{-1}(\epsilon-\frac{U}{2})(\epsilon+\frac{U}{2})\mathbf{I}-\mathbf{H}_\mathrm{T}-\mathbf{H}_\mathrm{SOC}$, where the matrix $\mathbf{n}$ has elements $n_{ks,k's'} = \langle n_{k\bar{s}}\rangle\delta_{kk'}\delta_{ss'}$ (where $\bar{s}$ denotes that spin s is flipped). It follows that $\mathbf{G}^+(\epsilon)-\mathbf{G}^-(\epsilon) = \mathbf{G}^+(\epsilon)\Big(\boldsymbol{\Sigma}(\epsilon)-\boldsymbol{\Sigma}^\dagger(\epsilon)+(\mathbf{g}_0(\epsilon)^\dagger)^{-1}-\mathbf{g}_0(\epsilon)^{-1}\Big)\mathbf{G}^-(\epsilon)$. Since $\mathbf{g}_0(\epsilon)$ contains no anti-hermitian parts, $\mathbf{g}_0(\epsilon)$ is an hermitian matrix. Here $\boldsymbol{\Sigma}(\epsilon) = \boldsymbol{\Sigma}_\mathrm{L}(\epsilon)+\boldsymbol{\Sigma}_\mathrm{R}(\epsilon)$ is the usual retarded self energy of the leads and $\boldsymbol{\Gamma}_\mathrm{L,R}(\epsilon) = -i(\boldsymbol{\Sigma}_\mathrm{L,R}(\epsilon)-\boldsymbol{\Sigma}_\mathrm{L,R}(\epsilon)^\dagger)$. Thus it follows that $\mathbf{G}^+(\epsilon)-\mathbf{G}^-(\epsilon) = -i\mathbf{G}^+(\epsilon)\Big(\boldsymbol{\Gamma}_\mathrm{L}(\epsilon)+\boldsymbol{\Gamma}_\mathrm{R}(\epsilon)\Big)\mathbf{G}^-(\epsilon)$ in the HIA.

Eq. (4.48) reduces to the Landauer-Büttiker formula in the case that the lesser Green's function is given by $\boldsymbol{G}^<(\epsilon) = i\boldsymbol{G}^+(\epsilon)\Big(\boldsymbol{\Gamma}_\mathrm{L}(\epsilon)f(\epsilon,\mu_\mathrm{L})+\boldsymbol{\Gamma}_\mathrm{R}(\epsilon)f(\epsilon,\mu_\mathrm{R})\Big)\boldsymbol{G}^-(\epsilon)$ and the retarded and advanced Green's function are related as $\boldsymbol{G}^+(\epsilon)-\boldsymbol{G}^-(\epsilon) = -i\boldsymbol{G}^+(\epsilon)\Big(\boldsymbol{\Gamma}_\mathrm{L}(\epsilon)+\boldsymbol{\Gamma}_\mathrm{R}(\epsilon)\Big)\boldsymbol{G}^-(\epsilon)$. We always assume this expression for the lesser Green's function. The latter expression holds for the HFA and HIA , justifying the use of the Landauer-Büttiker formula.

In the analysis of the electron-phonon coupling, the Lang-Firsov transformation is usually applied.[36] This induces a coupling between the vibrational system on the molecule and the leads, preventing us from requiring the leads to be in equilibrium, which is necessary for writing eq. (4.48).

REFERENCES

(1) Huisman, K. H.; Heinisch, J. B. M. Y.; Thijssen, J. M. CISS effect: Magnetocurrent–voltage characteristics with Coulomb interactions. II. *The Journal of Chemical Physics* **2023**, *158*, 174108, DOI: 10.1063/5.0148748.

(2) Onsager, L. Reciprocal Relations in Irreversible Processes. I. *Phys. Rev.* **1931**, *37*, 405–426.

(3) Onsager, L. Reciprocal Relations in Irreversible Processes. II. *Phys. Rev.* **1931**, *38*, 2265–2279.

(4) Casimir, H. B. G. On Onsager's Principle of Microscopic Reversibility. *Rev. Mod. Phys.* **1945**, *17*, 343–350.

(5) Büttiker, M. Symmetry of Electrical Conduction. *IBM Journal of Research and Development* **1988**, *32*, 317–334.

(6) Kulkarni, C.; Mondal, A.; Das, T.; Grinbom, G.; Tassinari, F.; Mabesoone, M.; Meijer, E.; Naaman, R. Highly Efficient and Tunable Filtering of Electrons' Spin by Supramolecular Chirality of Nanofiber-Based Materials. *Advanced Materials* **2020**, *32*, DOI: 10.1002/adma.201904965.

(7) Lu, H.; Xiao, C.; Song, R.; Li, T.; Maughan, A. E.; Levin, A.; Brunecky, R.; Berry, J. J.; Mitzi, D. B.; Blum, V., et al. Highly Distorted Chiral Two-Dimensional Tin Iodide Perovskites for Spin Polarized Charge Transport. *Journal of the American Chemical Society* **2020**, *142*, PMID: 32602710, 13030–13040.

(8) Huizi-Rayo, U.; Gutierrez, J.; Seco, J. M.; Mujica, V.; Diez-Perez, I.; Ugalde, J. M.; Tercjak, A.; Cepeda, J.; San Sebastian, E. An Ideal Spin Filter: Long-Range, High-Spin Selectivity in Chiral Helicoidal 3-Dimensional Metal Organic Frameworks. *Nano Letters* **2020**, *20*, PMID: 33170013, 8476–8482.

(9) Al Bustami, H.; Koplovitz, G.; Primc, D.; Yochelis, S.; Capua, E.; Porath, D.; Naaman, R.; Paltiel, Y. Single Nanoparticle Magnetic Spin Memristor. *Small* **2018**, *14*, 1801249.

(10) Koplovitz, G.; Primc, D.; Ben Dor, O.; Yochelis, S.; Rotem, D.; Porath, D.; Paltiel, Y. Magnetic Nanoplatelet-Based Spin Memory Device Operating at Ambient Temperatures. *Advanced Materials* **2017**, *29*, 1606748.

(11) Liu, T.; Wang, X.; Wang, H.; Shi, G.; Gao, F.; Feng, H.; Deng, H.; Hu, L.; Lochner, E.; Schlottmann, P., et al. Linear and Nonlinear Two-Terminal Spin-Valve Effect from Chirality-Induced Spin Selectivity. *ACS Nano* **2020**, *14*, PMID: 33136367, 15983–15991.

(12) Nguyen, T. N. H.; Rasabathina, L.; Hellwig, O.; Sharma, A.; Salvan, G.; Yochelis, S.; Paltiel, Y.; Baczewski, L. T.; Tegenkamp, C. Cooperative Effect of Electron Spin Polarization in Chiral Molecules Studied with Non-Spin-Polarized Scanning Tunneling Microscopy. *ACS Applied Materials & Interfaces* **2022**, *14*, PMID: 35960822, 38013–38020.

(13) Rahman, M. W.; Firouzeh, S.; Pramanik, S. Carrier localization and magnetoresistance in DNA-functionalized carbon nanotubes. *Nanotechnology* **2021**, *32*, 455001.

(14) Kiran, V.; Mathew, S.; Cohen, S.; Hernandez Delgado, I.; Lacour, J.; Naaman, R. Helicenes-A New Class of Organic Spin Filter. *Advanced materials (Deerfield Beach, Fla.)* **2016**, *28*, DOI: `10.1002/adma.201504725`.

(15) Xie, Z.; Markus, T. Z.; Cohen, S. R.; Vager, Z.; Gutierrez, R.; Naaman, R. Correction to Spin Specific Electron Conduction through DNA Oligomers. *Nano Letters* **2012**, *12*, PMID: 22132798, 523–523.

(16) Bullard, G.; Tassinari, F.; Ko, C.-H.; Mondal, A. K.; Wang, R.; Mishra, S.; Naaman, R.; Therien, M. J. Low-Resistance Molecular Wires Propagate Spin-Polarized Currents. *Journal of the American Chemical Society* **2019**, *141*, PMID: 31411873, 14707–14711.

(17) Tassinari, F.; Jayarathna, D.; Kantor-Uriel, N.; Davis, K.; Varade, V.; Achim, C.; Naaman, R. Chirality Dependent Charge Transfer Rate in Oligopeptides. *Advanced Materials* **2018**, *30*, 1706423.

(18) Bloom, B. P.; Kiran, V.; Varade, V.; Naaman, R.; Waldeck, D. H. Spin Selective Charge Transport Through Cysteine Capped Cdse Quantum Dots. *Nano Letters* **2016**, *16*, PMID: 27336320, 4583–4589.

(19) Aiello, C. D.; Abendroth, J. M.; Abbas, M.; Afanasev, A.; Agarwal, S.; Banerjee, A. S.; Beratan, D. N.; Belling, J. N.; Berche, B.; Botana, A., et al. A Chirality-Based Quantum Leap. *ACS Nano* **2022**, *16*, PMID: 35318848, 4989–5035.

(20) Yang, X.; van der Wal, C. H.; van Wees, B. J. Detecting Chirality in Two-Terminal Electronic Nanodevices. *Nano Letters* **2020**, *20*, PMID: 32672980, 6148–6154.

(21) Huisman, K. H.; Thijssen, J. M. CISS Effect: A Magnetoresistance Through Inelastic Scattering. *The Journal of Physical Chemistry. C, Nanomaterials and Interfaces* **2021**, *125*, 23364–23369.

(22) Das, T. K.; Tassinari, F.; Naaman, R.; Fransson, J. Temperature-Dependent Chiral-Induced Spin Selectivity Effect: Experiments and Theory. *The Journal of Physical Chemistry C* **2022**, *126*, 3257–3264.

(23) Huisman, K. H.; Heinisch, J.-B. M.-Y.; Thijssen, J. M. Chirality-Induced Spin Selectivity (CISS) Effect: Magnetocurrent–Voltage Characteristics with Coulomb Interactions I. *The Journal of Physical Chemistry C* **2023**, *127*, 6900–6905.

(24) Rebergen, M. A Study of Induced Spin Selectivity in Chiral Molecules, MSc thesis, Delft University of Technology, 2018.

(25) Fransson, J. Chirality-Induced Spin Selectivity: The Role of Electron Correlations. *The Journal of Physical Chemistry Letters* **2019**, *10*, PMID: 31657931, 7126–7132.

(26) Haug, H. J. W.; Jauho, A. P., *Quantum Kinetics in Transport and Optics of Semiconductors*; Springer: 2008.

(27) Newns, D. M. Self-Consistent Model of Hydrogen Chemisorption. *Phys. Rev.* **1969**, *178*, 1123–1135.

(28) Verzijl, C. J. O.; Seldenthuis, J. S.; Thijssen, J. M. Applicability of the wide-band limit in DFT-based molecular transport calculations. *The Journal of Chemical Physics* **2013**, *138*, 094102.

(29) Ramasesha, S.; Sinha, B.; Albert, I. Nature of exchange interactions in stacked radicals/radical-ions of cyclic polyenes. *Journal of Molecular Structure* **1994**, *327*, 173–180.

(30) Bursill, R. J.; Castleton, C.; Barford, W. Optimal parametrisation of the Pariser–Parr–Pople Model for benzene and biphenyl. *Chemical Physics Letters* **1998**, *294*, 305–313.

(31) Verzijl, C. J. O.; Gil, J. A. C.; Perrin, M. L.; Dulić, D.; van der Zant, H. S. J.; Thijssen, J. M. Image effects in transport at metal-molecule interfaces. *The Journal of Chemical Physics* **2015**, *143*, 174106.

(32) Jacquet, P. A. ThermoElectric Transport Properties of a Chain of Quantum Dots with Self-Consistent Reservoirs. *Journal of Statistical Physics* **2009**, *134*, 709–748.

(33) Groth, C. W.; Wimmer, M.; Akhmerov, A. R.; Waintal, X. Kwant: A Software Package for Quantum Transport. *New Journal of Physics* **2014**, *16*, 063065.

(34) Varjas, D.; Rosdahl, T.; Akhmerov, A. Qsymm: Algorithmic symmetry finding and symmetric Hamiltonian generation. *New Journal of Physics* **2018**, *20*, DOI: `10.1088/1367-2630/aadf67`.

(35) Meir, Y.; Wingreen, N. S. Landauer formula for the current through an interacting electron region. *Phys. Rev. Lett.* **1992**, *68*, 2512–2515.

(36) Galperin, M.; Nitzan, A.; Ratner, M. A. Inelastic effects in molecular junctions in the Coulomb and Kondo regimes: Nonequilibrium equation-of-motion approach. *Phys. Rev. B* **2007**, *76*, 035301.

5

MAGNETOCURRENT WITH VIBRATIONAL MODES

We consider the effect of vibrational interactions on the off-resonant tunneling regime through chiral molecules. Using the theory of Troisi, Ratner and Nitzan,[1] *we verify that the Onsager reciprocity theorem is satisfied and that the magnetocurrent arising in the non-linear regime is even in bias voltage with a size of the order* 0.1%. *Furthermore we find that the effect of the spin-orbit coupling, chirality and magnetization can lead to large effects in the second order differential conductance of the magnetocurrent.*

5.1. INTRODUCTION

In chapters 2, 3 and 4 we have seen that a finite magnetocurrent can only be generated in the presence of interactions. Fransson[2] showed that, in transport through chiral molecules, on-site Coulomb repulsion between electrons with opposite spin, in combination with the spin-orbit coupling leads to a finite magnetocurrent. In chapters 3 and 4 we also took into account on-site Coulomb interactions and spin-orbit coupling to generate a magnetocurrent in chiral molecules. We found a magnetocurrent that is even or odd as a function of bias voltage depending on the type of spin-orbit coupling (nearest-neighbour or next-nearest neighbour), the alignment of the Fermi level with the molecular spectrum and the type of leads used (wide band limit versus semi-infinite leads). Furthermore, the largest size of the effect was only of the order 0.1% when using realistic model parameters.

In this chapter we focus on vibrational modes of the molecule to generate a magnetocurrent in the inelastic tunneling regime. Nuclei in the molecule can move and electrons 'feel' this movement through the Coulomb force. When the potential associated to this force is expanded to first order in the displacement of the nuclei, a coupling between electron and phonons (vibrational modes) appears, this is the electron-phonon coupling. For small electron-phonon coupling one can for example resort to the self-consistent Born approximation[3–5] (which is computationally expensive), the lower order expansion,[6] or the method of Troisi et al..[1,7] These methods are known to reproduce the inelastic tunneling spectroscopy (IETS) spectra that are measured in experiment. For a strong electron-phonon coupling one can solve the system by performing the polaron (Lang-Firsov) transformation.[8,9] This transformation modifies the coupling of the electron to the leads as well and in the work of Chen et al.[10] an expression for the Green's function is obtained by taking the average over this modified coupling. For an extensive overview of the theory of vibrational modes see chapter 17 of Cuevas and Scheer.[11]

In the context of the CISS effect it is known that vibrational modes[12,13] can give a finite magnetocurrent as well. Fransson[12] found an effect of the order $1-10\%$ when the electron-phonon coupling was spin-dependent. Klein and Michaeli[14] pointed out that the inclusion of interactions (vibrational modes) can lead to spurious violation of current conservation. This motivated them to adjust the Meir-Wingreen formula[14] such that the total current is conserved : $I_\mathrm{L} + I_\mathrm{R} = 0$. When they implemented this adjusted formula in a system with strong electron-phonon coupling,[13] an effect of the order 1% was found for large values of the spin-orbit coupling parameter.

In this chapter we will study vibrational modes in the off-resonant regime using the method of Troisi et al..[1,7] In molecular junctions the transport is mostly elastic in nature. There can however be inelastic transport due to vibrational modes. Inelastic transport occurs when the applied bias voltage matches the vibrational mode's energy. The signature of inelastic transport can be observed as a step in the first and as a peak in the second order differential conductance ($\frac{dI}{dV}$ and $\frac{d^2I}{dV^2}$ respectively). We will investigate the bias dependence of these conductances for the opposite magnetization of the leads, when spin-orbit coupling is present. We will also verify Onsager-Casimir reciprocity, the absence of currents for zero bias and current conservation.

5.2. VIBRATIONAL MODES

The Hamiltonian for a two-terminal system with vibrational modes is given by:

$$H = H_{\text{mol.}} + H_{\text{lead-mol.}} + H_{\text{leads}} + H_{\text{el-ph}} + H_{\text{vib.}} \tag{5.1}$$

Here $H_{\text{mol.}}$ describes the Hamiltonian of the molecule and is taken as the chiral tight binding chain from chapter 3, $H_{\text{lead-mol.}}$ describes the coupling of the molecule to the leads, and H_{leads} describes the Hamiltonian of the leads. The coupling of the molecular vibrational modes to the electrons is described by:

$$H_{\text{el-ph}} = \sum_{i,\alpha,\beta,s,s'} \lambda^{i}_{\alpha s,\beta s'} c^{\dagger}_{\alpha s} c_{\beta s'} (b_i + b_i^{\dagger}) \tag{5.2}$$

and the vibrational modes are described by $H_{\text{vib.}} = \sum_i \hbar\omega_i b_i^{\dagger} b_i$, where $b_i^{\dagger}, b_i$ are bosonic creation and annihilation operators with frequency ω_i. We define the vibrational modes coupling matrix $\boldsymbol{\lambda}^i = \sum_{\alpha,\beta,s,s'} \lambda^{i}_{\alpha s,\beta s'} c^{\dagger}_{\alpha s} c_{\beta s'}$, which describes the coupling of vibrational mode i to the electrons. The matrix $\boldsymbol{\lambda}^i$ is finite and does not depend on the spin of the electron (since it originates from interactions between the electrons and the nuclei, which is a spin-independent interaction). Fransson[12] however argued that in the presence of spin-orbit coupling the vibrational modes couple to the spin of the electron and in principle it is possible that the $\boldsymbol{\lambda}^i$ is not diagonal in the spins anymore. Since both the interaction between the electrons and the nuclei and the spin-orbit coupling are invariant under the time-reversal operator $\hat{\mathscr{T}} = i\sigma_{\text{y}}\hat{\mathscr{K}}$ (with $\hat{\mathscr{K}}$ the conjugation operator and σ_{y} the y Pauli-matrix), the vibrational matrix $\boldsymbol{\lambda}^i$ is so as well: $\mathscr{T}\boldsymbol{\lambda}^i\mathscr{T}^{-1} = \boldsymbol{\lambda}^i$.

Now we turn to the formula for the current for a system with vibrational modes. It is possible that electrons gain or lose energy due to the vibrational modes, when travelling across the molecular junction. They then enter the scattering region with electron ϵ and leave it with a different energy ϵ' i.e. inelastic scattering. The Landauer-Büttiker formula gives the current for elastic processes, therefore we need to adjust it to include inelastic processes as well. The current into the left lead is given by:

$$I = \frac{e}{h} \iint \mathscr{T}^{\text{LR}}(\epsilon,\epsilon') f_{\text{L}}(\epsilon)[1 - f_{\text{R}}(\epsilon')] - \mathscr{T}^{\text{RL}}(\epsilon,\epsilon') f_{\text{R}}(\epsilon)[1 - f_{\text{L}}(\epsilon')] d\epsilon d\epsilon'. \tag{5.3}$$

Here f_α is the Fermi-Dirac function of contact $\alpha : f_\alpha = \left[\exp\left(\beta(\epsilon - \mu_\alpha)\right) + 1\right]^{-1}$ with $\mu_{\text{L,R}} = E_{\text{F}} \pm \frac{V}{2}$ with E_{F} the Fermi level and V the bias voltage. Note that the current into the right lead is obtained by swapping the indices L ↔ R in eq. (5.3) and it follows that $I_{\text{L}} + I_{\text{R}} = 0$.

The transmission is the sum of an elastic and inelastic part and expressions for them are obtained with the method of Troisi et al.[1,7] in the off-resonant regime. For elastic processes $\mathscr{T}^{\text{LR}}_{\text{el.}}(\epsilon,\epsilon') = \mathscr{T}^{\text{RL}}_{\text{el.}}(\epsilon,\epsilon') = \delta(\epsilon - \epsilon') T_{\text{el.}}(\epsilon)$, with $T_{\text{el.}}(\epsilon) = \text{Tr}\left[\boldsymbol{G}^{+}_{\text{el.}}(\epsilon)\boldsymbol{\Gamma}_{\text{L}}(\epsilon)\boldsymbol{G}^{-}_{\text{el.}}(\epsilon)\boldsymbol{\Gamma}_{\text{R}}(\epsilon)\right]$. Here $\boldsymbol{G}^{+}_{\text{el.}}$ is the retarded, elastic Green's function:

$$\boldsymbol{G}^{+}_{\text{el.}}(\epsilon) = \left(\epsilon\boldsymbol{I} - \boldsymbol{H}_{\text{mol.}} - \boldsymbol{\Sigma}_{\text{leads}}(\epsilon)\right)^{-1}, \tag{5.4}$$

with $\mathbf{\Sigma}_{\text{leads}}(\epsilon) = \mathbf{\Lambda}_{\text{L}}(\epsilon) + \mathbf{\Lambda}_{\text{R}}(\epsilon) - \frac{i}{2}\Big(\mathbf{\Gamma}_{\text{L}}(\epsilon) + \mathbf{\Gamma}_{\text{R}}(\epsilon)\Big)$. The formula for the elastic current reduces to the Landauer-Büttiker formula:

$$I_{\text{el.}} = \frac{e}{h}\int T_{\text{el.}}(\epsilon)\Big(f_{\text{L}}(\epsilon) - f_{\text{R}}(\epsilon)\Big)d\epsilon. \tag{5.5}$$

Near equilibrium and at low temperatures the system is in its ground state. Therefore we consider an initial state where all vibrational modes are unoccupied $|\boldsymbol{n}\rangle = |\mathbf{0}\rangle$ and a final state $|\boldsymbol{n}'\rangle$ which has modes i occupied with one boson and all other modes remain unoccupied. In that case the inelastic transmission is given by: $\mathscr{T}^{\text{LR}}(\epsilon,\epsilon') = \sum_i \delta(\epsilon - \epsilon' - \hbar\omega_i)T_i^{\text{LR}}(\epsilon)$, where:

$$T_i^{\text{LR}}(\epsilon) = \text{Tr}\Big[\boldsymbol{G}^+_{\text{inel.}}(\epsilon)\mathbf{\Gamma}_{\text{L}}(\epsilon)\boldsymbol{G}^-_{\text{inel.}}(\epsilon)\mathbf{\Gamma}_{\text{R}}(\epsilon - \hbar\omega_i)\Big]. \tag{5.6}$$

Restricting ourselves to single quantum excitations from the ground state, the inelastic retarded Green's function is given by:[1]

$$\boldsymbol{G}^+_{\text{inel.}}(\epsilon) = \sum_i \boldsymbol{G}^+_{\text{el.}}(\epsilon)\boldsymbol{\lambda}^i\boldsymbol{G}^+_{\text{el.}}(\epsilon). \tag{5.7}$$

and the advanced Green's function is obtained through Hermitian conjugation $\boldsymbol{G}^-_{\text{inel.}}(\epsilon) = \Big(\boldsymbol{G}^+_{\text{inel.}}(\epsilon)\Big)^\dagger$. The inelastic current is then given by (via eq. (5.3)):

$$I_{\text{inel.}} = \frac{e}{h}\int\sum_i T_i^{\text{LR}}(\epsilon)f_{\text{L}}(\epsilon)[1 - f_{\text{R}}(\epsilon - \hbar\omega_i)] - T_i^{\text{RL}}(\epsilon)f_{\text{R}}(\epsilon)[1 - f_{\text{L}}(\epsilon - \hbar\omega_i)]d\epsilon. \tag{5.8}$$

In Appendix 5.6.1 we show that the inelastic current vanishes at $V = 0$ provided $\hbar\omega_i \gg k_{\text{B}}T$.

5.3. MAGNETOCURRENT & IETS OBSERVABLES

The magnetocurrent is given by the difference in the total current for opposite magnetizations. The elastic current does not contribute to the magnetocurrent, due to Büttiker reciprocity $T_{\text{el.}}(\epsilon, m) = T_{\text{el.}}(\epsilon, -m)$ for two terminal systems,[15] making the magnetocurrent inelastic in nature:

$$\begin{aligned}\Delta I(m,V) &\equiv I(m) - I(-m)\\ &= \frac{e}{h}\sum_i\int\Big(T_i^{\text{LR}}(\epsilon,m) - T_i^{\text{LR}}(\epsilon,-m)\Big)f_{\text{L}}(\epsilon)[1 - f_{\text{R}}(\epsilon - \hbar\omega_i)]\\ &\quad -\Big(T_i^{\text{RL}}(\epsilon,m) - T_i^{\text{RL}}(\epsilon,-m)\Big)f_{\text{R}}(\epsilon)[1 - f_{\text{L}}(\epsilon - \hbar\omega_i)]d\epsilon.\end{aligned} \tag{5.9}$$

In the wide band limit the inelastic transmission satisfies $T_i^{\text{LR}}(\epsilon, m) = T_i^{\text{RL}}(\epsilon, -m)$ (see Appendix 5.6.2), which we use to rewrite the magnetocurrent as (for $\eta = \frac{1}{2}$):

$$\begin{aligned}\Delta I(m,V) = \frac{e}{h}\sum_i\int\Big(T_i^{\text{LR}}(\epsilon,m) - T_i^{\text{LR}}(\epsilon,-m)\Big)\Big(&f(\epsilon - E_{\text{F}} - \frac{V}{2})[1 - f(\epsilon - \hbar\omega_i - E_{\text{F}} + \frac{V}{2})]\\ &+f(\epsilon - E_{\text{F}} + \frac{V}{2})[1 - f(\epsilon - \hbar\omega_i - E_{\text{F}} - \frac{V}{2})]\Big)d\epsilon,\end{aligned} \tag{5.10}$$

with $f(x) = \left[\exp(\beta x) + 1\right]^{-1}$. From eq. (5.10) we immediately conclude that: $\Delta I(m,V) = \Delta I(m,-V)$. The magnetocurrent is exactly even in bias voltage, independent of the choice of Fermi level and type of spin-orbit coupling (NN versus NNN) if the junction is biased symmetrically. The capacitive coupling to the left and right lead can differ and we can write $\mu_L = E_F + \eta V, \mu_R = E_F + (\eta - 1)V$ with $0 < \eta < 1$. For $\eta \neq \frac{1}{2}$, the magnetocurrent in the wide-band limit is no longer exactly even in the bias voltage. For finite temperatures inelastic process will contribute to the total current around the bias voltages $V = \pm\hbar\omega$ and below this voltage the current is exclusively determined by elastic process. Therefore the magnetocurrent is expected to be zero for $|V| < \hbar\omega$ (due to Büttiker reciprocity) and around $V = \pm\hbar\omega$ inelastic process contribute such that a non-zero magnetocurrent will appear. In Appendix 5.6.2 we explicitly show that the magnetocurrent satisfies Onsager reciprocity.

In IETS the linear conductance : $G_1(m,V) = \frac{dI(m,V)}{dV}$ and second order conductance $G_2(m,V) = \frac{d^2 I(m,V)}{dV^2}$ are measured as a function of bias voltage. The difference between the linear conductance for opposite magnetizations is given by:

$$\Delta G_1(m,V) = G_1(m,V) - G_1(-m,V) = \frac{d\Delta I(m,V)}{dV}. \tag{5.11}$$

Given the fact that $\Delta I(m,V)$ (the magnetocurrent) is perfectly even in bias voltage, the quantity $\Delta G_1(m,V)$ is perfectly odd in bias voltage (and vanishes at $V = 0$ due to Onsager reciprocity). At the voltages $V = \pm\hbar\omega$ a sudden change is expected in $\Delta G_1(m,V)$. For $G_2(m,V)$ the second order magnetoconductance $\Delta G_2(m,V) = G_2(m,V) - G_2(-m,V) = \frac{d^2 \Delta I(m,V)}{dV^2}$ is introduced and it follows that $\Delta G_2(m,V)$ is perfectly even in bias voltage.

5.4. NUMERICAL RESULTS

We will model the molecule as the chiral chain of Fransson,[2] also used in chapter 3. We take one winding ($M = 1$) with four sites ($N = 4$). The radius and pitch of the helix are taken as $a = c = 1$. The spin-orbit coupling parameter λ_{soc} is chosen as : $\lambda_{\text{soc}} = 0.1t$ (due to large spin-orbit coupling in the leads) with $t = 2$ eV the hopping parameter. The on-site energy is taken to be zero $\epsilon_0 = 0$. The left (right) two outermost sites are coupled to the left (right) lead. The leads are taken in the wide band limit. The elements that are coupled to the lead α are given by: $\gamma_\alpha(\mathbf{1} + \sigma_z p_z^\alpha)$ and zero otherwise. Here p_z^α is the magnetic polarization of lead α. We only magnetize the left lead with $p_z^L = 0.5$ and $p_z^R = 0$. If not noted otherwise, the coupling strength to the left and right lead are taken symmetrically $\gamma_L = \gamma_R = 0.4$ eV and we take the capacitive coupling $\eta = \frac{1}{2}$ and temperature $T = 100$ K. We will consider one vibrational mode with energy $\hbar\omega = 0.25$ eV and the vibrational matrix coupling matrix is considered between nearest neighbours, where the coupling strength is given by $\lambda_{\text{vib.}} = 0.4t$. To stay in the off-resonant regime we apply a bias voltage such that the chemical potentials μ_R, μ_L do not reach any eigenvalues of $H_{\text{mol.}}$. Our code can be found on `https://github.com/khhuisman/VibrationalModes_Troisi_Compact`. The Hamiltonian of the $\boldsymbol{H}_{\text{mol.}}$ is constructed with the Kwant code[16] and the Qsymm code.[17]

In figure 5.1 the current, magnetocurrent and their first and second derivatives are shown. In 5.1a the total current for positive and negative magnetization is plotted and around $V = \pm\hbar\omega$, 'kinks' are observed, which arise due to the inelastic processes. In fig. 5.1b the difference between the currents for opposite magnetizations (i.e. the magnetocurrent) is plotted as a function of bias voltage. For $|V| < \hbar\omega$ the magnetocurrent is numerically zero and around $V = \pm\hbar\omega$ a finite magnetocurrent appears since inelastic processes start to contribute. The magnetocurrent is perfectly even in bias and the size of the effect $P_I = \frac{I(m,V)-I(-m,V)}{I(m,V)+I(-m,V)}$ is of the order 0.1%.

In fig. 5.1c the linear conductance for positive and negative magnetization are plotted. As expected there is a sudden increase at $V = \pm\hbar\omega$. In fig. 5.1d the difference between the linear conductances, i.e. $\Delta G_1(m,V)$, is plotted. It is seen to be perfectly odd in the bias voltage.

In 5.1e the second order differential conductance is plotted as a function of the bias voltage for positive and negative magnetization. As expected there are are two peaks, one at $V = \hbar\omega$ and at $V = -\hbar\omega$. The difference between these coefficients i.e. $\Delta G_2(m,V)$ is plotted in 5.1f as a function of bias voltage and as expected it is perfectly even in the bias. The size of the effect $P_{G_2} = \frac{G_2(m,V)-G_2(-m,V)}{G_2(m,V)+G_2(-m,V)}$ at $V = \pm\hbar\omega$ is of the order 1%, which should be detectable in experiment.

Further note that this effect vanishes if the spin-orbit coupling is set to zero. However we anticipate it could emerge due to the spin-orbit interaction in the leads. When the vibrational modes are made spin dependent, an increase in the size of the effect P_I, P_{G_2} was observed while the magnetocurrent remains even in the bias voltage.

5.5. CONCLUSION

In this chapter we investigated magnetocurrent caused by vibrational modes in the off-resonant regime for helicenes, using the method of Troisi et al..[1,7] We modeled a chiral molecule with spin-orbit coupling in the wide-band limit. We found that the total current is conserved $I_L + I_R = 0$ and no equilibrium currents arise $I(V=0) = 0$ in the regime where IETS is valid.

The magnetocurrent is found to be perfectly even if the capacitive coupling is chosen as $\eta = \frac{1}{2}$, this follows from the definition of the magnetocurrent. This evenness can in principle be verified experimentally by looking at the second order magnetoconductance. This quantity is expected to be dominantly even in the bias voltage and the size of the effect at $|V| = \hbar\omega$ is of the order of a few percent. When the capacitive coupling deviates from this value (i.e. $\eta \neq \frac{1}{2}$) the magnetocurrent is no longer perfectly even and obtains an odd signature. The discrepancy between odd magnetocurrent found in experiment and even magnetocurrent found in theory dependence remains a puzzling problem. We explicitly showed that the magnetocurrent satisfies Onsager reciprocity. The size of the effect is of the order 0.1%. It is remarkable that the (relative) size of the effect in the currents is of the same order as the relative MR found in previous chapters for resonant transport.

For future theoretical studies the self-consistent Born approximation or lower order expansion could be used to get a more accurate estimate for the size of the effect and the bias dependence of the magnetocurrent, although we expect similar results.

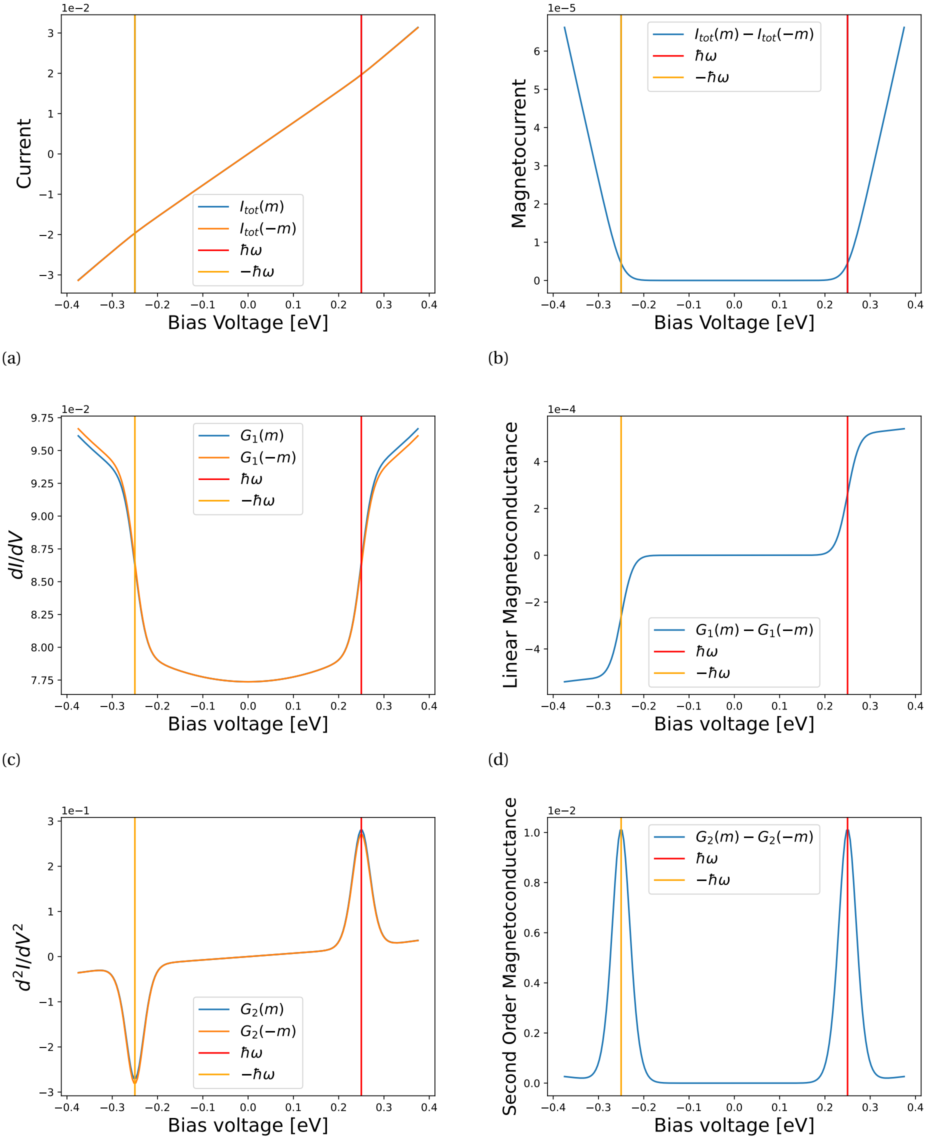

(a)

(b)

(c)

(d)

(e)

(f)

Figure 5.1: IETS spectrum for opposite magnetizations for the helical chain. 5.1a The total current as function of bias voltage. 5.1b The magnetocurrent as a function of bias voltage. 5.1c The linear differential conductance. 5.1d The difference between the linear differential conductance for opposite magnetizations. 5.1e The second order differential conductance.5.1f The difference between the second order differential conductance for opposite magnetizations.

5.6. APPENDIX

5.6.1. VANISHING EQUILIBRIUM CURRENT

At zero bias $V = 0$ the inelastic current in eq. (5.8) should vanish,this provides us with the sanity check that:

$$I_{\mathrm{inel.}}(V=0) = \frac{e}{h}\int\sum_i\left(T_i^{\mathrm{LR}}(\epsilon) - T_i^{\mathrm{RL}}(\epsilon)\right)f_0(\epsilon)[1-f_0(\epsilon-\hbar\omega_i)]\,d\epsilon, \tag{5.12}$$

must be zero. Here $f_0(\epsilon) = \left[\exp\left(\beta(\epsilon - E_{\mathrm{F}})\right)+1\right]^{-1}$. If $T_i^{\mathrm{LR}}(\epsilon) \neq T_i^{\mathrm{RL}}(\epsilon)$ the current can only vanish by virtue of the overlap of the two Fermi-Dirac functions: $f_0(\epsilon)[1-f_0(\epsilon-\hbar\omega_i)]$. Take for example $T = 0$ K and $\hbar\omega_i > 0$ (the latter must always be the case), then the overlap reduces: $\Theta(-\epsilon)\Theta(\epsilon-\hbar\omega_i)$ (with $\Theta(x)$ the Heaviside function), which is zero for all energies, resulting in a vanishing equilibrium current. For finite temperatures and positive $\hbar\omega_i$, this overlap will be finite, but it can be made numerically small by choosing: $\hbar\omega_i \gg k_{\mathrm{B}}T$. In this regime emission processes dominate, which is precisely the processes considered in IETS.[11] In our calculations we will explicitly verify that this equilibrium current vanishes (the equilibrium current does not become larger than $|I_{\mathrm{inel.}}(V=0)| < 10^{-10}$).

5.6.2. ONSAGER RECIPROCITY

We then consider a system where the left lead is magnetized with magnetization m, causing the transmission for elastic process to depend on this quantity:

$$T_{\mathrm{el.}}(\epsilon, m) = \mathrm{Tr}\left[\boldsymbol{G}^{+}_{\mathrm{el.}}(\epsilon, m)\boldsymbol{\Gamma}_{\mathrm{L}}(\epsilon, m)\boldsymbol{G}^{-}_{\mathrm{el.}}(\epsilon, m)\boldsymbol{\Gamma}_{\mathrm{R}}(\epsilon)\right], \tag{5.13}$$

and for inelastic processes as well:

$$T_i^{\mathrm{LR}}(\epsilon, m) = \mathrm{Tr}\left[\boldsymbol{G}^{+}_{\mathrm{el.}}(\epsilon, m)\boldsymbol{\lambda}^i\boldsymbol{G}^{+}_{\mathrm{el.}}(\epsilon, m)\boldsymbol{\Gamma}_{\mathrm{L}}(\epsilon, m)\boldsymbol{G}^{-}_{\mathrm{el.}}(\epsilon, m)\boldsymbol{\lambda}^i\boldsymbol{G}^{-}_{\mathrm{el.}}(\epsilon, m)\boldsymbol{\Gamma}_{\mathrm{R}}(\epsilon-\hbar\omega_i)\right]. \tag{5.14}$$

Now we verify Onsager reciprocity by calculating the linear differential conductance coefficient of the total current $I = I_{\mathrm{el.}} + I_{\mathrm{inel.}}$ at zero bias voltage, for any value of the capacitive coupling η. Via eqs. (5.5) and (5.8) this gives:

$$\begin{aligned}
G_1(m) &= \frac{e}{h}\frac{\partial I(m)}{\partial V}\bigg|_{V=0} \\
&= -\frac{e}{h}\int T_{\mathrm{el.}}(\epsilon, m) f_0'(\epsilon)\,d\epsilon \\
&\quad -\frac{e}{h}\int\sum_i\left[T_i^{\mathrm{RL}}(\epsilon, m) + T_i^{\mathrm{LR}}(\epsilon, m)\right]\left(f_0'(\epsilon)[1-f_0(\epsilon-\hbar\omega_i)] + f_0(\epsilon)f_0'(\epsilon-\hbar\omega_i)]\right)d\epsilon.
\end{aligned} \tag{5.15}$$

Here $f_0'(\epsilon) = \partial_\epsilon f_0(\epsilon)$. Therefore the difference between the linear coefficients for opposite magnetizations is:

$$
\begin{aligned}
\Delta G_1 &= G_1(m) - G_1(-m) \\
&= -\frac{e}{h}\sum_i \int \Big[T_i^{\mathrm{RL}}(\epsilon,m) + T_i^{\mathrm{LR}}(\epsilon,m) - T_i^{\mathrm{RL}}(\epsilon,-m) - T_i^{\mathrm{LR}}(\epsilon,-m)\Big] \\
&\quad \times \Big(f_0'(\epsilon)[1-f_0(\epsilon-\hbar\omega_i)] + f_0(\epsilon)f_0'(\epsilon-\hbar\omega_i)]\Big)d\epsilon. \qquad (5.16)
\end{aligned}
$$

Where we used that $T_{\mathrm{el.}}(\epsilon,m) = T_{\mathrm{el.}}(\epsilon,-m)$, due to Büttiker reciprocity. The Green's functions in the expression for the inelastic transmission eq. (5.14) transform under the time-reversal operator as $\hat{\mathscr{T}}\boldsymbol{G}^{\pm}(m)\hat{\mathscr{T}}^{-1} = \boldsymbol{G}^{\mp}(-m)$, the matrix describing the coupling of the electrons to the vibrational modes are symmetric under time $\hat{\mathscr{T}}\boldsymbol{\lambda}^i\hat{\mathscr{T}}^{-1} = \boldsymbol{\lambda}^i$ (as is $\boldsymbol{\Gamma}_{\mathrm{R}}$) and the left lead coupling matrix transforms as: $\hat{\mathscr{T}}\boldsymbol{\Gamma}_{\mathrm{L}}(m)\hat{\mathscr{T}}^{-1} = \boldsymbol{\Gamma}_{\mathrm{L}}(-m)$. We first insert the identity matrix $\boldsymbol{I} = \hat{\mathscr{T}}\hat{\mathscr{T}}^{-1}$ between each matrix in eq. (5.14), we then use the transformation rules under $\mathscr{T}$ for each matrix in the product and finally we use the cyclic property of the trace to obtain:

$$
T_i^{\mathrm{LR}}(\epsilon,m) = \mathrm{Tr}\Big[\boldsymbol{G}^{+}_{\mathrm{el.}}(\epsilon,-m)\boldsymbol{\lambda}^i\boldsymbol{G}^{+}_{\mathrm{el.}}(\epsilon,-m)\boldsymbol{\Gamma}_{\mathrm{R}}(\epsilon-\hbar\omega_i)\boldsymbol{G}^{-}_{\mathrm{el.}}(\epsilon,-m)\boldsymbol{\lambda}^i\boldsymbol{G}^{-}_{\mathrm{el.}}(\epsilon,-m)\boldsymbol{\Gamma}_{\mathrm{L}}(\epsilon,-m)\Big]. \qquad (5.17)
$$

In the wide band limit $\boldsymbol{\Gamma}_{\mathrm{L}}, \boldsymbol{\Gamma}_{\mathrm{R}}$ are independent of energy and we obtain $T_i^{\mathrm{LR}}(\epsilon,m) = T_i^{\mathrm{RL}}(\epsilon,-m)$ and $T_i^{\mathrm{RL}}(\epsilon,m) = T_i^{\mathrm{LR}}(\epsilon,-m)$, from which it follows that ΔG_1 in eq. (5.16) vanishes: $\Delta G_1 = 0$. On the other hand, if the leads are energy dependent then the transmissions in the integrand of eq. (5.16) do not always cancel out and ΔG_1 can only vanish by virtue of the overlap of the Fermi-Dirac functions: $f_0'(\epsilon)[1-f_0(\epsilon-\hbar\omega_i)] + f_0'(\epsilon-\hbar\omega_i)f_0(\epsilon)$. At zero temperature ($T = 0\ K$) this overlap becomes: $\delta(0)\Theta(\epsilon-\hbar\omega_i) + \delta(\hbar\omega_i)\Theta(-\epsilon)$ and for $\hbar\omega_i > 0$ this overlap is always zero. For finite temperatures this overlap is finite, but becomes numerically small when $\hbar\omega_i \gg k_B T$. In this regime emission processes dominate, which is precisely the processes considered in IETS.[11] Therefore we do not expect any violation of Onsager-reciprocity in IETS measurements.

REFERENCES

(1) Troisi, A.; Ratner, M. A.; Nitzan, A. Vibronic effects in off-resonant molecular wire conduction. *The Journal of Chemical Physics* **2003**, *118*, 6072–6082.

(2) Fransson, J. Chirality-Induced Spin Selectivity: The Role of Electron Correlations. *The Journal of Physical Chemistry Letters* **2019**, *10*, PMID: 31657931, 7126–7132.

(3) Frederiksen, T.; Brandbyge, M.; Lorente, N.; Jauho, A.-P. Inelastic Scattering and Local Heating in Atomic Gold Wires. *Phys. Rev. Lett.* **2004**, *93*, 256601.

(4) Paulsson, M.; Frederiksen, T.; Brandbyge, M. Modeling inelastic phonon scattering in atomic- and molecular-wire junctions. *Phys. Rev. B* **2005**, *72*, 201101.

(5) Frederiksen, T.; Paulsson, M.; Brandbyge, M.; Jauho, A.-P. Inelastic transport theory from first principles: Methodology and application to nanoscale devices. *Phys. Rev. B* **2007**, *75*, 205413.

(6) Viljas, J. K.; Cuevas, J. C.; Pauly, F.; Häfner, M. Electron-vibration interaction in transport through atomic gold wires. *Phys. Rev. B* **2005**, *72*, 245415.

(7) Troisi, A.; Ratner, M. A. Modeling the inelastic electron tunneling spectra of molecular wire junctions. *Phys. Rev. B* **2005**, *72*, 033408.

(8) Lang, I. G.; Firsov, Y. A. Kinetic Theory of Semiconductors with Low Mobility. *Journal of Experimental and Theoretical Physics (U.S.S.R.)* **1963**, *16*, 1301–1312.

(9) Mahan, G. D., *Many Particle Physics*; Plenum Publishers: 2005.

(10) Chen, Z.-Z.; Lü, R.; Zhu, B.-f. Effects of electron-phonon interaction on nonequilibrium transport through a single-molecule transistor. *Phys. Rev. B* **2005**, *71*, 165324.

(11) Cuevas, J. C.; Scheer, E., *Molecular Electronics: An Introduction to Theory and Experiment*; World Scientific, 2010: 2010.

(12) Fransson, J. Vibrational Origin of Exchange Splitting and Chirality Induced Spin Selectivity. *Physical Review B* **2020**, DOI: 10.1103/PhysRevB.102.235416.

(13) Klein, D.; Michaeli, K. Giant chirality-induced spin selectivity of polarons. *Phys. Rev. B* **2023**, *107*, 045404.

(14) Klein, D.; Michaeli, K. Landauer formula for interacting systems: a consistent nonperturbative approximation, 2022.

(15) Büttiker, M. Symmetry of Electrical Conduction. *IBM Journal of Research and Development* **1988**, *32*, 317–334.

(16) Groth, C. W.; Wimmer, M.; Akhmerov, A. R.; Waintal, X. Kwant: A Software Package for Quantum Transport. *New Journal of Physics* **2014**, *16*, 063065.

(17) Varjas, D.; Rosdahl, T.; Akhmerov, A. Qsymm: Algorithmic symmetry finding and symmetric Hamiltonian generation. *New Journal of Physics* **2018**, *20*, DOI: 10.1088/1367-2630/aadf67.

ACKNOWLEDGEMENTS

First of all I want to thank my supervisor Jos Thijssen. Words cannot express the gratitude I feel that you gave me the opportunity to pursue my dream to become a scientist. I have come to know you as a reliable, kind and knowledgeable supervisor. You know a lot about physics and I could always tap into your source of knowledge. I enjoyed our weekly meetings which I experienced as relaxed, low-key and yet very productive. When I really needed something from you, you were there for me and I could always count on you. I wish nothing but the best for you, your wife, sons and grand-child(ren). Herre van der Zant, thank you for welcoming me with your jovial, friendly character. I would also like to thank you for letting me join your group meeting. You always had suggestions and were listening intently to what I was saying. I could also always rely on you when I needed something from you.

I would like to thank Bart van Wees, Jan van Ruitenbeek, Ferdinand Grozema for the interesting discussions during the CISS-consortium meetings and for being on the promotion committee. I would like to thank Yarsolav Blanter for acting as a reserve member for my promotion committee. Finally I would also like to thank Jonas Fransson for being on the promotion committee, the interesting discussions we had via email and live at Bad Honnef and giving me the opportunity to present my first publication at the online CISS-seminar. I would also like to thank Sense Jan van der Molen for interesting discussions during the CISS-consortium meetings.

I owe a great deal of gratitude to Michael Wimmer and Antonio Manesco for helping me with the Kwant code. I would also like to express my gratitude to the former master students Marnix Rebergen, Huib van Rijt, Grigori Giannakoudakis and last but certainly not least Jan-Brian Heinisch. Jan-Brian, I am very happy that you decided to do your master project with Jos and me. Not only are you a very talented physicist but also a very nice person to work with.

I would also like to thank my colleagues the Quantum Nanoscience department. Chunwei, I think you are a talented physicists and a kind person. I enjoyed the Elecmol conference in Lyon with you and the chats we had over coffee breaks. Jacqueline & Damian, thanks for inviting me to play Mariokart. Sonakshi, I think you are a very kind person and a nice office-mate. My thanks to you and the rest of the C&C committee for organizing cool events. Talieh, thank you for always chatting with me. You are a very kind person and I wish you the best of luck with your career. To Antonio, Marilia and Kostas (my man!) I will never forget the Mariokart evening, which was loco. I would also like to thank my fellow PhD students from the CISS-consortium or who work(ed) on the CISS-effect : Peter Neu, Jędrzej Tepper, Zimu Wei, Xu Yang and Sytze Tirion for interesting discussions.

Marc, from cradle to Quantum Nanoscience, we have know each other. I am happy we are friends for so long and I want to thank you for the relaxing times after work by navigating a coloured jellybean-like being across a ridiculous assault course, driving a car together across some life-threatening, insane circuit or just biking around Delft/on the Cauberg. **Laurens & Caspar**, or “broski” and “amicum” respectively. Over the last four years our gatherings have been more virtual than live. I will never forget the online evenings, from Verdansk to Vondel or our live trips from Domburg to Düsseldorf. I want to thank you for the relaxing times which made me forget about the stress that accompanied my work.

Alba, I am so happy that watching a stupid football match on my phone in the train made me miss my transfer to Delft. Otherwise the two of us most likely never would have met. I want to thank you for the amazing time we had ever since that moment and for the (emotional) support (yes I do have emotions) during my PhD. **Suegros**, yo he recibido una “bienvenido a la familia ” que siempre deseaba. Sois personas muy buenas, gracias por todo. **Familie Huisman & Snip**, ik wil jullie bedanken voor jullie mentale steun en de nodige afleiding tijdens mijn promotietraject. **Edzo & Madeleine** of gewoon **pap & mam**, mijn dank voor jullie steun tijdens mijn promotietraject. Ik draag deze thesis aan jullie op omdat ik alles aan jullie te danken heb. Ik kan me geen betere ouders wensen, was getekend jullie liefhebbende zoon Kars.

CURRICULUM VITAE

Karssien Hero HUISMAN

12-12-1993	Born in Amsterdam, the Netherlands.

EDUCATION

2019–2023	Promovendus, Technische Universiteit Delft *Thesis:* Two Terminal Transport Theory Of Chirality Induced Spin Selectivity *Promotors:* prof. dr. J. M. Thijssen prof. dr. ir. H.S.J. van der Zant
2017–2019	Master Theoretische Natuurkunde, Univeristeit van Amsterdam *Thesis:* $W \to l\bar{\nu}_l$ at Next to Leading Order in the Standard Model Effective Field Theory *Supervisors:* dr. W. J. Waalewijn dr. D. J. Scott
2012–2017	Bachelor Univeristeit van Amsterdam, Bachelor Econometrie (2012) Bachelor Beta-Gamma, major Natuurkunde (2013-2017) *Thesis:* Higgs Boson Production via Gluon - Gluon Fusion And Decay Through: $H \to WW \to l\nu l\nu$ Cutbased Analyses Of The Run Two ATLAS Data *Supervisors:* prof. dr. W. Verkerke dr. L. Brenner
2006–2012	Coornhert Lyceum Haarlem, Atheneum
1998–2006	Openbare Basisschool Bos & Vaart, Haarlem

LIST OF PUBLICATIONS

3. **K. H. Huisman, J.M. Thijssen**, *CISS Effect: A Magnetoresistance Throught Inelastic Scattering*, J. Phys. Chem. C 2021, 125, 42, 23364–23369.

2. **K. H. Huisman, J.B.M.Y. Heinisch and J.M. Thijssen**, *Chirality-Induced Spin Selectivity (CISS) Effect: Magnetocurrent–Voltage Characteristics with Coulomb Interactions I*, J. Phys. Chem. C 2023, 127, 14, 6900–6905.

1. **K. H. Huisman, J.B.M.Y. Heinisch and J.M. Thijssen**, *CISS Effect: Magnetocurrent–Voltage Characteristics with Coulomb Interactions. II*, J. Chem. Phys. 158, 174108 (2023).